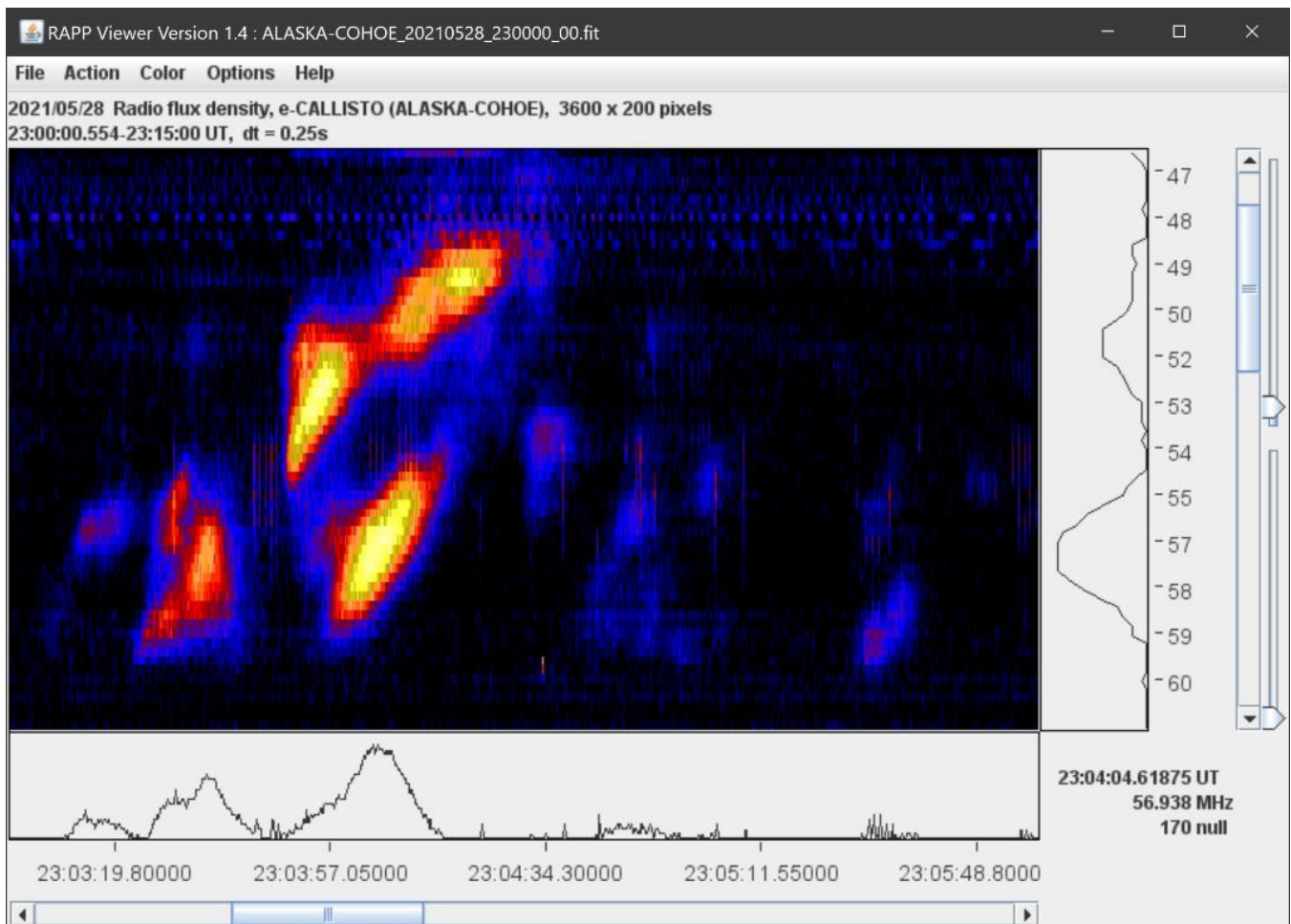


RADIO ASTRONOMY

Journal of the Society of Amateur Radio Astronomers
May-June 2021



Observation of VHF Type II Solar Radio Burst on 28 May 2021
Type II slow-drift radio bursts between 47 and 62 MHz.



Dennis Farr
SARA President

Dr. Richard A. Russel
Editor

Whitham D. Reeve
Contributing Editor

Radio Astronomy is published bimonthly as the official journal of the Society of Amateur Radio Astronomers. Duplication of uncopyrighted material for educational purposes is permitted but credit shall be given to SARA and to the specific author. Copyrighted materials may not be copied without written permission from the copyright owner.

Radio Astronomy is available for download only by SARA members from the SARA web site and may not be posted anywhere else.

It is the mission of the Society of Amateur Radio Astronomers (SARA) to: Facilitate the flow of information pertinent to the field of Radio Astronomy among our members; Promote members to mentor newcomers to our hobby and share the excitement of radio astronomy with other interested persons and organizations; Promote individual and multi station observing programs; Encourage programs that enhance the technical abilities of our members to monitor cosmic radio signals, as well as to share and analyze such signals; Encourage educational programs within SARA and educational outreach initiatives. Founded in 1981, the Society of Amateur Radio Astronomers, Inc. is a membership supported, non-profit [501(c) (3)], educational and scientific corporation. Copyright © 2019 by the Society of Amateur Radio Astronomers, Inc. All rights reserved.

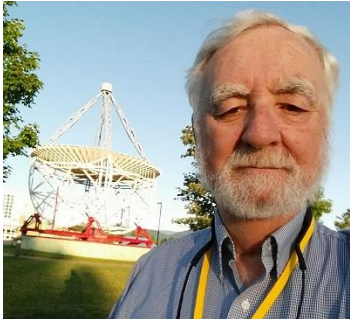
Cover photo:
Whitham D. Reeve

Contents

Radio Waves	3
President’s Page.....	3
Editor’s Notes.....	4
News	5
For Your Radio Astronomy Bookshelf	10
SuperSID	11
John Cook's VLF Report	14
News: (May-Jun 2021).....	28
Feature Articles	32
nanoVNA Calibration Standards.....	32
Getting the Best from the Pulsar Folding Algorithm.....	43
Observation of HF Sudden Frequency Deviation on 22 May 2021	53
Sky raster fly map with satellite rotors, DiSEqC-controller and CALLISTO.....	54
Observation of VHF Type II Solar Radio Burst on 28 May 2021.....	59
Poor man's amateur radio astronomy with small dishes.....	61
Comparative Observations of the 12 May 2021 Geomagnetic Event.....	92
HI Observation with RTL-SDR & IF Average.....	96
Membership	102
New Members.....	102
Journal Archives & Other Promotions.....	103
SARA Online Discussion Group.....	103
What is Radio Astronomy?.....	104
Administrative	104
Officers, directors, and additional SARA contacts	104
Resources	106
Great Projects to Get Started in Radio Astronomy	106
Radio Astronomy Online Resources.....	108
For Sale, Trade and Wanted	110
SARA Advertisements	112
SARA Brochure	113

Radio Waves

President's Page



SARA members are making great strides in astronomy! Dr. Wolfgang Herrmann and his Astropfeiler Stockert group have detected the repeating fast radio burst FRB 20201124A twice. The observation even made a record for one of the strongest pulses observed so far!

Other members are using the new technology of software defined radios to do neutral hydrogen observations and even maser observations.

The Drakes lounge monthly ZOOM meetings are a great hit! Where else can you talk to amateur radio astronomers from all over the world? The meetings are held the 3rd Sunday of each month starting at 1400 ET. All SARA members should receive an email notice.

The listserv forum is very interactive and provides 24/7 contact with other SARA members who appear to have a great time assisting each other with their amateur radio projects and observations. [Email Discussion List | Society of Amateur Radio Astronomers \(radio-astronomy.org\)](#)

The scope in a box program is fully implemented and we have sold out Amazon a number of times as we try to fill orders. Remember, the kit could be made available as a grant to worthy programs. If you know of a group that might qualify, please have them contact us at grants@radio-astronomy.org

The 2021 Eastern conference is a virtual ZOOM conference. This year, the conference dates will be July 31 and August 1. Significant raffle prizes will be picked for those registering, this includes: 2 Scope in the Box kits, 2 SuperSID kits, 3 Radio Sky licenses, a signal generator, and SARA shirts. Register for the Eastern Conference at: [2021 SARA Eastern Conference payments | Society of Amateur Radio Astronomers \(radio-astronomy.org\)](#)
We are very hopeful that 2022 will be the year we return to Green Bank for an in-person conference.

Please take a moment to check out the new online SARA store. It should be much easier now to order anything we offer using one site for both PayPal and Credit card payments.
<https://www.radio-astronomy.org/store/>

Welcome to the new SARA Store Manager, Lester Veenstra!

Keep your antennas pointed up!

Dennis

Editor's Notes

We are always looking for basic radio astronomy articles, radio astronomy tutorials, theoretical articles, application and construction articles, news pertinent to radio astronomy, profiles and interviews with amateur and professional radio astronomers, book reviews, puzzles (including word challenges, riddles, and crossword puzzles), anecdotes, expository on "bad astronomy," articles on radio astronomy observations, suggestions for reprint of articles from past journals, book reviews and other publications, and announcements of radio astronomy star parties, meetings, and outreach activities.

New Journal Feature – Observation Reports

We are now accepting 1-2 page observation reports. These reports should include the astronomical objects RA/DEC plus UTC of the observation. Also include the telescope configuration, process used to observe the object and results. Picture of the setup and plots of the observation are a plus to the report.

If you would like to write an article for Radio Astronomy, please follow **the newly updated Author's Guide** on the SARA web site:

http://www.radio-astronomy.org/publicat/RA-JSARA_Author's_Guide.pdf.

Let us know if you have questions; we are glad to assist authors with their articles and papers and will not hesitate to work with you. You may contact your editors any time via email here: edit@radio-astronomy.org.

The editor(s) will acknowledge that they have received your submission within two days. If they do not reply, assume they did not receive it and please try again.

Please consider submitting your radio astronomy observations for publication: any object, any wavelength. Strip charts, spectrograms, magnetograms, meteor scatter records, space radar records, photographs; examples of radio frequency interference (RFI) are also welcome.

Guidelines for submitting observations may be found here: http://www.radio-astronomy.org/publicat/RA-JSARA_Observation_Submission_Guide.pdf

Issue	Articles	Review	Distribution
Jul – Aug	August 12	August 25	August 31
Sep – Oct	October 12	October 25	October 31
Nov – Dec	December 12	December 20	December 31
Jan – Feb	February 12	February 20	February 28

News

SARA Election Ballot July 2021 RO Bruce Randall, Secretary

Because of the Eastern Conference being a web-based event, this year Elections will be done differently. The president will request nominations from floor at the conference.

Email ballots before the conference will be handled the same as previous years.

SARA 2021 Voting Ballot

Secretary: Vote for One (1)

Bruce Randall
 Write-In _____

Treasurer: Vote for One (1)

Brian C. O'Rourke
 Write-In _____

Director: Vote for Two (2)

Tom Jacobs
 Charles Osborne
 Write-In _____
 Write-In _____

Director at Large: Vote for Two (2)

Jon Wallace
 Wolfgang Herrmann
 Write-In _____
 Write-In _____

Members voting by e-mail should send their completed ballot to

brandall@comporium.net

no later than July 30, 2021, 11:00 PM EDT. **Copying and pasting the ballot into the email will work. Then you can then mark your choices in the email.**

Web conference voting procedure is to be announced at the conference.

SARA Student & Teacher Grant Program

All, SARA has a grant program that is, sad to say very underutilized. We will provide kits or money to students and teachers including college students to help them with a radio telescope project. SARA can supply any of the following kits:

- SuperSID
- Scope in a Box
- IBT (Itty Bitty Telescope)
- Radio Jove kit
- Inspire
- Sky Scan

We can also provide up to five hundred dollars (\$500.00 USD) for an approved radio telescope project.

We have on occasion provided more money based on the merits of the project and the SARA Grant Committee approval.

More information on the grant program can be found at the URL below.

[SARA Student and Teacher Project Grants | Society of Amateur Radio Astronomers \(radio-astronomy.org\)](https://www.radio-astronomy.org/SARA-Student-and-Teacher-Project-Grants)

All that is required is the SARA grant request form be filled out and sent in. If it needs more work for approval, we will work with the student to help ensure their success.

Please pass the word that SARA will fund any legitimate radio telescope project anywhere in the world.

If you have a question, contact me at [crowleytj at hotmail](mailto:crowleytj@hotmail.com) dot com.

Tom Crowley
SARA Grant Program Administrator

Drake's Lounge

Join the SARA community as we discuss the latest astronomy and radio astronomy news. The lounge also provides a forum to share and get advice on your radio astronomy projects from very experienced amateur radio astronomers.

Drake's Lounge is every month on the 3rd Sunday at 2 pm Eastern time. ZOOM email notifications will be sent to all members.

See you there!

2021 SARA Eastern Conference is Virtual Only Again (Hopefully for the last time!)

We are sorry that we will not be able to see each other at Green Bank this year but we are planning to restart the physical conferences next year at the VLA for the Western Conference and Green Bank for the Eastern Conference. The 2021 SARA Eastern virtual conference will be held on Saturday and Sunday to allow for peoples work. The new dates are **July 31 – August 1, 2021**. The schedule will include sessions all day Saturday and half of the day Sunday afternoon to accommodate peoples worship services in the morning.

Conference cost will be \$25 to cover expenses.

Register at: <https://www.radio-astronomy.org/node/318>

Contact Rich Russel (Conference Coordinator) if you would like to present a paper.

drichrussel@netscape.net

Door Prizes for Eastern Conference Registrants

If you are registered and signed into the Eastern Conference, you are eligible to win one of the following door prizes:

- 2 SuperSIDs:
- 2 Scope in a Box Radio Telescopes
- 2 2022 SARA Memberships
- 4 SARA Shirts (S, M, L)
- 1 Signal Generator
- 3 Radio Sky Software Licenses:
- 1 Book: An Introduction to Radio Astronomy

SARA 2021 Eastern Conference Keynote Speaker

Dr. Sander Weinreb

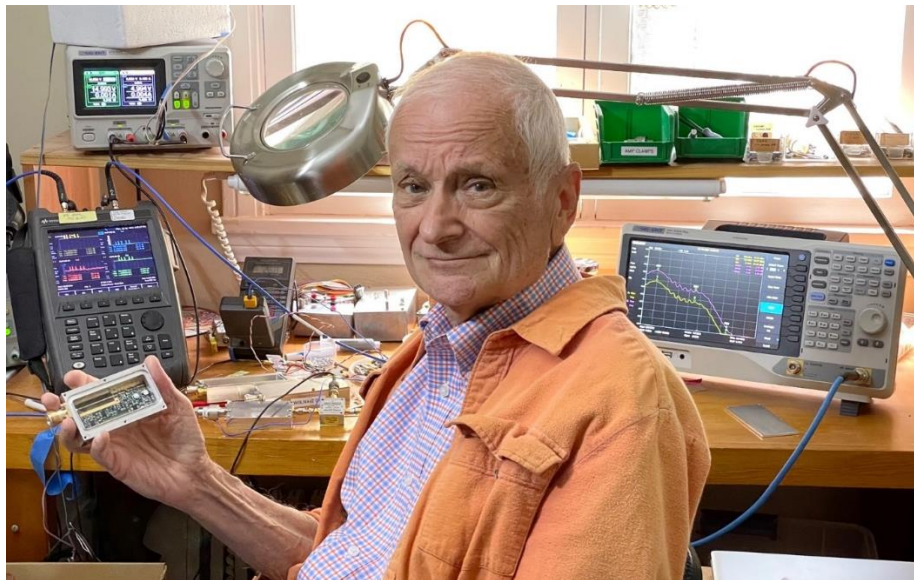
Dr. Weinreb was awarded the 2008 Grote Reber Medal for lifetime innovative contributions to radio astronomy. His pioneering developments of novel techniques and instrumentation over nearly half a century helped to define modern radio astronomy. <http://www.weinreb.org/sandy/index.html>

Presentation

New Directions in Radio Astronomy

In the past we believed that astronomical sources other than planets only varied over times of millions of years. In the recent several years, a whole new world of sources with variations in the time scales of milliseconds to months have become exciting targets for new research. The most widely studied time-variable sources in radio astronomy are the Fast Radio Bursts, FRBs – a ms pulse of radiation in the low microwave range which sweeps in frequency and in most cases does not repeat. The search and characterization for these single-event objects are tantalizing objectives for amateur radio astronomers.

This talk will begin with discussion of FRBs followed by descriptions of new radio astronomy arrays, and new LNAs with noise of the order of 10 K without a need for costly cryogenic cooling.





British Astronomical Association

Supporting amateur astronomers since 1890

Radio Astronomy Section

BAA RA Section Autumn programme 2021

Our meetings are open to all. Once you are registered on the RA Section email list the Zoom link will be sent out to you before the meeting. If you are not on the email list, please request registration from Paul Hearn (paul@hearn.org.uk).

All recordings will be posted on our BAA YouTube channel. <https://www.youtube.com/user/britishastronomical/playlists>

Sep 3 rd .	19:30 BST (18:30 UTC)	Whit Reeve HAARP High-Frequency Active Auroral Research. Exploring the obscurities of the upper atmosphere.
Sep 18 th	GNU Training Seminar 15:00 – 18:00 BST (14:00 – 17:00 UTC)	Marcus Leech, Science Radio Laboratories, Inc. Unpacking the mysteries of GNU Radio A complement to our ‘Python for Radio Astronomers’ course.
Oct 1 st	19:30 BST (18:30 UTC)	Dr. Gemma Richardson, Space Weather scientist in the British Geological Survey geomagnetism team. The changing environmental conditions in near-Earth space.
Oct 16 th	10:00 – 17:00 BST (09:00 – 16:00 UTC)	BAA RAG21 day conference. Keynote speakers: Prof Ian McHardy, Prof Ian McHardy School of Physics & Astronomy, University of Southampton. The mysteries of X-ray Cosmology. Dr Spencer Axani MIT CosmicWatch – the counting of muons. Other speakers to be announced – watch this space. Conference organizer – Paul Hyde
Nov 5 th	19:30 GMT (19:30 UTC)	Prof Lyndsay Fletcher Glasgow University <i>School of Physics and Astronomy</i> The Physics, Analysis and Imaging of Solar flares. A perspective for Radio Astronomers
Dec 3 rd	19:30 GMT (19:30 UTC)	‘SARA presents...’ Pablo Lewin Building a Radio Telescope for HI observations Dr Richard Russel Deep Space Exploration Society (DSES) ‘Pulsars for Galactic Navigation’
Dec 10 th	19:30 GMT (19:30 UTC)	Christmas Lecture Prof. Anna Scaife. Professor of Radio Astronomy at the University of Manchester and Head of the Jodrell Bank Centre for Astrophysics ‘Jodrell Bank, the cold war and the space race’



For Your Radio Astronomy Bookshelf

(Prices in USD)

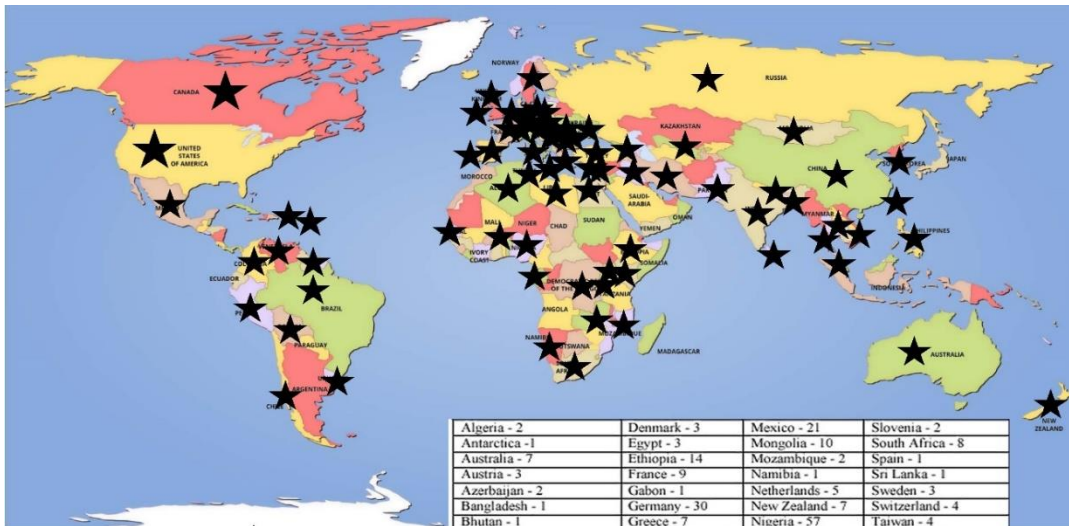
- ⚙ **Statistics, Data Mining & Machine Learning in Astronomy: A Practical Python Guide for the Analysis of Survey Data**, Z. Ivezić, A.J. Connolly, J. T. Vanderplas, A. Gray; (Princeton Series in Modern Observational Astronomy Book 8), 2020, Princeton University Press, \$68.95 (hardcover)
- ⚙ **A Student's Guide to the Mathematics of Astronomy**; D. Fleisch, J. Kregenow; Cambridge University Press, 2013, \$21.00



SuperSID
*Collaboration of Society
of Amateur Radio
Astronomers and
Stanford Solar Center*



- ✓ Stanford provides data hosting, database programming, and maintains the SuperSID website
- ✓ Society of Amateur Radio Astronomers (SARA) sells the SuperSID monitors for 48 USD to amateur radio astronomers and the funds are then used to support free distribution to students all over the world (image below as of Fall 2017)
- ✓
- ✓ Jonathan Pettingale at SARA is responsible for building and shipping the SuperSID monitor kits: SuperSID@radio-astronomy.org
- ✓ SuperSID kits may be ordered through the SARA SuperSID webpage: <http://radio-astronomy.org/node/210>
- ✓ Questions about the SuperSID project may be directed to Steve Berl at Stanford: steveberl@gmail.com
- ✓ Jaap Akkerhuis at Stanford is responsible for the SuperSID software and SARA has provided financial support for his efforts
- ✓ SuperSID website hosted by Stanford: <http://solar-center.stanford.edu/SID/sidmonitor/>
- ✓ SuperSID database: <http://sid.stanford.edu/database-browser/>
- ✓ The data is searchable by time, station, date, and multiple plots may be placed on the same graph for comparison.



★
**SID Monitor
Distribution**
1078 instruments
82 countries
7 continents

Algeria - 2	Denmark - 3	Mexico - 21	Slovenia - 2
Antarctica - 1	Egypt - 3	Mongolia - 10	South Africa - 8
Australia - 7	Ethiopia - 14	Mozambique - 2	Spain - 1
Austria - 3	France - 9	Namibia - 1	Sri Lanka - 1
Azerbaijan - 2	Gabon - 1	Netherlands - 5	Sweden - 3
Bangladesh - 1	Germany - 30	New Zealand - 7	Switzerland - 4
Bhutan - 1	Greece - 7	Nigeria - 57	Taiwan - 4
Bolivia - 1	Guyana - 1	Pakistan - 4	Thailand - 5
Bosnia-Herzegovina - 2	Hungary - 1	Peru - 10	Tunisia - 9
Brazil - 11	India - 33	Philippines - 3	Turkey - 2
British Virgin Islands - 1	Indonesia - 2	Poland - 2	Uganda - 5
Bulgaria - 2	Iran - 4	Portugal - 3	UK - 32
Burkina Faso - 1	Iraq - 1	Rep of Congo - 3	Uruguay - 9
Canada - 33	Ireland - 9	Romania - 4	US Virgin Islands - 2
Chile - 1	Italy - 42	Russia - 3	USA - 491
China - 38	Kenya - 23	Rwanda - 1	Uzbekistan - 2
Columbia - 9	Korea (South) - 2	S Africa - 4	Venezuela - 2
Croatia - 7	Lebanon - 11	Senegal - 1	Vietnam - 1
Cyprus - 1	Libya - 1	Serbia - 1	Zambia - 2
Czech Republic - 1	Malaysia - 19	Singapore - 3	
D Rep of Congo - 4	Malta - 1	Slovak Repub - 2	

For official use only
 Monitor assigned: _____
 Site name: _____
 Country: _____

SuperSID Space Weather Monitor Request Form

<i>Your information here</i>				
Name of site/school (if an institution):				
Choose a site name: (3-6 characters) No Spaces				
Primary contact person:				
Email:				
Phone(s):				
Primary Address:	Name School or Business Street Street City Country State/Province Postal Code			
Shipping address, if different:	Name School or Business Street Street City Country State/Province Postal Code			
Shipping phone number:	<table border="1" style="width: 100%; border-collapse: collapse;"> <tr> <td style="width: 33%; height: 20px;"></td> <td style="width: 33%; height: 20px;"></td> <td style="width: 33%; height: 20px;"></td> </tr> </table>			
Latitude & longitude of site:	Latitude: _____ Longitude: _____			

I understand that neither Stanford nor the Society of Amateur Radio Astronomers is responsible for accidents or injuries related to monitor use. I will assure that a surge protector and other lightning protection devices are installed if necessary.

Signature: _____ **Date:** _____

I will need:

<i>What</i>	<i>Cost</i>	<i>How many?</i>
SuperSID distribution USB Power	\$48 (assembled)	
USB Sound card 96 kHz sample rate (or provide this yourself)	\$40 (optional)	
Antenna wire (120 meters) (or you can provide this yourself)	\$23 (optional) with connectors attached and tested	
RG 58 Coax Cable (9 meters) (or provide this yourself)	\$14 (optional) with connectors attached and tested	
Shipping	US \$12 Canada & Mexico \$40 all other \$60	
	TOTAL	\$

_____ I have included a \$_____ check (payable to SARA)

_____ I will make payment thru www.paypal.com to treas@radio-astronomy.org

or

_____ If you are a Minority-serving institution, in a Developing or economically deprived nation, and/or you are using the monitor with students for educational purposes, you may qualify for obtaining a monitor at reduced or no cost. Check here if you wish to apply for this designation. Then tell us how you want to use the SuperSID monitor. Include type of site, number of students involved, whether public or private school, grade levels, etc. and describe your program. The goal of the SuperSID project is to provide as many students with systems as possible. If you are able to pay for a system, even if you qualify for a free one, please do so and help support our goal.

For more details on the Space Weather Monitor project, see: <http://sid.stanford.edu>

To set up a SuperSID monitor you will need:

1. Access to power and an antenna location that is relatively free of electric interference (could be indoors or out)
2. A **PC**** with the following minimal specifications:
 - A sound card that can record (sample) up to 96 kHz, or a USB port to connect such a sound card (for North and South America)
 - All other countries can use AC97 sound card with 48 kHz record (sample) rate. Most computers made after 1997 will have AC97.
 - Windows 2000 or more recent operating system
 - 1 GHz Processer with 128 mb RAM
 - Ethernet connection & internet browser (desirable, but not required)
 - Standard keyboard, mouse, monitor, etc.
3. An inexpensive antenna that you build yourself. You'll need about 120 meters (400 feet) of **insulated** wire. Solid wire is easier to wind than stranded. Magnet wire will work but be more fragile. You can use anything from #18 to #26 size wire. The antenna frame can be made of wood, PVC pipe, or similar materials. We'll provide instructions. You can purchase the wire from us or obtain your own.
4. RG58 coax cable with a BNC connector at one end to run from the antenna to the SuperSID receiver. 9 meters is recommended, but the length will depend on where you place the antenna. You can purchase the coax from us or obtain your own.
5. Surge protector and other protection against a lightning strike

Return this form to: SuperSID@radio-astronomy.org

or mail to: SARA
Brian O'Rourke, SARA Treasurer
337 Meadow Ridge Rd,
Troy, VA 22974-3256



Founded in 1890

The British Astronomical Association

A company limited by guarantee

Registered Charity No. 210769

Burlington House, Piccadilly, London, W1J 0DU

Telephone: 020 7734 4145

Fax No.: 020 7439 4629

Email: office@britastro.org

Website: www.britastro.org



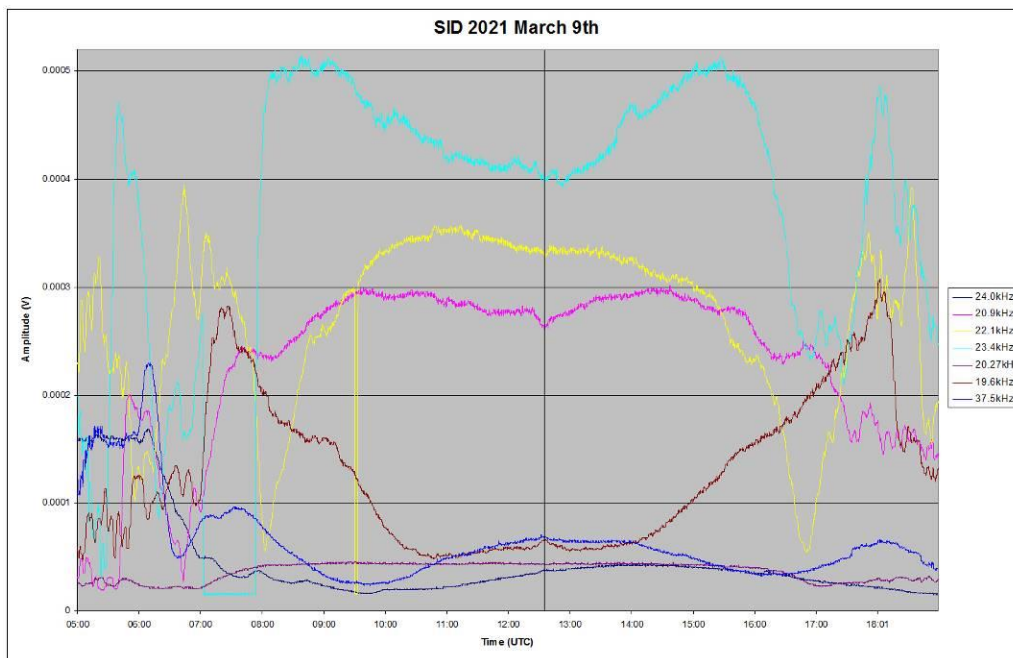
Please send all reports and observations to jacook@jacook.plus.com

John Cook's VLF Report

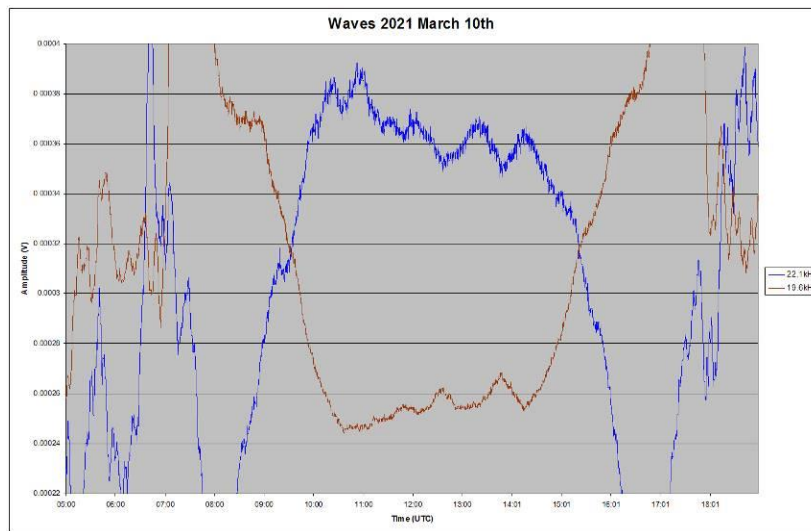
BAA Radio Astronomy Section

2021 MARCH

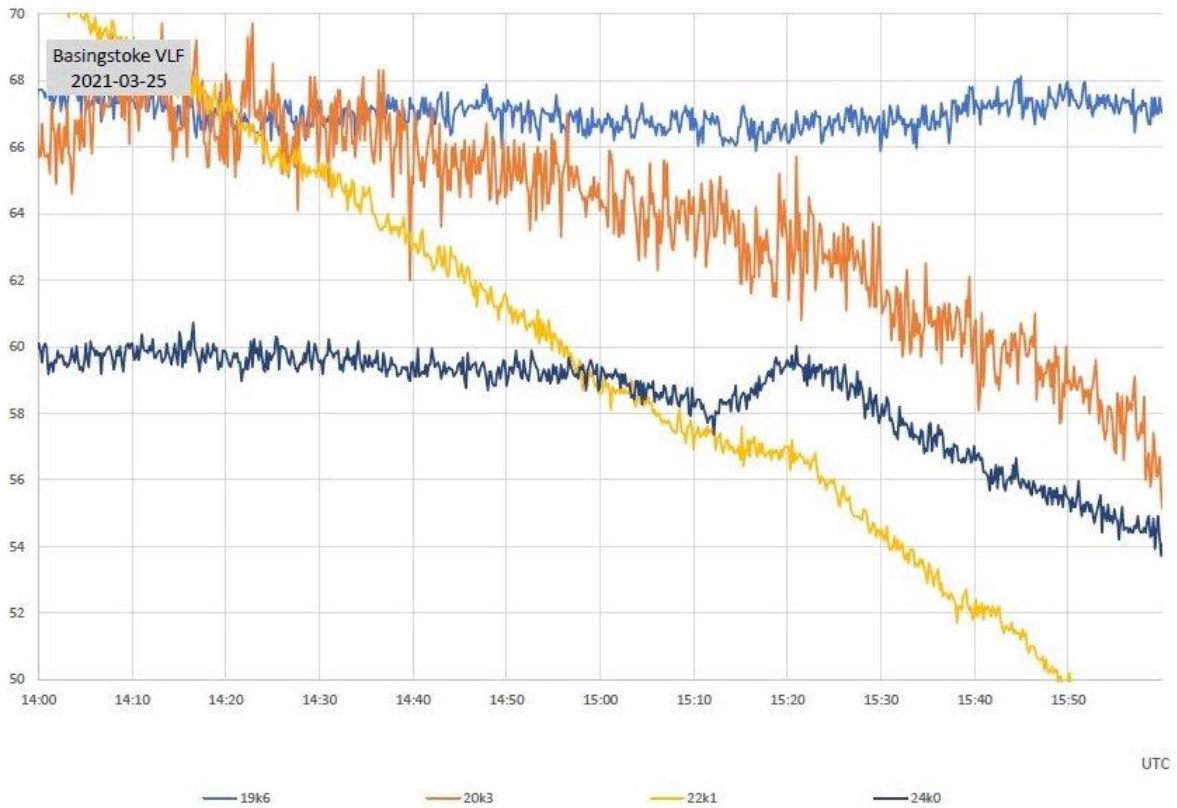
There was a general increase in sunspot numbers in March, with numerous small B-class flares shown in the space weather reports. There were just a couple of flares reaching C-class, the C1.6 recorded on the 9th being the strongest of the month and well timed for European observers.



This recording by Mark Edwards shows distinctive SIDs at 20.9 kHz (pink trace) and 19.6 kHz (brown trace). Some of the other signals show less distinct SIDs for this event. Mark also recorded ionospheric waves on the 22.1 kHz and 19.6 kHz signals. These were recorded on March 10th, the two frequencies being very close mirror images. There is no obvious cause for these, but we have recorded similar effects in the past.

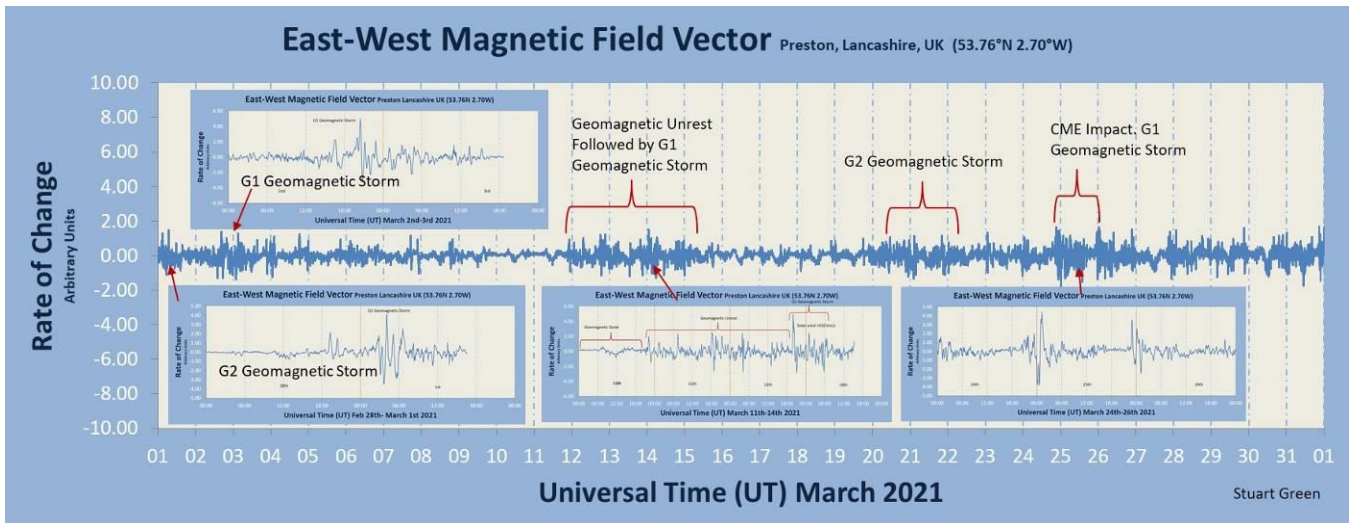


The B8.3 flare on the 25th shows well in this recording by Paul Hyde on the longer path at 24 kHz.

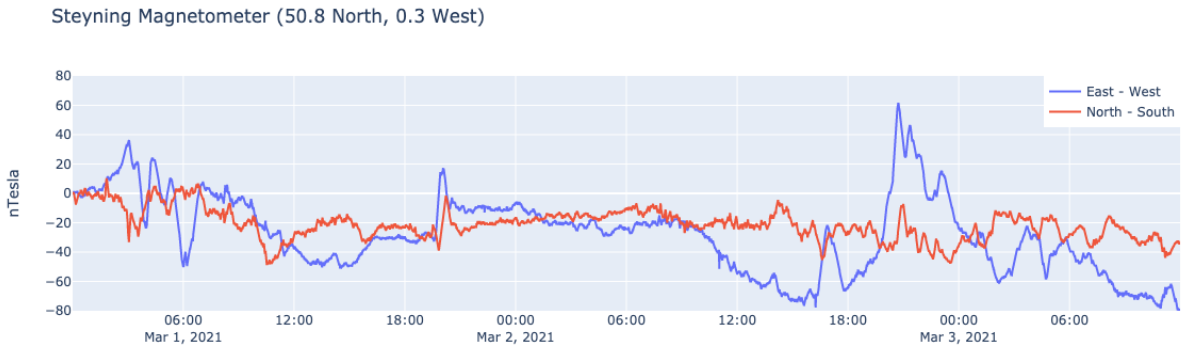


MAGNETIC OBSERVATIONS

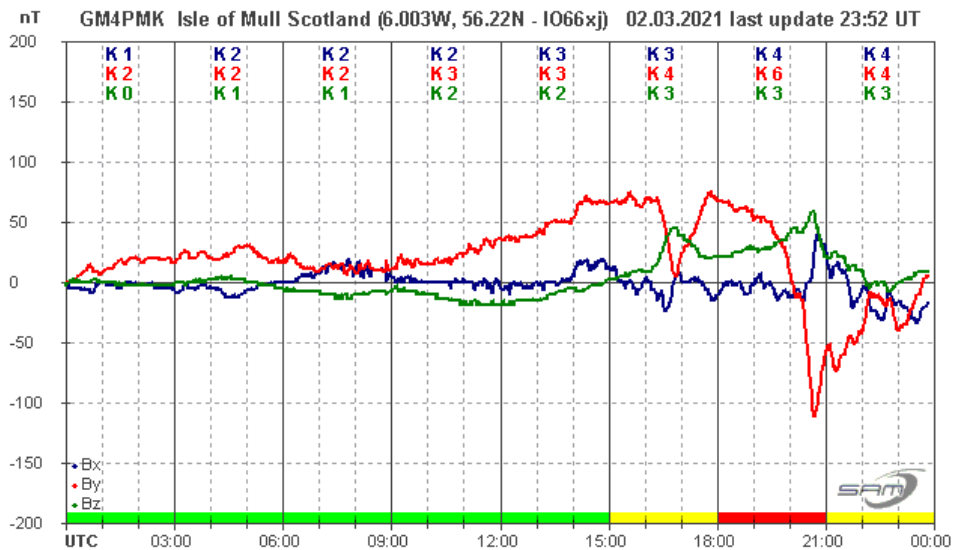
There was also a lot of magnetic activity in March, mostly from a complex coronal hole over the Sun's south polar region with extensions running northwards. Stuart Green's chart shows the Month's activity:



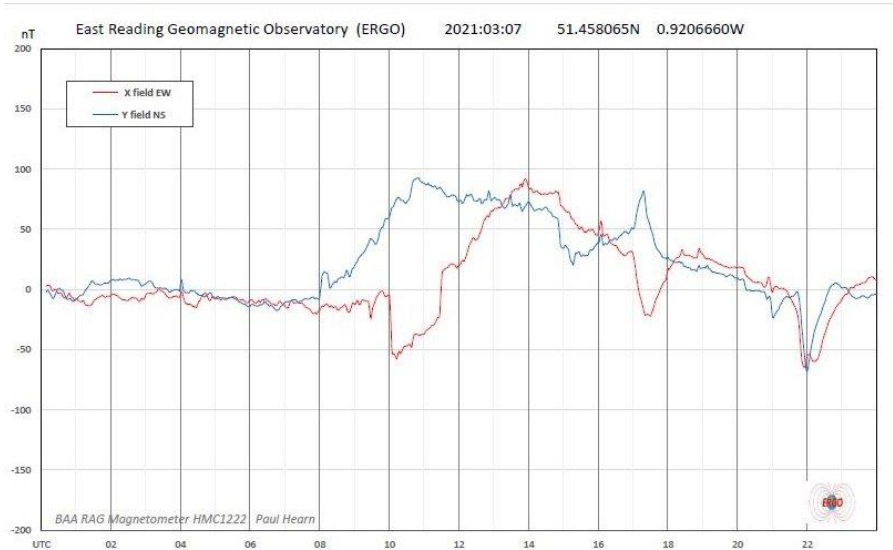
The south polar hole has been present for several months now, with some strong activity shown in late February on the previous rotation. Nick Quinn recorded its effects over March 1st to 3rd:



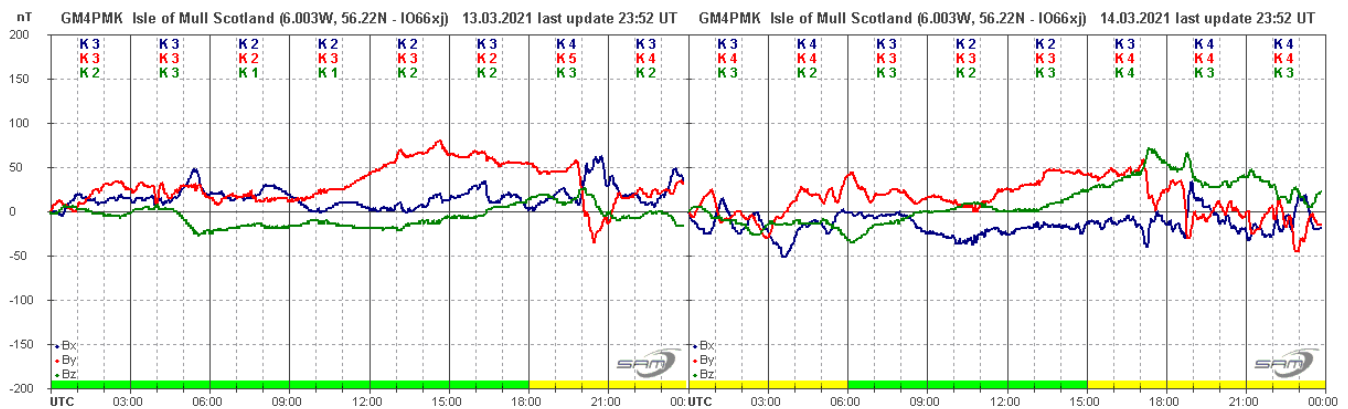
A period of strong disturbance can be seen in the evening of the 2nd with a large variation in the east-west component. Nick is located near the south coast, and so a comparison with the Mull magnetometer of Roger Blackwell, nearly 6 degrees further north, is of interest:



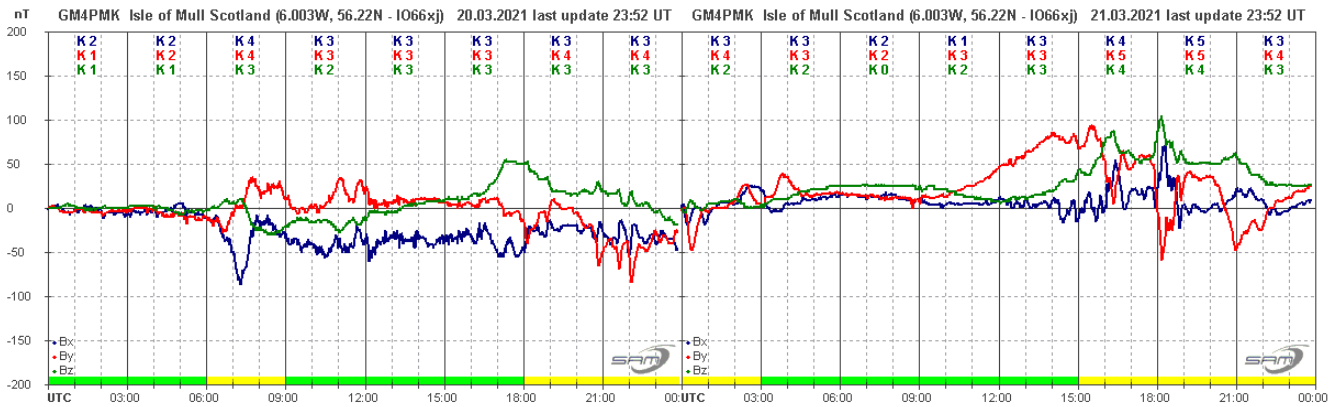
The By component of his 3-axis sensor matches very well the (inverted) east-west signal in Nick's recording. The peak-to-peak variation in Mull is about 20nT greater than in the south.



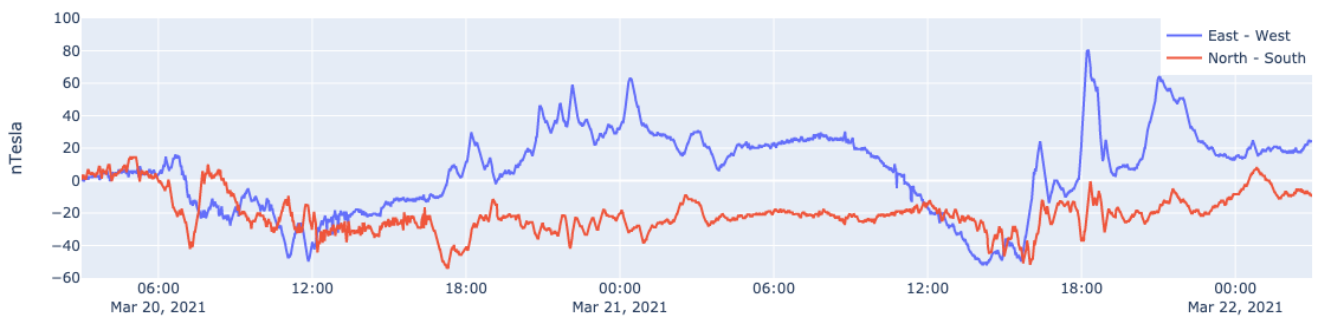
This recording by Paul Hearn shows a more moderate disturbance on March 7th, resulting from another coronal hole high speed wind. This was the least turbulent of the month, fading out on the 8th. The south polar hole became effective again in the afternoon of the 12th, with some strong disturbances seen on the 13th and 14th, shown here in the recording by Roger Blackwell:



A combination of minor CME's and the high speed wind produced further disturbances towards the end of March. Roger's recordings show some of this activity on the 20th and 21st:

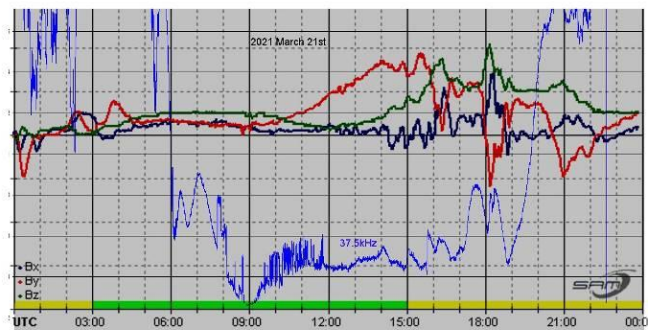
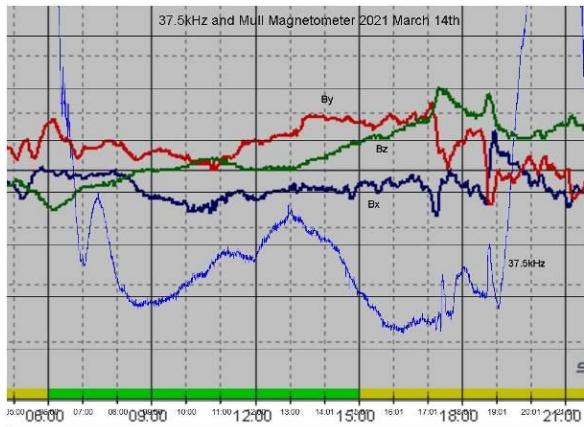


Steinyng Magnetometer (50.8 North, 0.3 West)



Nick Quinn's recording over the same period shows very similar disturbances, again at slightly lower magnitude. Mild activity continued on the 24th and 25th, fading out from the 26th to the end of the month.

Mark Edwards noted these magnetic disturbances on the 37.5kHz signal from Grindavik, Iceland, particularly on the 14th and 21st, shown in these charts:



Mark has overlaid his VLF recording on Roger Blackwell's magnetometer charts. The effects are again most noticeable in the late afternoon and evening, running into the VLF sunset around 19:00 UT. The recording from the 21st also shows some disturbance to the 37.5 kHz signal from 06:00 UT, followed by interference from 10 to 12 UT. The interference was from some broadband noise around the signal frequency. This recording also covers the period of volcanic activity in Iceland, in a region just to the north of the transmitter site. Luckily there were only small local lava flows from the volcano, with no threats to Grindavik itself.

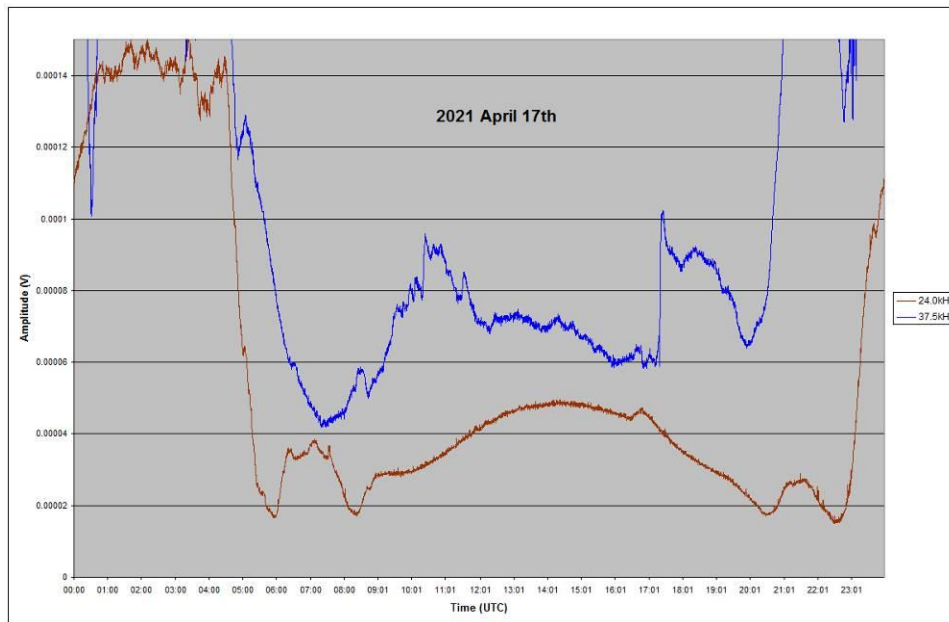
Magnetic observations received from Roger Blackwell, Colin Clements, Stuart Green, Andrew Thomas, Nick Quinn and John Cook.

The Zoom meetings organised by Paul Hearn have been a great success so far, with several more programmed over the next few weeks. Full details of the programme can be found on the BAA website, along with the other BAA meetings. If you are interested in joining any of these, please follow the notes given in the listing.

BAA Radio Astronomy Section

2021 APRIL

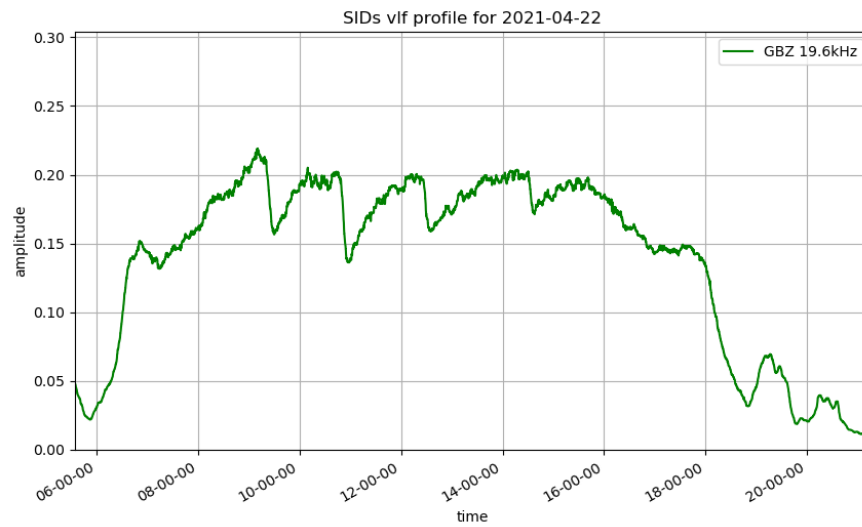
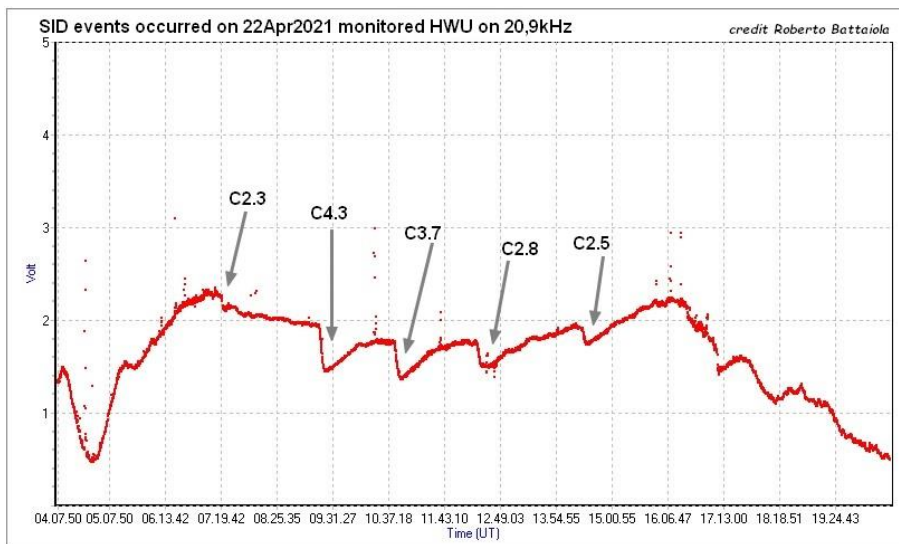
Solar activity increased in April with the appearance of several new sunspot regions. Most of these were either quiescent or produced only smaller B-class flares, but there was a small burst of C-class activity later in the month with eight flares being recorded as SIDs along with one B-class event. These events coincided with an extended period when both 23.4 kHz and 22.1 kHz signals were off-air. Luckily, we have a good range of signals covered by our observers, and so all of the best events were recorded.



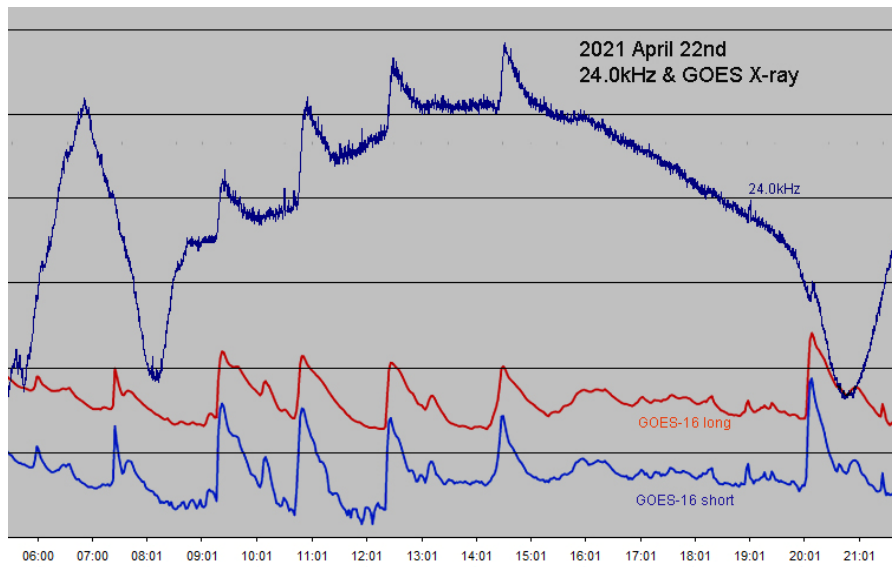
The B9.7 flare on the 17th was quite late in the afternoon, but does show well on the 24 kHz signal (brown trace) in this recording by Mark Edwards. A small 'kink' is also visible at 37.5 kHz (blue) just before the large magnetic induced transient. This was a very slow flare, lasting well into the sunset period of European signals. Mark noted that the peak timing listed in the SWPC bulletin was at 17:17 UT, much later than the peak of the SID. Looking at the X-ray data shows that the shorter wavelength signal peaked well before the longer wavelength, much nearer to our timing. The shorter wavelength also showed a much faster decay time.

The C1.9 flare on the 20th is also odd in that the SWPC bulletin lists the peak at 11:45 UT, compared with our SID observations around 12:15. The SID was only recorded by two observers, but their timings are very similar. Looking at the X-ray plot on the polarlicht website shows a flare matching our timings, starting well after the 11:45 peak listed. There is a few minutes delay between the short and long wavelength peaks, but neither match the 11:45 timing.

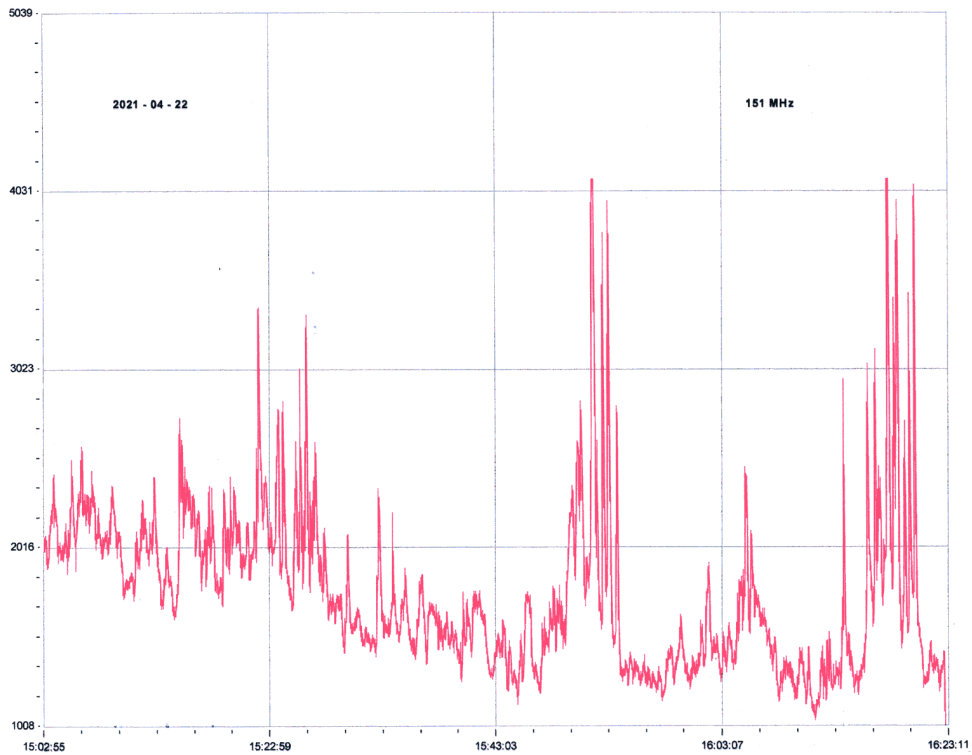
The most active day recorded so far in 2021 was on the 22nd, with a total of seven SIDs recorded, all of C-class. Roberto Battaiola shows the first five in his recording at 20.9 kHz:



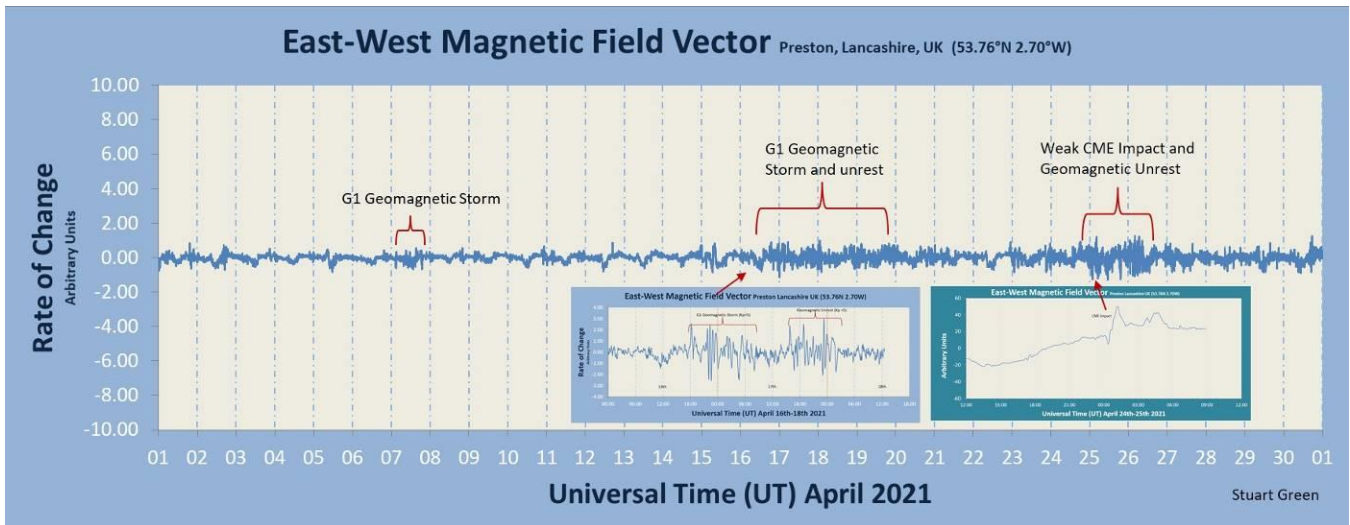
This recording by John Prescott at 19.6 kHz is also very clear, although with a later sunrise time the earlier C2.3 flare is not so obvious.



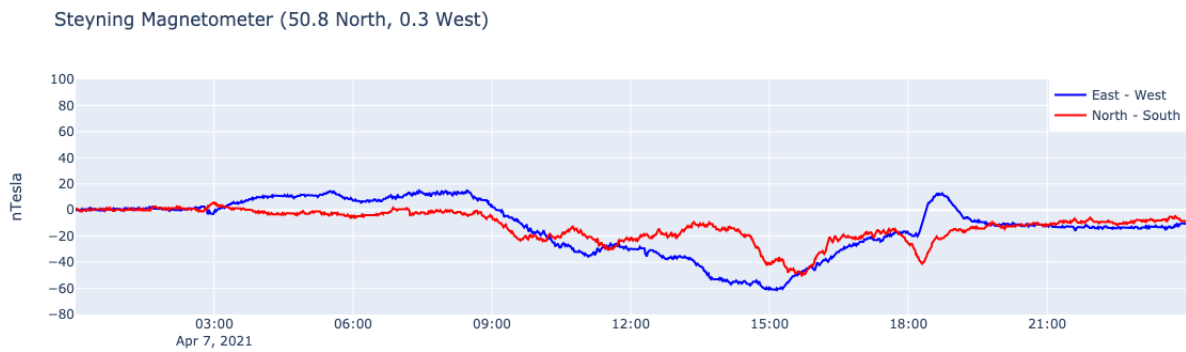
Mark has added the GOES X-ray data to his recording that also includes the later C8.5 flare caught on the 24 kHz signal. Colin Clements noted several radio bursts at 151 MHz, shown below. They are all following the C2.5 flare, although a connection is not clear. They were not detected at 408 MHz.



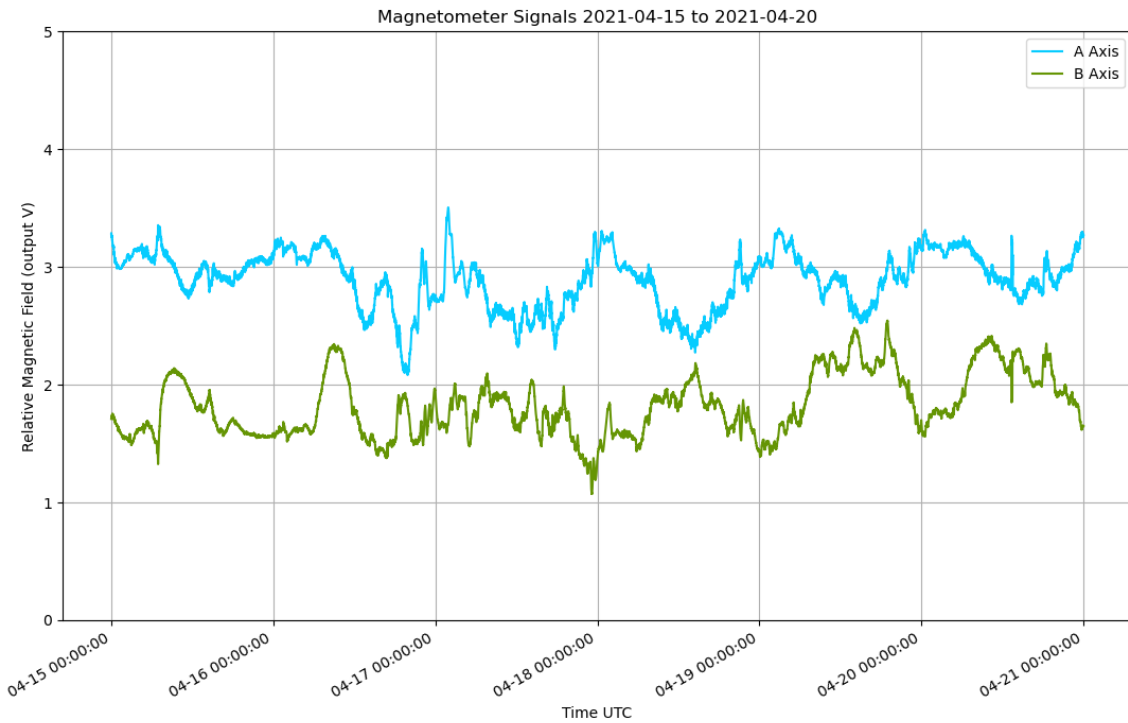
MAGNETIC OBSERVATIONS



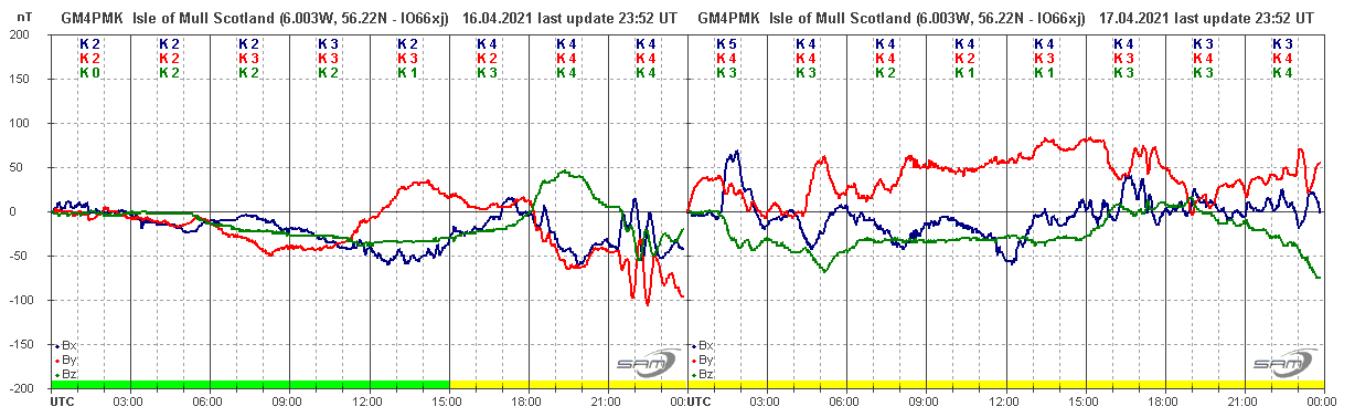
Magnetic disturbances in April were all very mild, shown in the month’s summary by Stuart Green. The coronal holes seen over previous months seem to have broken up, resulting in lower solar wind speeds. There were a number of CMEs associated with the increased flare activity, they were mostly not aimed towards Earth. A small CME from March 31st arrived on April 5th, with some minor disturbance on the 7th. Although classified as a G1 geomagnetic storm, its effects were very mild as shown in the recording by Nick Quinn:



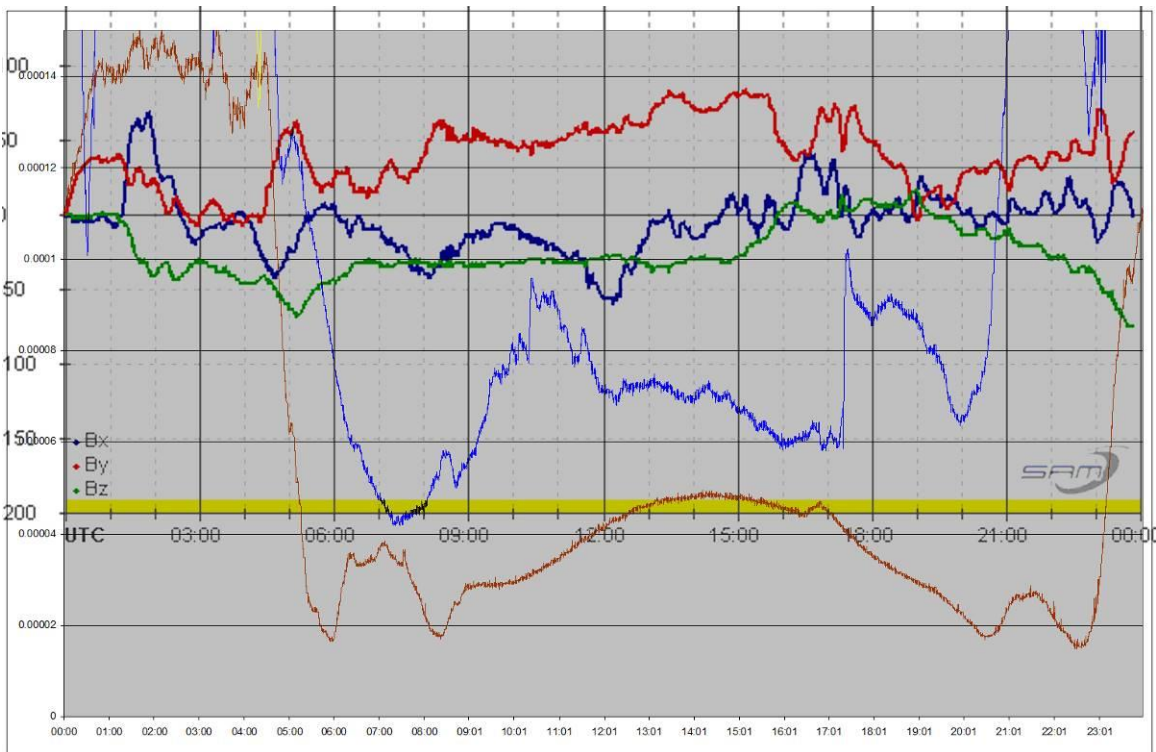
A combination of CMEs and coronal holes produced several days of activity starting on the 16th, shown in this recording by Andrew Thomas:



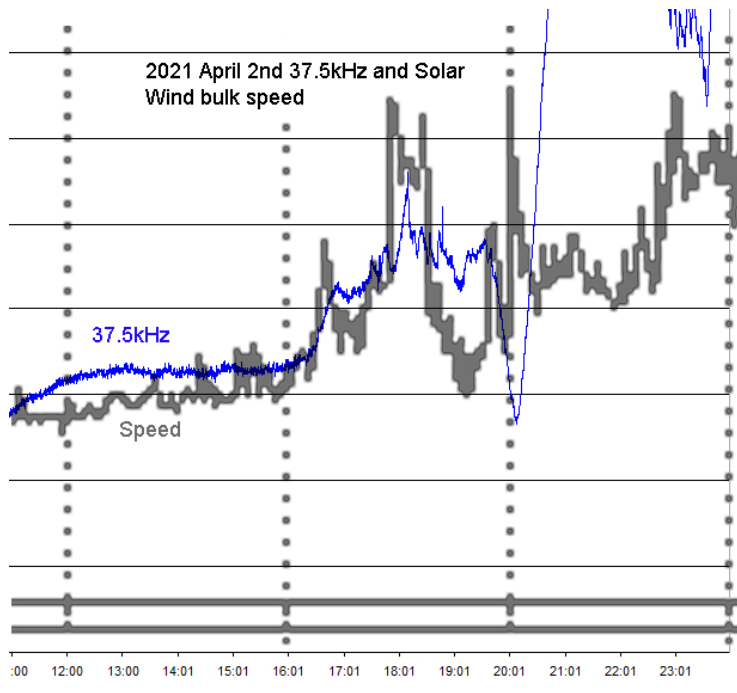
Rapid variations of 100nT were recorded in the evening of the 16th, continuing all day on the 17th as shown in Roger Blackwell's recording:



The discontinuity at midnight is due a reset of the sensor.

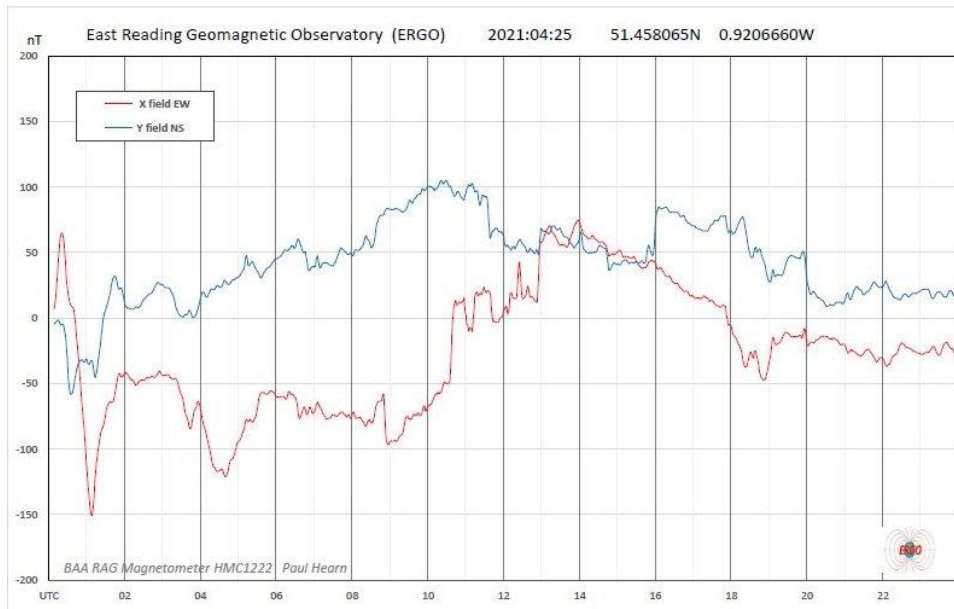


Mark Edwards has overlaid Roger's magnetic data from the 17th onto the 37.5 kHz (blue) and 24 kHz (brown) signals, showing the effects that the magnetic disturbance has had on the VLF signal. Mark also has an interesting observation from April 2nd:



The 37.5 kHz signal is shown overlaid on the Soho solar wind monitor signal, showing a possible link between the solar wind speed and the VLF signal in the hours before the sunset effect takes over. There were no matching magnetic disturbances at that time. This is an interesting connection, and open to debate.

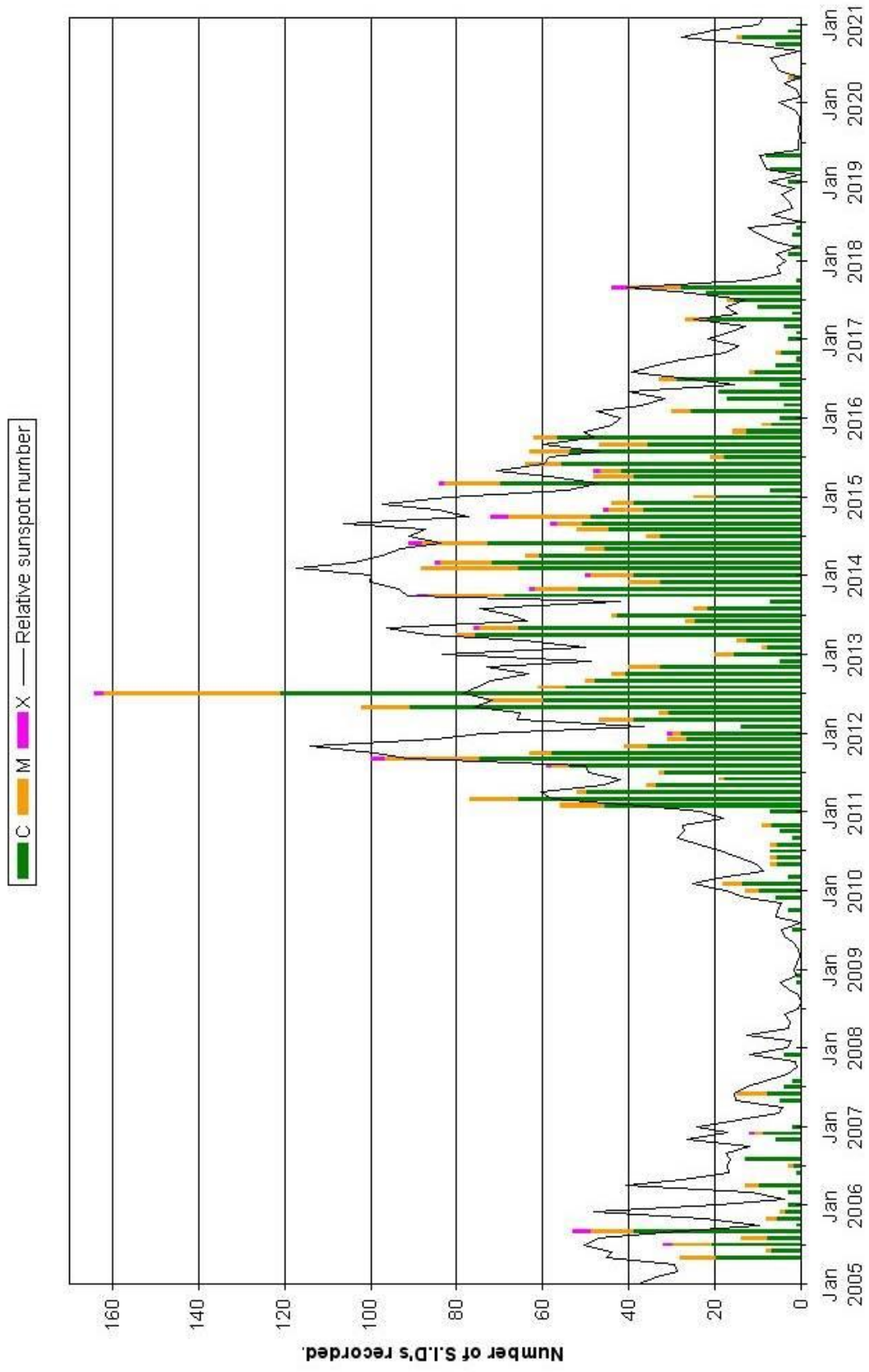
A CME recorded in Soho data from the 22nd arrived late in the evening of the 24th, close to midnight, with a period of stronger magnetic disturbance recorded on the 25th.



This recording by Paul Hearn shows a short period of strong activity up to 02UT, followed by a milder disturbance over the next few hours. Unfortunately, local interference has affected the recording from 12 to 16 UT, but the CME can still be seen through the rest of the day. Disturbance continued during the morning of the 26th, gently fading out.

Magnetic observations received from Roger Blackwell, Colin Clements, Paul Hearn, Andrew Thomas, Nick Quinn and John Cook.

VLF flare activity 2005/21



ROTATION	KEY:	DISTURBED.	ACTIVE	SFE	B, C, M, X = FLARE MAGNITUDE.	Synodic rotation start (carrington's)
2529	F	26	27 28 29 30 31	2019 January 1 2	3 4 5 6 7 8 9 10 11 12 13 14 15 16 17	2213 18 19 20 21
2530	F	22	23 24 25 26 CB	2019 February 27 28 29 C	30 31 1 2 3 4 5 6 7 8 9 10 11 12	2214 13 14 15 16 17
2531	F	18 19 20 21 22 23 24 25 26	27 28	2019 March 1 2	3 4 5 6 7 8 9 10 11 12	2215 13 14 15 16
2532	F	17 18 19 20 C	21 22 23 CCC	2019 April 24 25 26 27 CCCB	28 29 30 31 1 2 3 4 5 6 7 8	2216 9 10 11 12 B
2533	F	13 14 15 16 17 18 19 20 B	21 22 23 24	2019 May 25 26 27 28 29 30	1 2 3 4 5 6 7 8 9 10 11 12	2217 13 14 15 16 CCCC
2534	F	10 11 12 13 14 15 16 17 18 19 20 21 22 23 24 25 26 27 28 29 30 31	2019 June 1 2	2218 3 4 5		
2535	F	6 7 8 9 10 11 12 13 14 15 16 17 18 19 20 21 22 23 24 25 26 27 28 29	2019 July 30	2219 1 2		
2536	F	3 4 5 6 7 8 9 10 11 12 13 14 15 16 17 18 19 20 21 22 23 24 25 26	2019 August 27 28 29	2220		
2537	F	30 31 1 2 3 4 5 6 7 8 9 10 11 12 13 14 15 16 17 18 19 20 21 22	2019 September 23 24 25	2221		
2538	F	26 27 28 29 30 31 1 2 3 4 5 6 7 8 9 10 11 12 13 14 15 16 17 18	2019 October 19 20 21	2222		
2539	F	22 23 24 25 26 27 28 29 30 1 2 3 4 5 6 7 8 9 10 11 12 13 14 15 16	2019 November 17 18	2223		
2540	F	19 20 21 22 23 24 25 26 27 28 29 30 31 1 2 3 4 5 6 7 8 9 10 11 12	2019 December 13 14	2224		
2541	F	15 16 17 18 19 20 21 22 23 24 25 26 27 28 29 30 1 2 3 4 5 6 7 8 9	2020 January 10 11	2225		
2542	F	12 13 14 15 16 17 18 19 20 21 22 23 24 25 26 27 28 29 30 31 1 2 3 4 5 6 7	2020 February 28 29	2226		
2543	F	8 9 10 11 12 13 14 15 16 17 18 19 20 21 22 23 24 25 26 27 28 29 30 31 1 2 3	2020 March 26 27 28	2227		
2544	F	4 5 6 7 8 9 10 11 12 13 14 15 16 17 18 19 20 21 22 23 24 25 26 27 28 29 1	2020 April 22 23 24	2228		
2545	F	2020 March 2 3 4 5 6 7 8 9 10 11 12 13 14 15 16 17 18 19 20 21 22 23 24 25 26 27 28	2020 May 22 23 24	2229		
2546	F	29 30 31 1 2 3 4 5 6 7 8 9 10 11 12 13 14 15 16 17 18 19 20 21 22 23 24	2020 June 22 23 24			
2547	F	2230 25 26 27 28 29 30 1 2 3 4 5 6 7 8 9 10 11 12 13 14 15 16 17 18 19 20 21	2020 July 22 23 24			
2548	F	2231 22 23 24 25 26 27 28 29 30 31 1 2 3 4 5 6 7 8 9 10 11 12 13 14 15 16 17	2020 August 22 23 24			
2549	F	2032 18 19 20 21 22 23 24 25 26 27 28 29 30 1 2 3 4 5 6 7 8 9 10 11 12 13 14	2020 September 22 23 24			
2550	F	2033 15 16 17 18 19 20 21 22 23 24 25 26 27 28 29 30 31 1 2 3 4 5 6 7 8 9 10	2020 October 22 23 24			
2551	F	2234 11 12 13 14 15 16 17 18 19 20 21 22 23 24 25 26 27 28 29 30 31 1 2 3 4 5 6	2020 November 22 23 24			
2552	F	2235 7 8 9 10 11 12 13 14 15 16 17 18 19 20 21 22 23 24 25 26 27 28 29 30 1 2 3	2020 December 22 23 24			
2553	F	2236 4 5 6 7 8 9 10 11 12 13 14 15 16 17 18 19 20 21 22 23 24 25 26 27 28 29 30	2021 January 22 23 24			
2554	F	2237 31 1 2 3 4 5 6 7 8 9 10 11 12 13 14 15 16 17 18 19 20 21 22 23 24 25 26	2021 February 22 23 24			
2555	F	2238 27 28 29 30 1 2 3 4 5 6 7 8 9 10 11 12 13 14 15 16 17 18 19 20 21 22 23	2021 March 22 23 24			
2556	F	2239 24 25 26 27 28 29 30 31 1 2 3 4 5 6 7 8 9 10 11 12 13 14 15 16 17 18 19	2021 April 22 23 24			
2557	F	2240 20 21 22 23 24 25 26 27 28 29 30 31 1 2 3 4 5 6 7 8 9 10 11 12 13 14 15	2021 May 22 23 24			
2558	F	2241 16 17 18 19 20 21 22 23 24 25 26 27 28 1 2 3 4 5 6 7 8 9 10 11 12 13 14	2021 June 22 23 24			

News: (May-Jun 2021)

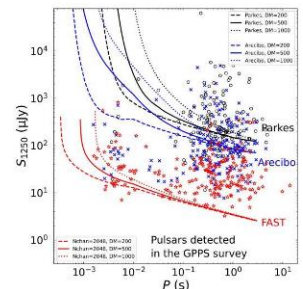


Quanta magazine ~ *How Radio Astronomy Reveals the Universe*: <https://www.quantamagazine.org/how-radio-astronomy-reveals-the-universe-20210413/>

The Astronomer's Telegram ~ *Extremely bright pulse from FRB20201124A observed with the 25-m Stockert Radio Telescope*: <https://www.astronomerstelegam.org/?read=14556>

Phys.org ~

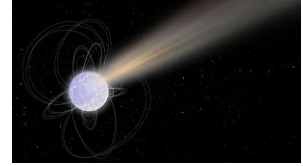
- ⚙ *On the pulse of pulsars and polar light*: <https://phys.org/news/2021-04-pulse-pulsars-polar.html>
- ⚙ *Video: Mapping the radio sky*: <https://phys.org/news/2021-04-video-radio-sky.html>
- ⚙ *Fast radio bursts shown to include lower frequency radio waves than previously detected*: <https://phys.org/news/2021-04-fast-radio-shown-frequency-previously.html>
- ⚙ *Outback radio telescope discovers dense, spinning, dead star*: <https://phys.org/news/2021-04-outback-radio-telescope-dense-dead.html>
- ⚙ *Radio astronomers discover 8 new millisecond pulsars*: <https://phys.org/news/2021-04-radio-astronomers-millisecond-pulsars.html>
- ⚙ *Hot and cold space radio testing*: <https://phys.org/news/2021-04-hot-cold-space-radio.html>
- ⚙ *Scientists invent method for predicting solar radio flux for two years ahead*: <https://phys.org/news/2021-05-scientists-method-solar-radio-flux.html>
- ⚙ *New FAST discoveries shed light on pulsars*: <https://phys.org/news/2021-05-fast-discoveries-pulsars.html>
- ⚙ *Hubble tracks down fast radio bursts to galaxies' spiral arms*: <https://phys.org/news/2021-05-hubble-tracks-fast-radio-galaxies.html>



Hey, Mac, did you mean to say 'crop circle'? : Phys.org ~ *Astronomers discover a new extragalactic circular radio source*: <https://phys.org/news/2021-05-astronomers-extragalactic-circular-radio-source.html>

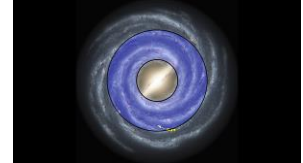
Jet Propulsion Laboratory ~ Lunar Crater Radio Telescope: Illuminating the Cosmic Dark Ages:
<https://www.jpl.nasa.gov/news/lunar-crater-radio-telescope-illuminating-the-cosmic-dark-ages>

Hey, Mac, here we go again: ScienceNews ~ *Fast radio bursts could help solve the mystery of the universe's expansion:* <https://www.sciencenews.org/article/fast-radio-bursts-universe-expansion-hubble-constant>

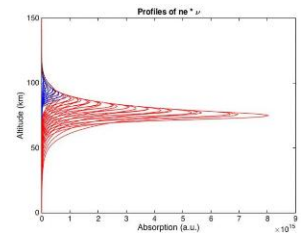


Hey, Mac, huh?: Phys.org ~ *How scientists are tuning in to the universe, man:*
<https://phys.org/news/2021-05-scientists-tuning-universe.html>

Universe Today ~ *Breakthrough Listen Searched for Signals From Intelligent Civilizations Near the Center of the Milky Way:*
<https://www.universetoday.com/151063/breakthrough-listen-searched-for-signals-from-intelligent-civilizations-near-the-center-of-the-milky-way/>



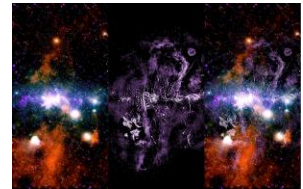
Universe Today ~ *60 Years Later, is it Time to Update the Drake Equation?:*
<https://www.universetoday.com/151174/60-years-later-is-it-time-to-update-the-drake-equation/>



Phys.org ~ *NASA rocket mission studying escaping radio waves:*
<https://phys.org/news/2021-05-nasa-rocket-mission-radio.html>

Phys.org ~ *Gravitational wave search no hum drum hunt:*
<https://phys.org/news/2021-05-gravitational.html>

Universe Today ~ *New Mosaic Shows the Galactic Core From Opposite Sides of the Electromagnetic Spectrum:* <https://www.universetoday.com/151339/new-mosaic-shows-the-galactic-core-from-opposite-sides-of-the-electromagnetic-spectrum/>



Technical Knowledge & Education: (May-Jun 2021)

Digi-Key ~ *Transistor Basics: NPN & PNP Using 2N3904, 2N3906, 2N2222, and 2N2907:*

<https://www.digikey.com/en/articles/transistor-basics>

Sierra Circuits, Inc. ~

- ⚙ *Trace Width and Current Capacity Calculator:* <https://www.protoexpress.com/pcb/trace-width-calculator/>
- ⚙ *Impedance Calculator:* <https://www.protoexpress.com/pcb/pcb-impedance-calculator/>

Copper Mountain Technologies ~ *VNA Measurements Demonstrations:*

- ⚙ *Videos:* <https://coppermountaintech.com/videos/>
- ⚙ *Webinars:* <https://coppermountaintech.com/webinars/>

ARWorld ~ *Guide to RF Coaxial Cables and Connectors:*

<https://arworld.us/resources/Guide-to-RF-Coaxial-Connectors-and-Cables.asp?ref=spotlight-coaxial-cables>



Hey, Mac, we'll keep measuring the Hubble "constant" until we finally decide the whole idea is wrong: Cornell University ~ *A new measurement of the Hubble constant using Fast Radio Bursts:*

<https://arxiv.org/abs/2104.04538>

Vimeo ~ *The 10th Annual Jansky Lecture, hosted by the National Radio Astronomy Observatory and presented at the Gilmer Hall Auditorium, UVA on November 19, 1975. Speaker is Dr. Grote Reber of CSIRO Tasmania, Australia. The lecture is entitled "Beginning of Radio Astronomy."* (poor video but good audio quality):

<https://vimeo.com/173657671>

History of Geo- and Space Sciences (HGSS) ~ *History of the Super Dual Auroral Radar Network (SuperDARN)-I: pre-SuperDARN developments in high frequency radar technology for ionospheric research and selected scientific results:*

<https://hgss.copernicus.org/articles/12/77/2021/>

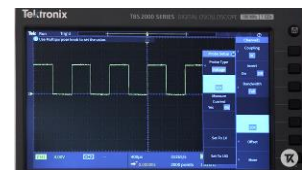


Community of European Solar Radio Astronomers (CESRA) ~ *Parametric simulation studies on the wave propagation of solar radio emission: the source size, duration, and position:*

<http://www.astro.gla.ac.uk/users/eduard/cesra/?p=2860>

Evaluation Engineering ~ *XYZs of Oscilloscopes Video Series:*

<https://www.youtube.com/playlist?list=PLt9TMIEXL79TdVcsAMEOUKVWtaB9Nfc1F>



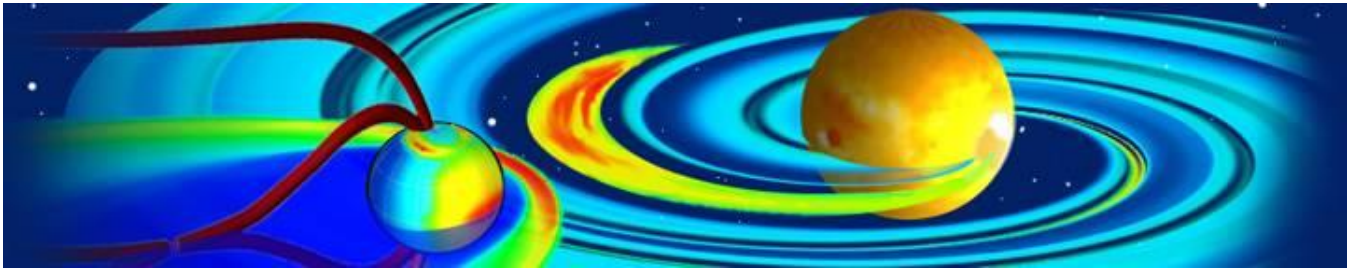
Marki Microwave ~ *Directivity and VSWR Measurements – Understanding Return Loss*

Measurements: https://www.markimicrowave.com/assets/appnotes/directivity_and_vswr_measurements.pdf

Keysight Technologies ~ *Keysight's new Smart Bench Essential Series' will help you make the most of the gear on your bench by covering the must-know basics of DMMs, function generators, power supplies, and oscilloscopes.:*

https://learn.keysight.com/learn/public/learning_plan/view/8/bench-essentials

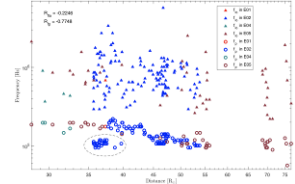




Community Coordinated Modeling Center, CCMC ~ *The CCMC is a multi-agency partnership to enable, support and perform the research and development for next-generation space science and space weather models:*

<https://ccmc.gsfc.nasa.gov/>

Community of European Solar Radio Astronomers (CESRA) ~ *Statistics of Low Frequency Cutoffs for Type III Radio Bursts Observed by Parker Solar Probe during Its Encounters 1–5:* <http://www.astro.gla.ac.uk/users/eduard/cesra/?p=2948>



Historical radio astronomy books:

Radio Astronomy and Cosmology 1977:

http://www.survivorlibrary.com/library/radio_astronomy_and_cosmology_1977.pdf

[PDF](#) 17 MB

Radio Astronomy for Amateurs 1962:

http://www.survivorlibrary.com/library/radio_astronomy_for_amateurs_1962.pdf

[PDF](#) 46 MB

Radio Astronomy Simplified 1963:

http://www.survivorlibrary.com/library/radio_astronomy_simplified_1963.pdf

[PDF](#) 23 MB

Radio Astronomy Today 1962:

http://www.survivorlibrary.com/library/radio_astronomy_today_1962.pdf

[PDF](#) 40 MB

Radio Astronomy - Jennison 1966:

http://www.survivorlibrary.com/library/radio_astronomy-jennison_1966.pdf

[PDF](#) 7 MB

Radio Astronomy - Piddington 1961:

http://www.survivorlibrary.com/library/radio_astronomy-piddington_1961.pdf

[PDF](#) 21 MB

Galactic Radio Astronomy 1974:

http://www.survivorlibrary.com/library/galactic_radio_astronomy_1974.pdf

[PDF](#) 30 MB

nanoVNA Calibration Standards

Whitham D. Reeve

1. Introduction

The nanoVNA is an inexpensive and very popular vector network analyzer (figure 1). I purchased the AURSINC nanoVNA-H4, which is one of many implementations of the nanoVNA platform. According to the Amazon listing, the -H4 has a 4 in (100 mm), 480x320 pixel TFT display and a 1950 mAh rechargeable battery. Its native frequency range is advertised as 10 kHz to 300 MHz with measurements up to 1500 MHz by using harmonics. The nanoVNA has some limitations, such as being capable of only 101 measurement points, but it is hard to beat the price at less than 100 USD.



Figure 1 ~ nanoVNA-H4 and measurement accessories supplied with it. These include two RG-316, 150 mm long coaxial jumper cables with SMA male connectors, SMA male Open, Short and Load calibration standards, and an SMA female barrel connector. It also included a couple USB cables and a Quick Start Guide (not shown). Note the guitar pick on the lanyard to be used as a stylus. I prefer a soft-tip stylus and added the one shown above the unit. The calibration standards have an identical outward appearance, so I color-coded them with fingernail polish for easy identification: Blue = Load; Red = Short; and White = Open. The SMA barrel connector, seen to the left of the Load, is not strictly part of the calibration standards but is necessary for Thru calibration and when using the standards with cables or devices that have male connectors. I also marked the two coaxial jumper cables red and green for identification. Image © 2021 W. Reeve

The nanoVNA assumes that all calibration standards are ideal. It has no provisions for entering the electrical characteristics (capacitance, inductance, resistance), and no such data are provided or available for the nanoVNA. The nanoVNA does have a Port Extension feature for entering delay.

Because of the low cost and lack of calibration features, I was quite skeptical about the quality of the supplied calibration standards and decided to measure their reflection coefficient (S_{11} scattering parameter) with a professional instrument. I report the measurements here. I also compare measurements of the nanoVNA jumper cables to similar measurements with precision test cables. This article is focused on the calibration standards and

does not discuss the performance of the nanoVNA itself. Readers should note that, because there are many nanoVNA versions, there also may be many versions of the calibration standards. The measurements and other information provided in this article may or may not apply to other versions.

2. Measurements Setup

I used a Keysight FieldFox N9917A Microwave Analyzer in *Network Analyzer* mode for all measurements. The FieldFox was setup for 50 kHz to 1500 MHz frequency range and 1001 measurement points. I set markers at 1000 MHz (arbitrary) and 1420 MHz (corresponding to the 21.1 cm wavelength of neutral hydrogen emissions).

All measurements involved reflection coefficients displayed in dB. My discussions use the equivalent return loss, where $\text{Return loss (dB)} = |\text{Reflection coefficient (dB)}|$.

For FieldFox calibration I used an HP 85033D 3.5 mm Calibration Kit and a type N-M to SMA-F adapter to adapt the FieldFox connector to the SMA connectors on the nanoVNA calibration standards and jumper cables. Unlike the nanoVNA calibration standards, the HP Calibration Kit is fully characterized. Its characteristics are stored on the FieldFox and recalled when needed. The adapter was part of the FieldFox calibration and all measurements. Because the nanoVNA calibration standards are male gender, I used the SMA female barrel connector (coupler) supplied with the unit to connect the standards to the coaxial jumper cables.

The nanoVNA barrel connector does not appear to be special in any way, and serious users of the nanoVNA should consider replacing it with one of higher quality (figure 2). The connector does not have flats for a wrench, so it is impossible to properly torque connections to it. Where the barrel connector was required, I only could make the connections finger-tight. Its characteristics (whatever they are) are included in the measurements discussed below.



Figure 2 ~ nanoVNA SMA barrel connector (upper-right) alongside a high-quality connector. The brass nanoVNA connector has no flats for a wrench and cannot be properly torqued. The RF Industries model RSA-3404 nickel-plated brass connector shown next to it has flats for a 5.5 mm wrench. I made all connections involving the brass barrel connector finger-tight. Image © 2021 W. Reeve

3. Calibration Standards and Cable Measurements

In this section I discuss the measured return loss for each standard, the two nanoVNA jumper cables alone, and the two jumper cables with the Load standard connected.

The three calibration standards showed very good results throughout the measurement frequency range (figure 3). The return loss of the Open and Short are very close to zero, as expected. The return loss of the Load is nearly 44 dB at 1420 MHz (equivalent to a VSWR of 1.013:1) and better than 41 dB throughout the entire measurement frequency range. The two jumper cables showed no unusual behavior when measured alone (figure 4) but, when connected to the Load, they markedly reduced the return loss of the Load from 44 dB to 20 dB at 1420 MHz (figure 5). The measurements of the cable and Load combination also showed some resonant effects that were not obvious when the cables were measured alone.

The nominal attenuation of RG-316 cable at 1420 MHz is 1.03 dB/m so, for a 150 mm long cable without connectors, the 1-way attenuation would be near 0.15 dB. With total reflection at an open end, the return loss would be double the 1-way attenuation or 0.3 dB. Connectorized cables will show slightly higher attenuation due to the connectors, particularly at higher frequencies. The measured return loss was 0.43 and 0.42 for the open-circuited cables, well within expectations when the connectors and instrument accuracy are taken into account.

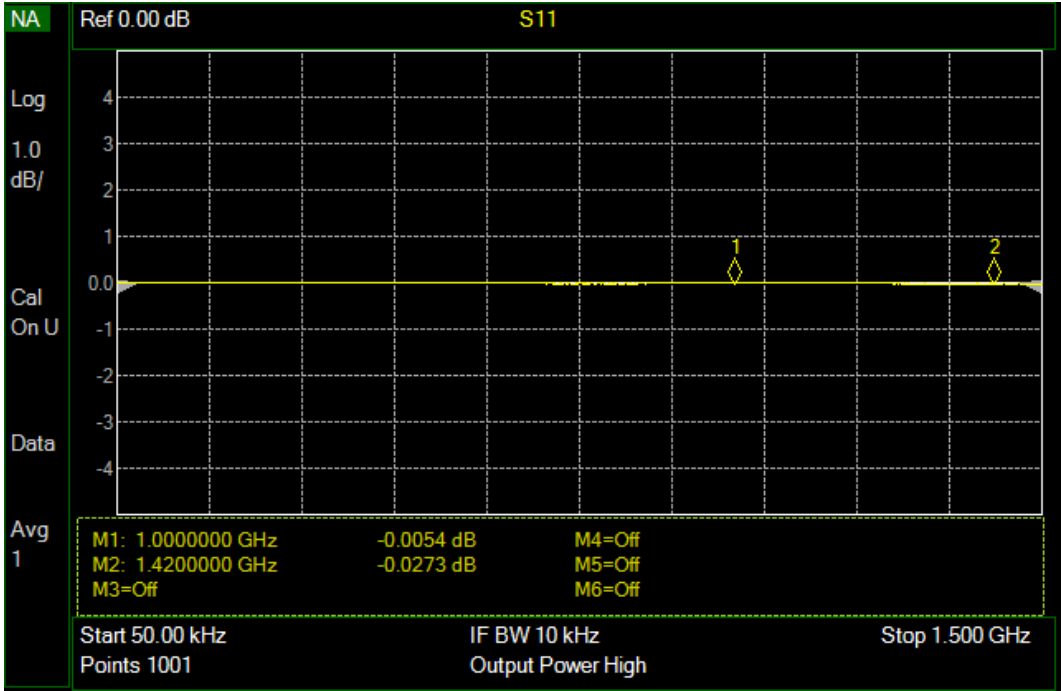


Figure 3.a ~ nanoVNA Open standard. Vertical scale is 1 dB/div with the reference (at center) set to 0.0 dB. These measurements are for direct connection of the Open standard to the FieldFox port adapter.

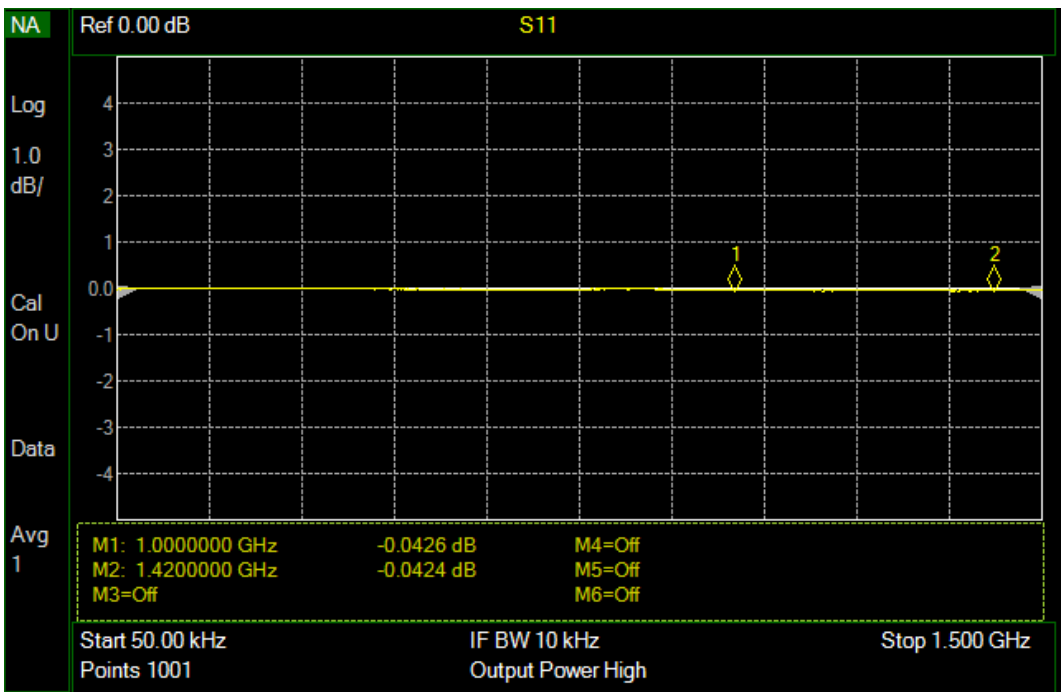


Figure 3.b ~ nanoVNA Short standard. Vertical scale is 1 dB/div with the reference (at center) set to 0.0 dB. These measurements are for direct connection of the Short standard to the FieldFox port adapter.

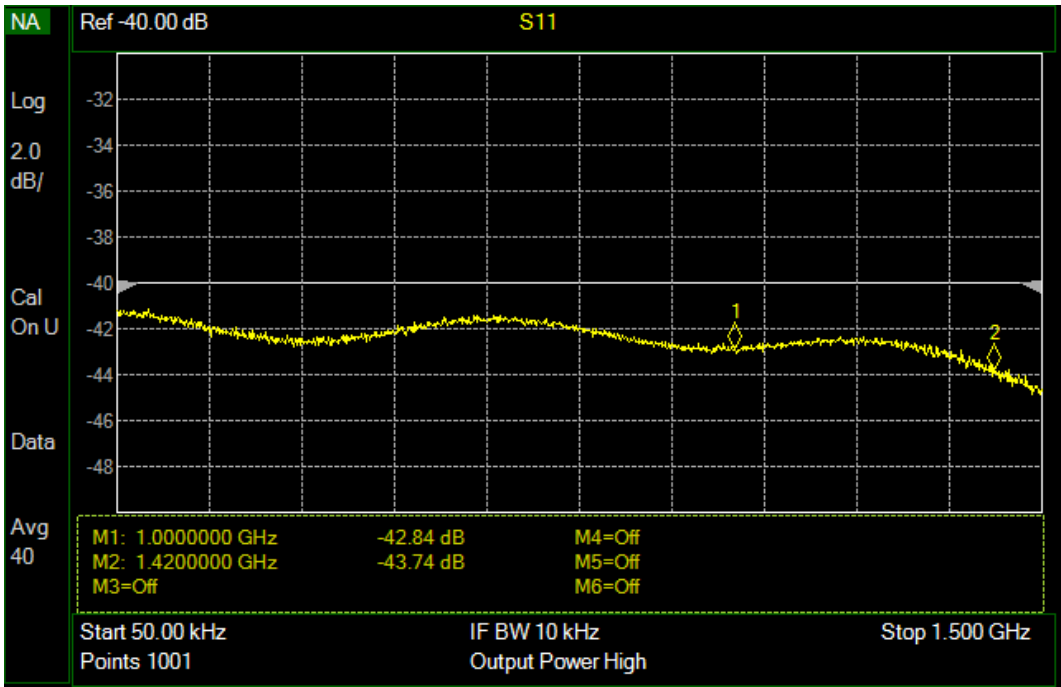


Figure 3.c ~ nanoVNA Load standard. Vertical scale is 2 dB/div with the reference (at center) set to -40.0 dB. These measurements are for direct connection of the Load standard to the FieldFox port adapter.

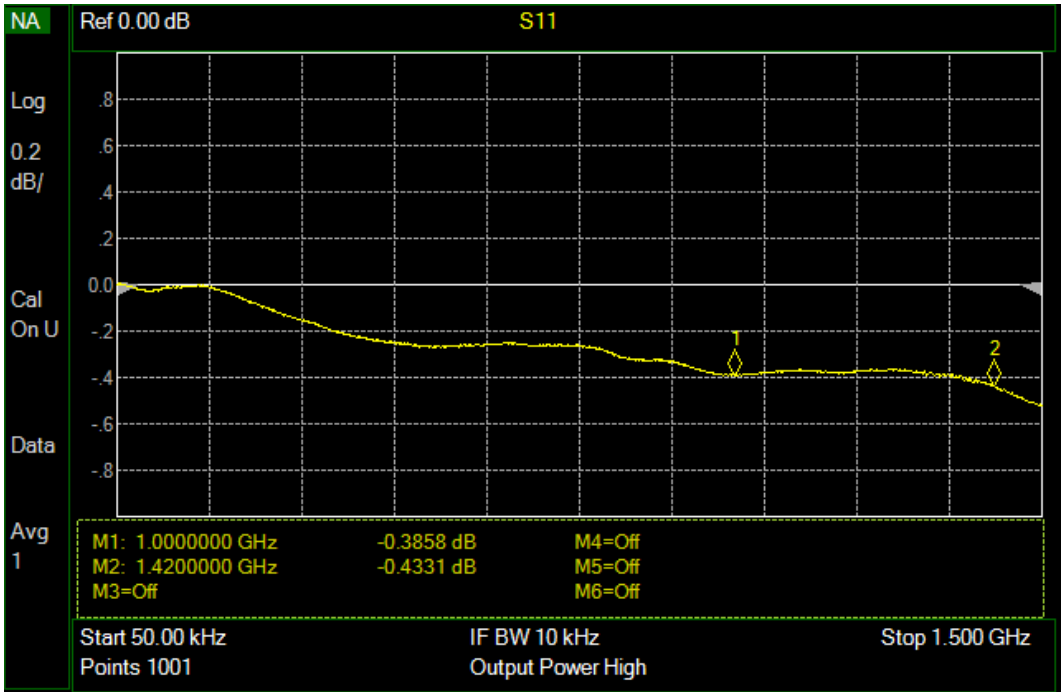


Figure 4.a ~ nanoVNA Red coaxial jumper cable alone, no termination and no barrel connector. Vertical scale is 2 dB/div with the reference (at center) set to 0.0 dB.

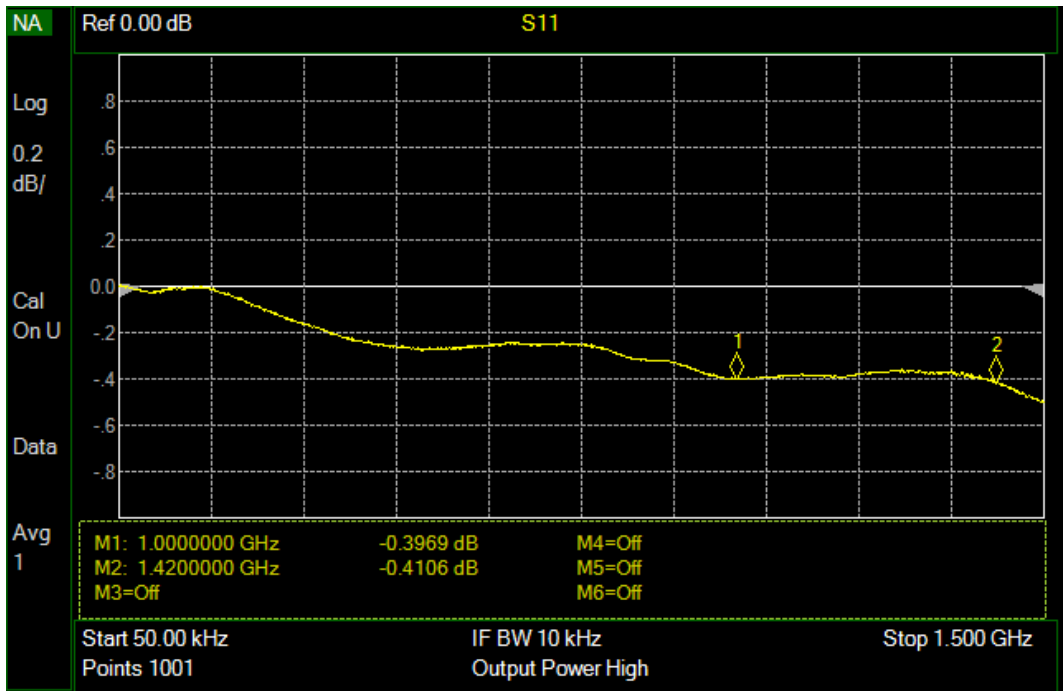


Figure 4.b ~ nanoVNA Green coaxial jumper cable alone, no termination and no barrel connector. Vertical scale is 2 dB/div with the reference (at center) set to 0.0 dB.

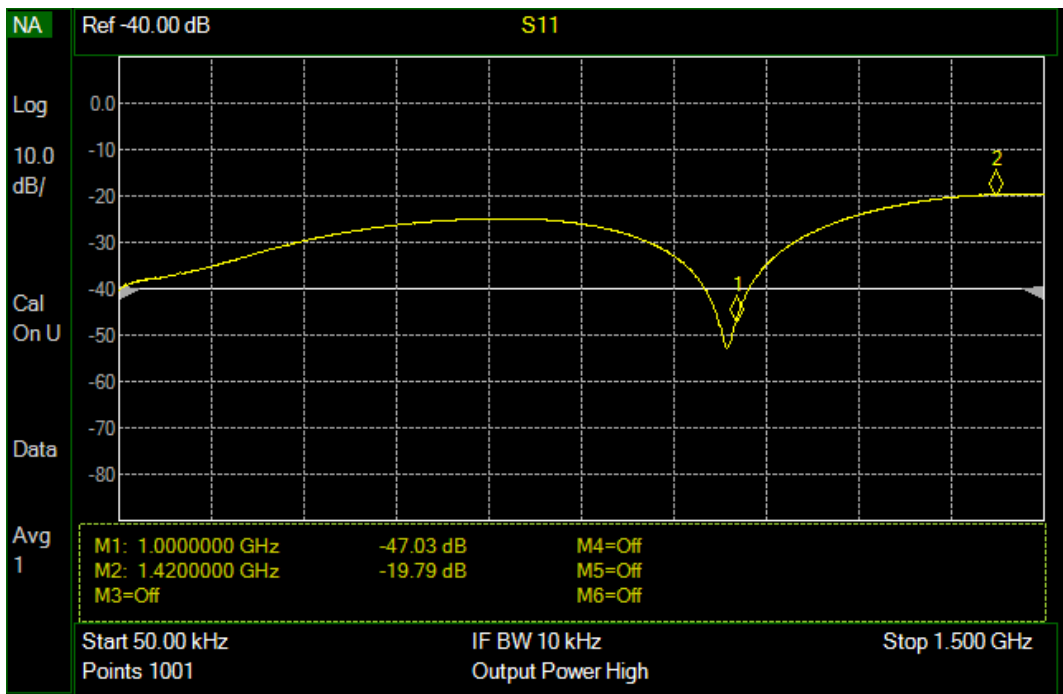


Figure 5.a ~ nanoVNA Red coaxial jumper cable with barrel connector and Load standard. Vertical scale is 10 dB/div with the reference (at center) set to -40.0 dB.

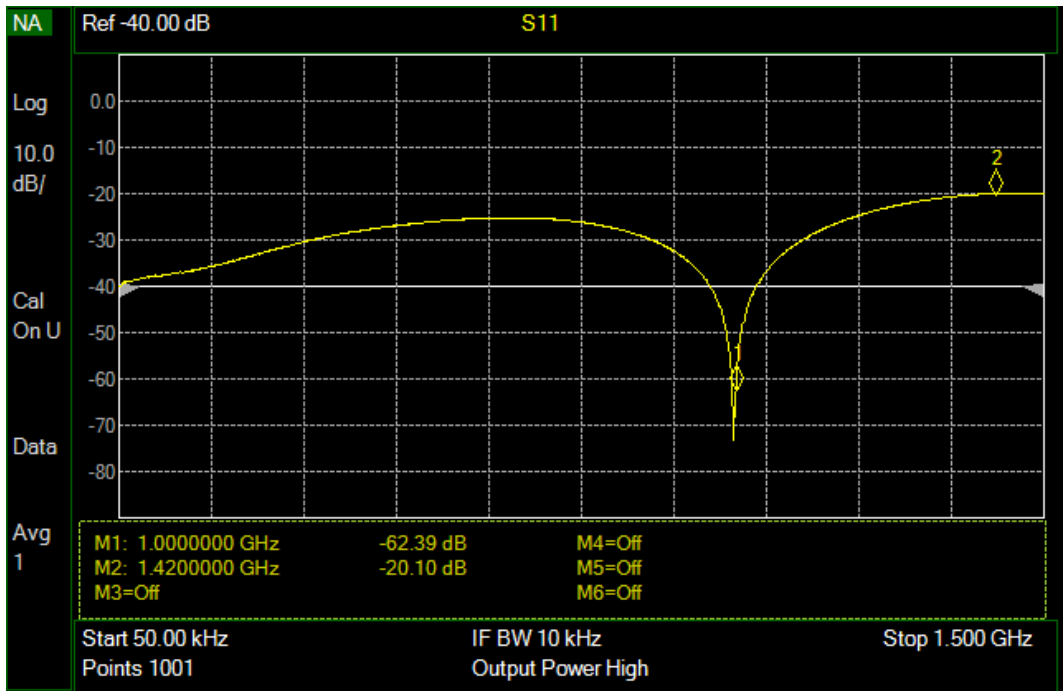


Figure 5.b ~ nanoVNA Green coaxial jumper cable with barrel connector and Load standard. Vertical scale is 10 dB/div with the reference (at center) set to -40.0 dB.

RG-316 cable has a PTFE dielectric with a nominal velocity factor of 0.69 to 0.7. Therefore, the wavelength at 1420 MHz in the cables would be 146 to 148 mm, which coincidentally is close to the physical cable lengths. When terminated with the Load, both cables showed a resonance dip just below the 1000 MHz markers, one cable about 20 dB deeper than the other. This difference could be due to measurement resolution, which is about 1.5 MHz.

The resonance effects and return loss degradations caused by the cables call into question their usefulness with the nanoVNA. For example, if the measured return loss of a very good Load standard (44 dB in the case of the nanoVNA Load) in combination with the cable is 20 dB, no measurement of a device will ever be better than 20 dB no matter what its actual return loss is. It should be noted that 20 dB return loss corresponds to a VSWR of 1.22:1 and is not that bad. It is the degradation from 44 to 20 dB that is of concern. It is good practice to include any jumper or test cables in the calibration, and this is done in the next section.

4. Comparison with Precision Test Cables

I performed additional measurements with the nanoVNA coaxial jumper cables and several precision test cables. The test cables were Pasternack PE300.24 (24 in length) and Gore OKR01R71024.0 (24 in length) (figure 6). The Pasternack cables have a straight SMA-M connector on each end. The Gore cables have a straight SMA-M connector on one end and a right-angle SMA-M connector on the other. For the measurements with the Gore cables, I connected the straight connector to the FieldFox port (through the adapter) and the right-angle connector to the nanoVNA Load standard.

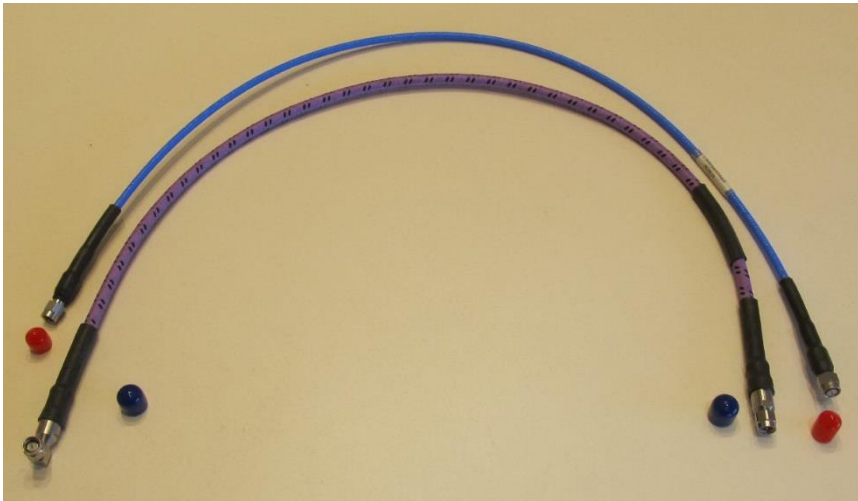


Figure 6 ~ Precision test cables with protective caps removed. The upper cable is a Pasternack PE300-24 and the lower cable is a Gore. The Gore cable has a tough, braided fabric protective cover over the jacket. Its right-angle connector is visible in the lower-left corner.

First, for comparison with figure 5 above, I measured the nanoVNA Load standard return loss when connected to the precision test cables (figure 7). For these measurements, the calibration plane was at the adapter on the FieldFox as with all previous measurements. The precision test cables showed ripple in their reflection coefficient traces, but this is common and indicates imperfect impedance matching. The variations due to ripple were on the order of 10 dB for the Pasternack cables and 20 dB for the Gore cables. Note that these precision cables show a much different response than the nanoVNA jumper cables, partly because they are longer.

The test cables reduced the measured return loss of the Load from 44 dB to 34 dB (Pasternack) and 29 dB (Gore with right-angle connector) at 1420 MHz – neither as severe as the shorter RG-316 cables supplied with the nanoVNA. I was expecting the right-angle connectors on the Gore cables to degrade the Load measurements, and this apparently was the case. Compared to the Pasternack test cables, the Gore cables showed lower return loss at 1420 MHz by about 5 dB.

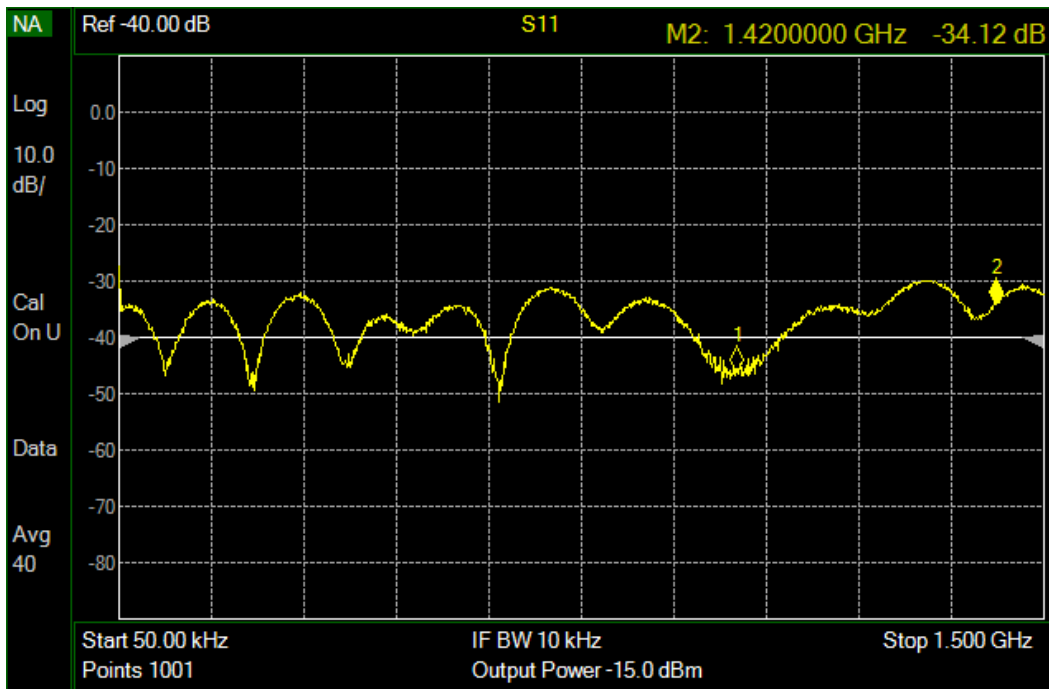


Figure 7.a ~ Pasternack PE300.24 test cable and Load standard with barrel connector, typical of four cables. Vertical scale is 10 dB/div with the reference (at center) set to -40.0 dB.

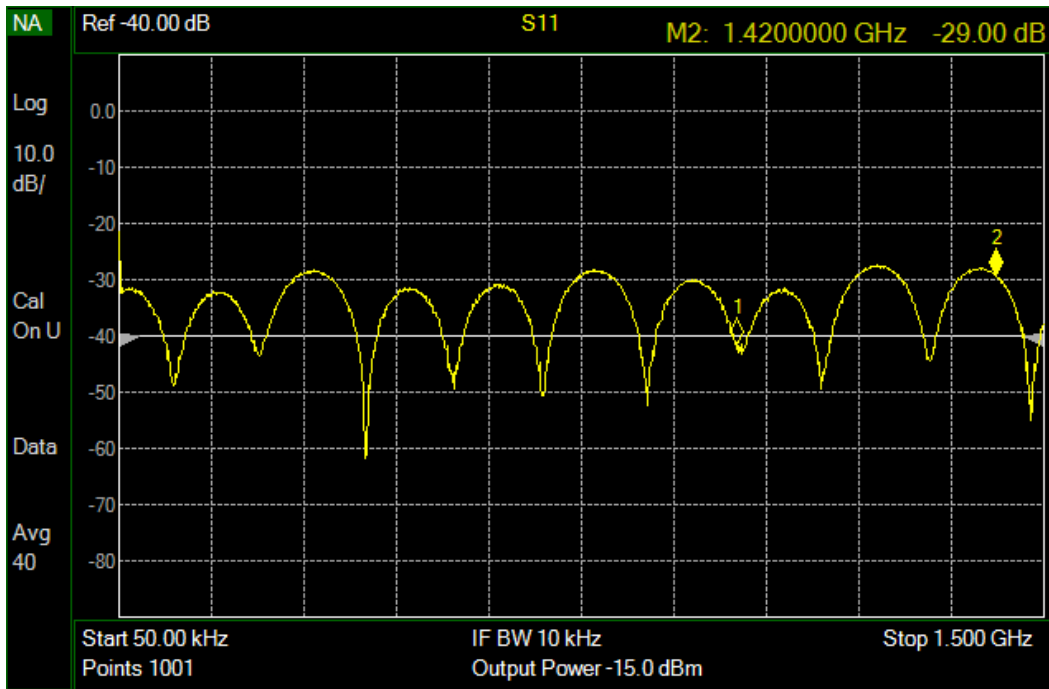


Figure 7.b ~ Gore OKR01R71024.0 test cable and Load standard with barrel connector, typical of two cables. Vertical scale is 10 dB/div with the reference (at center) set to -40.0 dB.

I then moved the calibration plane to the end of the cable and barrel connector by recalibrating the FieldFox with the HP 85033D Calibration Kit at that position. Three calibrations were made, first using the nanoVNA jumper cables, then a Pasternack cable and, finally, a Gore cable. These calibrations included the SMA barrel connector because it is required for connecting all of the nanoVNA calibration standards to the cables. After each calibration, I again measured the return loss of the Load standard.

This set of measurements yielded better results, as expected (figure 8). In these measurements, the cable and barrel connector characteristics were embedded in the calibration so, ideally, they have no effect, and the Load standard would measure as if it was connected directly to the instrument. However, in practical measurements, especially at frequencies in the GHz range, any movement of the test cables during and after calibration can affect the results. Precision test cables generally are less susceptible to this effect, but I noticed the RG-316 jumper cables supplied with the nanoVNA showed considerable differences when moved around - I could easily change the return loss by 10 dB by moving and bending (but not kinking) the cable.

The measurement results show return losses more in line with those shown previously in figure 3.c. Curiously, the return loss is a few dB higher with one of the nanoVNA jumper cables than either the Load alone or the Load with the precision test cables. These differences are easily explained by the comments above about cable movement during and after calibration affecting the measurements. The precision test cables showed more consistent results.

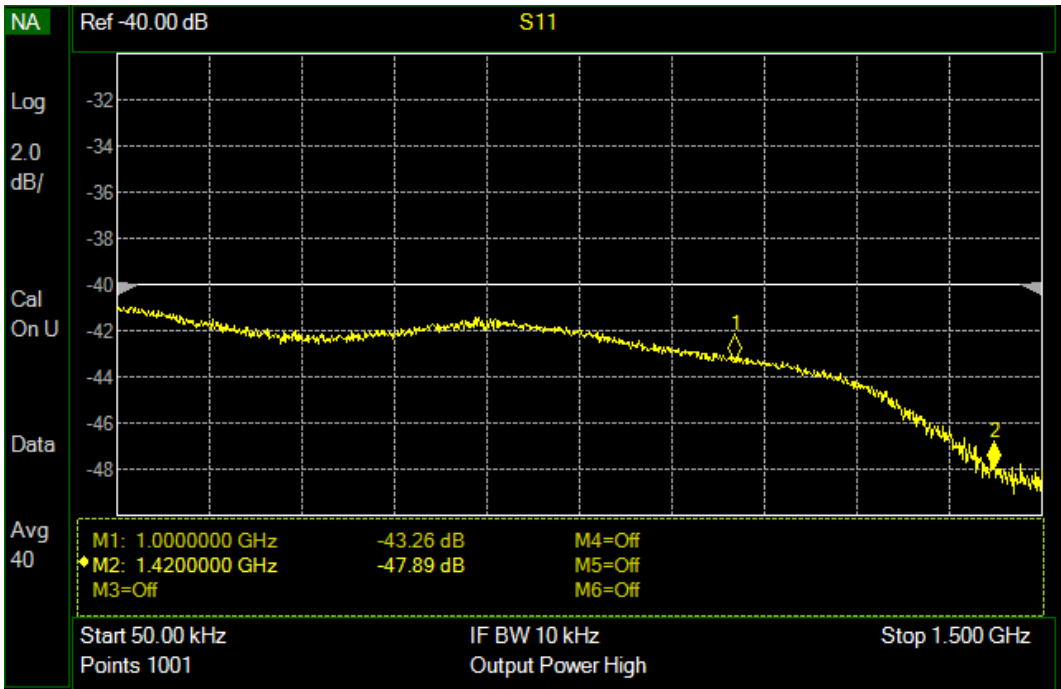


Figure 8.a.1 ~ Return loss of the Load standard on the Red nanoVNA coaxial jumper cable. The barrel connector was included in the FieldFox calibration. Vertical scale is 2 dB/div with the reference (at center) set to -40.0 dB. Note that the resonance effect seen in figure 5 is not present because the calibration plane has been moved to the end of the barrel connector on the cable.

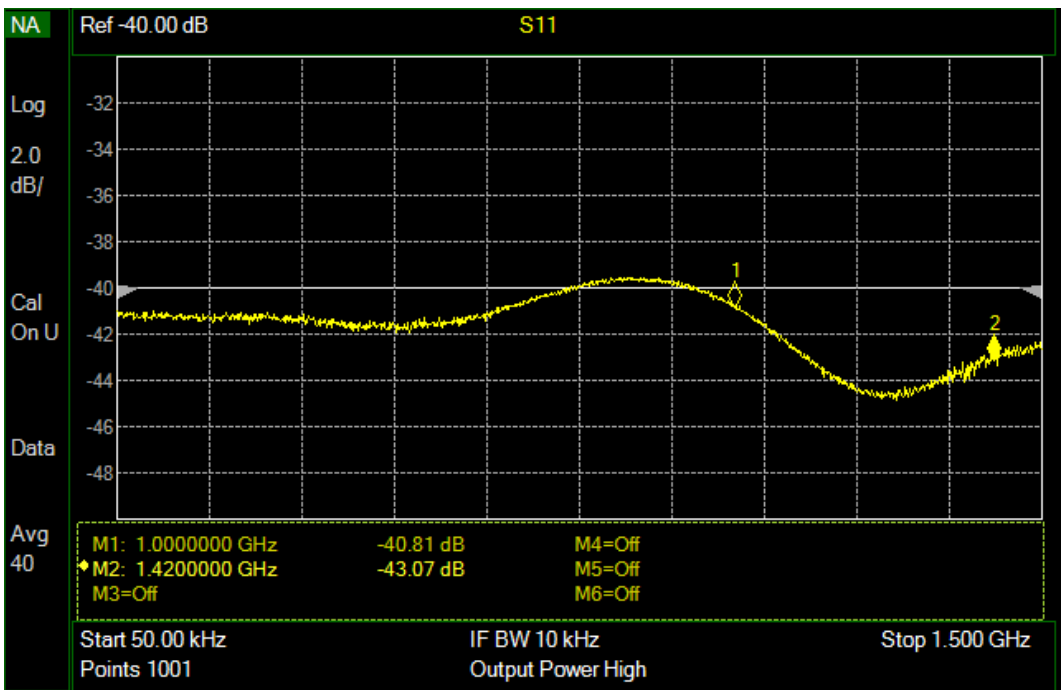


Figure 8.a.2 ~ Return loss of the Load standard on the Green nanoVNA coaxial jumper cable. The barrel connector was included in the FieldFox calibration. Vertical scale is 2 dB/div with the reference (at center) set to -40.0 dB. Note that the resonance effect seen in figure 5 is not present because the calibration plane has been moved to the end of the barrel connector on the cable.

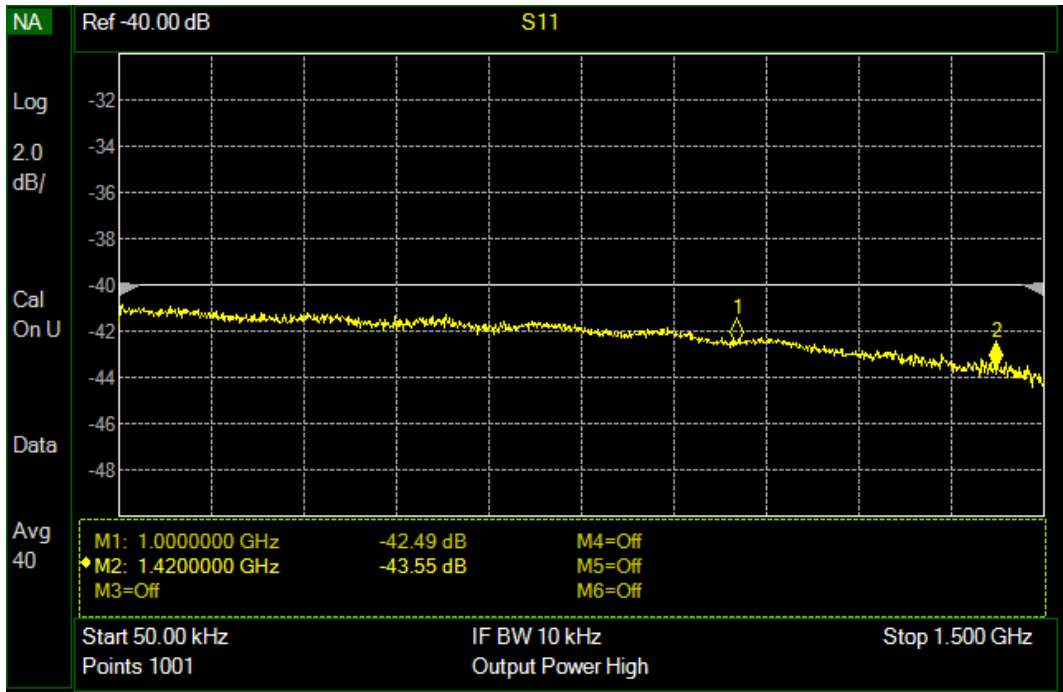


Figure 8.b ~ Return loss of the Load standard connected to one of four Pasternack test cables. Vertical scale is 2 dB/div with the reference (at center) set to -40.0 dB. Note that the ripple seen in figure 7 is not present because the calibration plane has been moved to the end of the barrel connector on the cable.

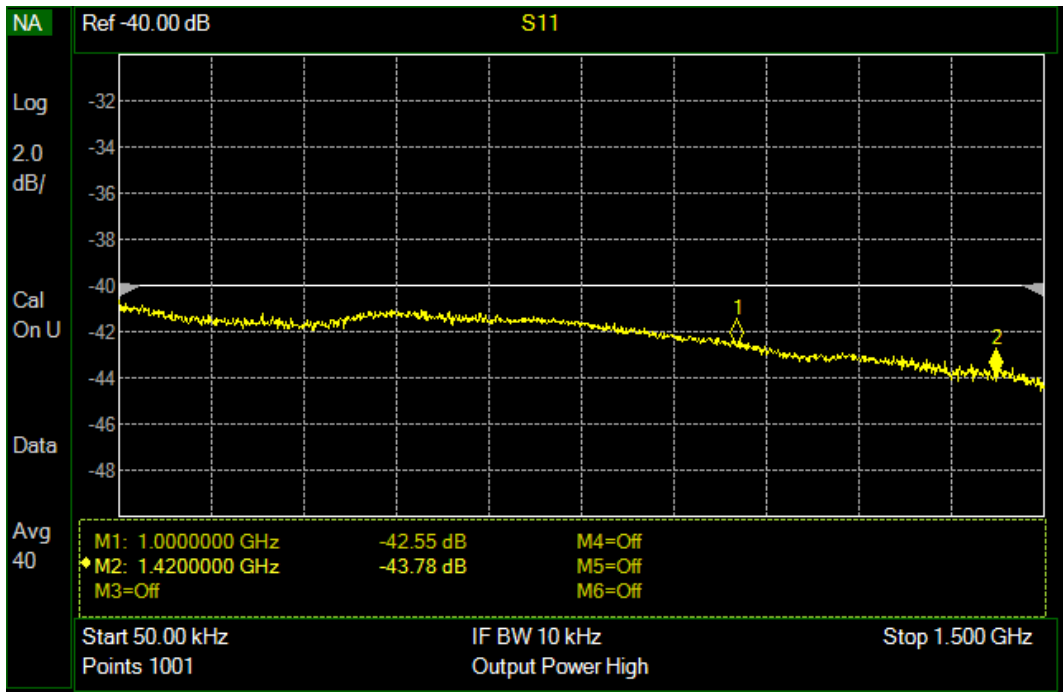


Figure 8.c ~ Return loss of the Load standard connected to one of two Gore test cables. Vertical scale is 2 dB/div with the reference (at center) set to -40.0 dB. Note that the ripple seen in figure 7 is not present because the calibration plane has been moved to the end of the barrel connector on the cable.

5. Conclusions

The measurements eliminated my skepticism of the nanoVNA calibration standards but not of the test cables. The calibration standards by themselves looked very good but the supplied coaxial jumper cables do not have comparable performance and are not useful for repeatable measurements. Test cables normally are connected to a VNA during calibration and their effects are *calibrated out*. Doing this significantly improved the measurements as expected, but any movement of the jumper cables affected the measurements especially at higher frequencies.



Author: Whitham Reeve obtained B.S. and M.S. degrees in Electrical Engineering at University of Alaska Fairbanks, USA. He worked as a professional engineer and engineering firm owner/operator in the airline and telecommunications industries for more than 40 years and now manufactures electronic equipment used in radio astronomy. He also is a part-time space weather advisor for the High-frequency Active Auroral Research Program (HAARP) and a member of the HAARP Advisory Committee. He has lived in Anchorage, Alaska his entire life. Email contact: whitreeve@gmail.com

Getting the Best from the Pulsar Folding Algorithm

Peter East

Abstract

The signal-to-noise ratio (SNR) prediction of the pulsar radiometer equation is achieved by matching the folding algorithm bandwidth to that required to just pass the pulsar pulse spectrum. The basic folding algorithm has SNR limitations but still has its uses. This article investigates folding theory and applies the recommended process to measurements made on the Vela and B0329+54 pulsars covering SNR extremes and finally interprets the results.

Introduction

The folding algorithm is used for enhancing the visibility of a pulsar by synchronously adding a number of pulsar periods along the data record. Simply explained, the pulsar signal integrates linearly whilst the background noise integrates as the square root, so improving the detection signal-to-noise ratio (SNR). As with most digital signal processing tasks, there are several ways of implementing this algorithm. A typical amateur method, simply divides the pulsar period into a number of time bins and sums each consecutive period synchronously. The final graphical indication of both the pulse shape and noise depend upon the number of time bins set in the pulsar period; many time bins improve the pulse detail but in the simplest case can degrade the SNR. This basic process can be improved as implied by the pulsar radiometer equation and the aim of this document is to show how to achieve both optimum SNR and folded time resolution simultaneously. Firstly the pulsar radiometer equation is reviewed to understand what should be achieved.

The Pulsar Radiometer Equation

Equation 1 is the pulsar radiometer equation derived by Lorimer⁽¹⁾ which describes the folding algorithm performance in generating an observable signal-to-noise ratio (SNR) for a single received polarization,

$$SNR = \frac{S_p A_e \sqrt{t_{int} \Delta f}}{2\beta k_b T_{sys}} \sqrt{\frac{P-W}{W}} \quad (1)$$

where, S_p is the pulsar mean flux at the observation frequency, as listed in the ATNF data base in Janskys (1 Jansky = 10^{-26} W/Hz/m²).

A_e is the receiving antenna effective collecting area in m².

t_{int} is the total data acquisition time in seconds.

Δf is the receiver RF bandwidth in Hz.

P is the predicted accurate pulsar period in ms.

W is the pulsar pulse half-height width in ms.

the factor 2 halves the pulsar flux to conform with the flux with a single polarization.

β is a modifying factor to account for digitization losses for coarser digital increments.

k_b is Boltzmann's constant(= 1.380649×10^{-23} W/°K/Hz).

T_{sys} is the antenna terminal system noise temperature in °K.

This equation actually describes the best possible mean SNR and, as discussed in this article, to achieve this optimum value in practice requires some careful attention.

Since the raw data is sampled, to ensure some timing resolution the pulsar folding period is normally divided into a number of bins N for display. This effectively factors the integration time, so that it seems logical that the value N should appear in the Equation 1 as a t_{int} divisor. Also, the pulsar flux S_p is catalogued as a mean value but for SNR calculation we are more interested in the peak value, so it might be thought that S_p should really be increased by the pulse peak-to-mean factor $(P-W)/W$, rather than its square root.

However, if the number of bins chosen, $N = (P-W)/W$, then Equation 1 appears to be satisfied. Indeed, this is the number of bins usually recommended for the basic folding method to obtain the best indicated SNR; but this may

not always be the case. In addition, pulsar duty cycles (P - W): W vary over quite a wide range and as a consequence the timing resolution of the basic method may be very poor for pulsars with low duty cycles.

Information in Recorded Data

The recorded data is assumed to comprise multi-level digital in-phase and quadrature (I/Q) samples sampled at a rate $1/t_c (= \Delta f)$. An analogue representation of the digital square-law detection process following a software defined radio (SDR) is shown in Figure 1.

The data sample amplitudes ($I^2 + Q^2$) contain both DC and AC components; both of these DC and AC components are proportional to T_{sys} (powers $\approx kT_{sys} \Delta f$).

After low-pass filtering (LPF), often simply by data series averaging, the AC component power is reduced to $kT_{sys} \sqrt{\Delta f \Delta lpf}$, where $\Delta lpf (\rightarrow 1/t_{int})$ is the effective low-pass filter cut-off frequency. For block averaging of N samples, $\Delta f \rightarrow 1/Nt_c$.

In the presence of a pulsar pulse T_{sys} increases by T_p - the pulsar peak equivalent temperature. The pulsar DC contribution sits on the system noise DC component and it is the difference between these components that is of interest.

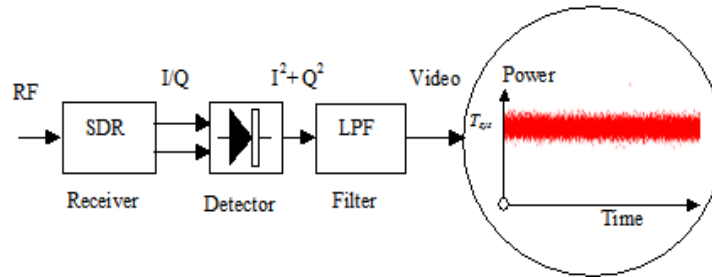


Figure 1. Raw Data Analogue-equivalent Detection Process.

With a large antenna and a strong pulsar, pulses may be visible on the noise section in Figure 1. This is a 30 minute section of real B0329+54 system data downsampled to 1ksps. The noise rms level here is approximately equivalent to 2 K and the expected pulsar pulse amplitude for this system is 0.05 K - a fair task for the folding algorithm.

Describing the detected system AC noise signal by $v_n(t)$ and the pulsar DC level by $v_p(t)$ - the pulsar AC component can usually be ignored compared to T_{sys} - then the equivalent pulsar input SNR is,

$$SNR_{in} = \overline{v_p^2(t)} / \overline{v_n^2(t)} = T_p / T_{sys}.$$

Basic Bin Folding Analysis

In preparation for folding, the data recording for the duration T is notionally divided into R sections exactly equal to the pulsar period P so that, if present, the pulsar pulse will appear at the same relative position 't' amongst the random system noise as depicted in Figure 2.

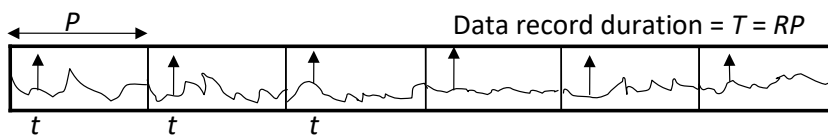


Figure 2. Data Record T Divided into R Blocks Equal in Time to the Pulsar Period P .

In folding, each period block of data is divided into N bins and the R periods added synchronously together. After synchronously adding/folding, RP/Nt_c of the original data samples on average fall in each bin*. In a bin filled with a pulse, the summed DC detected voltage increases linearly to $\overline{v_p(t)} \cdot RP / Nt_c$.

Once all RP/t_c data samples are folded in, the AC rms noise voltage increases by power to $\sqrt{\overline{v_n^2(t)} \cdot RP / Nt_c}$ in all bins.

The indicated output voltage SNR_o is the ratio of the in-bin pulsar DC and the system noise AC terms from noise-only bins, or,

$$SNR_o = \frac{\overline{v_p(t)} RP / Nt_c}{\sqrt{\overline{v_n^2(t)} \sqrt{RP / Nt_c}} = \frac{T_p}{T_{sys}} \cdot \sqrt{\frac{RP}{Nt_c}}$$

The peak equivalent pulsar temperature for one received polarization, based on the radiometer equation definitions above is, $T_p = \frac{S_p}{2} \frac{P-W}{W} \cdot \frac{A_e}{k_b}$ and since, $1/t_c = \Delta f$ (for complex I/Q samples), $t_{int} = RP$. With these substitutions, a basic version of the pulsar radiometer equation is derived for when the pulsar lies centrally in a bin,

$$SNR_o \approx \frac{S_p A_e \sqrt{\frac{t_{int} \Delta f}{N}}}{2 k_b T_{sys}} \frac{P-W}{W} \quad (2)$$

When, $N = (P-W)/W$, this equation can be rewritten as suggested earlier,

$$SNR_o \approx \frac{S_p A_e \sqrt{t_{int} \Delta f}}{2 k_b T_{sys}} \sqrt{\frac{P-W}{W}}$$

and now this basic pulsar radiometer equation for the folding algorithm agrees with the official Equation 1 form.

* Due to the bin quantization, it is unlikely that equal numbers of data samples fill every bin, so in practice, the bin samples are counted and the bin sums normalized.

Improving the Basic Folding Algorithm for Large Bin Numbers

As described, the basic folding algorithm of Equation 2 matches the performance of the pulsar radiometer Equation 1 at one value of $N = (P-W)/W$; for larger bin numbers the output SNR is reduced by the square-rooting function, \sqrt{N} .

Now, P/N ms represents the time resolution of the folded result, which has a corresponding noise frequency bandwidth of N/P kHz. So, the larger bin numbers are associated with increased noise frequencies whilst the pulsar signal integration is unaffected and this is the mechanism that reduces the SNR. When $N = (P-W)/W$ the time resolution and bandwidth are just sufficient to pass the pulse so by restricting or filtering the noise bandwidth of large N folded results to this value, the matched SNR can be recovered.

Bin Folding with Filtering

Imagine again that the data record is divided into R periods and that these are added at the sample rate. In this case, the folded pulsar-to-noise SNR, increases by $R/\sqrt{R} = \sqrt{R}$. Passing this result through a low-pass filter sufficient

to just pass the pulse, the filter cut-off frequency = $1/W$, and the SNR becomes, $\frac{T_p}{T_{sys}} \sqrt{R} \sqrt{\frac{W}{t_c}}$. Now since, $\sqrt{t_{int} \Delta f} = \sqrt{RP/t_c}$, substituting for t_c , we get,

$$SNR_o = \frac{T_p}{T_{sys}} \sqrt{R} \sqrt{t_{int} \Delta f} \sqrt{\frac{W}{RP}}$$

The peak equivalent pulsar temperature is again, $T_p = \frac{S_p}{2} \frac{P-W}{W} \cdot \frac{A_e}{k_b}$

Substituting for T_p we get the official radiometer equation form showing that the predicted SNR is no longer dependent upon the number of folding bins.

$$SNR_o = \frac{S_p A_e \sqrt{t_{int} \Delta f}}{2 k_b T_{sys}} \sqrt{\frac{P-W}{W}}$$

This last statement is not quite true, as for low bin numbers, the bin time window can get wider than the pulse, so the pulse contribution to the bin SNR reduces producing the low bin number tail off in SNR, as shown later by the green curve in Figure 3. The theoretically predicted curve with bin size taken into account is explored in the Appendix 1.

Matched Filtering Approach

Band limiting the data can be accomplished in a number of ways, but noting that the required filtering operation is equivalent to convolving the folded result with a similarly shaped clean pulse target, it can be accomplished digitally and with minimum time penalty by the process,

- 1) Fourier transform the folded output.
- 2) Fourier transform a target pulse shape closely matching the pulsar pulse.
- 3) Determine the spectrum product of 1) and the normalized modulus of 2).
- 4) Inverse Fourier transform the product to produce the filtered result.

By this means, the signal-to-noise ratio of the resulting folded data is improved without affecting the delay shape or fidelity of the pulse. Improved pulse detail with the penalty of some SNR reduction is possible by increasing the filter cut-off by reducing the width of the pulse target.

A MathCad code outline is given in Appendix 2.

Alternatively, of course, noise bandwidth reduction is achievable by suitably filtering the pre-folded detected data.

Practical Folding Results

Vela Pulsar Example, SNR = 55:1, P/W ≈ 43

Figure 3 compares the folding results as a function of number of folding bins for the basic folding method and the enhanced post-filtering scheme, using some Vela pulsar data collected by G. Gancio on the Argentine Institute's 30 m dish. The plots indicate the SNR resulting as a function of the number of bins dividing the pulsar period. All integer bin numbers are represented from 10 to 800.

The red dots indicate the SNR for various period bin numbers using the basic folding method clearly showing the \sqrt{N} reduction in SNR. The blue dots indicate the enhanced performance with spectral band limiting on the same data set. Both methods demonstrate similarity as the number of bins reduces below the optimum value of N due to the folded data bandwidth now being controlled by the bin number rather than the pulse bandwidth. The wider uncertainty here occurs due to the pulse power being shared between adjacent bins; best performance being achieved when the pulsar position lies centrally in a bin.

The green and magenta curves are the predicted values assuming Gaussian statistics background noise and a Gaussian-shaped pulsar pulse of equal half-height to the expected pulsar, arriving at a bin center, as derived in the Appendix 1.

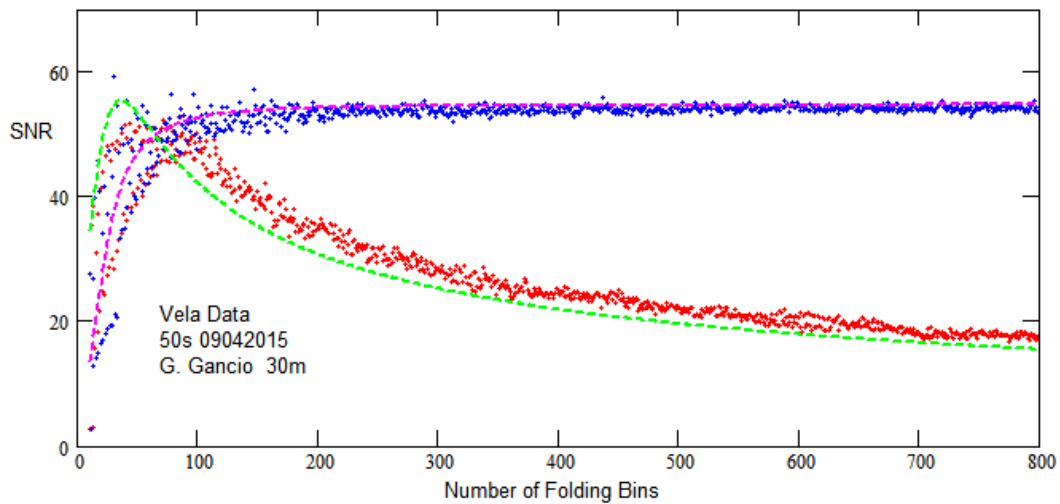


Figure 3. Vela Pulsar Data SNR as a Function of Number of Folding Bins (red - basic; blue - matched).

For the basic folding method (green curve), the theory predicts a peak SNR at around the bin value, $42 \approx (P-W)/W = (89.3-2.1)/2.1$ - the Vela pulsar period, and half-height width parameters. The uncertainties at the higher bin numbers are due to the data quantization and the odd/even bin numbers varying the pulsar phase across bin boundaries. The plots highlight the limitations of the basic algorithm implementation. The basic approach only offers modest SNR performance over a small range of bin numbers between 40 and 100. Even within this range, care must be taken to ensure the pulsar phase is such that the peak lies centrally in a bin. Over this region, there is little difference between the folding methods as stated earlier, the bandwidth-limiting becomes dominated by the lower bin number averaging reducing the effective bandwidth (N/P). Very low bin numbers are to be avoided, due to the serious roll-off as the bin duration exceeds the pulse width allowing in more noise.

Matched-filtering really comes into its own at large bin numbers as shown by the blue dots plot in Figure 3; above 250 bins in this example, the SNR uncertainty reduces.

Figure 4 plots the relative offset error/period ratio indicating the position of the pulsar pulse peak within the period data block. The red plot has been offset slightly to improve visibility where there is data overlap.

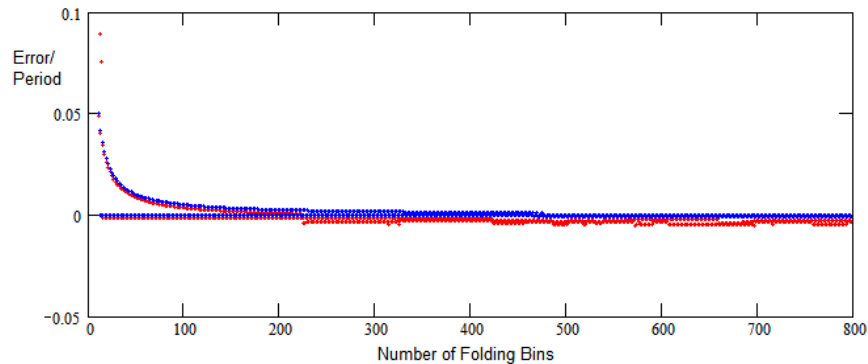


Figure 4. Vela Pulsar Pulse Bin Position Error v Number of Folding Bins, N .

The red, basic folding scheme shows increasing bin pulsar peak error uncertainty at higher bin numbers due to the reducing indicated SNR. Below about 150 bins, both schemes illustrate the effect of pulse energy being split

between adjacent bins, mainly driven by odd/even bin number values. For example, if the pulsar phase lies in the center of a period, it would be naturally either split by or fill a bin. No attempt was made to control the pulsar phase in this instance.

B0329+54 Pulsar Example SNR = 4.4:1, P/W ≈ 108

Figure 5(a) compares the two folding methods on much lower SNR data. The performance below 100 bins for both methods is again similar with the matched filter approach slightly superior. Here the ‘optimum’ bin number is ≈108. Above this bin number range the matched filter method dominates, but exhibits some wide SNR variation due to the increased noise level as a result of the low intrinsic SNR. Note that the basic method (red dots) does exhibit some tendency to respond to the predicted curve peak (green plot) at low bin numbers. Up to about 300 bins, the basic method median is showing some consistency with the expected \sqrt{N} SNR roll-off. This is confirmed in Figure 5(b) where the pulsar peak bin position error is very small. The matched-filter method shows much less peak uncertainty.

Above 300 bins however, the basic method red dots deviate from the theoretical green curve and appear to maintain a wide random range but level off in mean SNR at around 3:1. In this region, the pulsar pulse is swamped by the ambient noise peaks and it is these noise peak SNR values that are being reported as can be inferred from the error plots in Figure 5b.

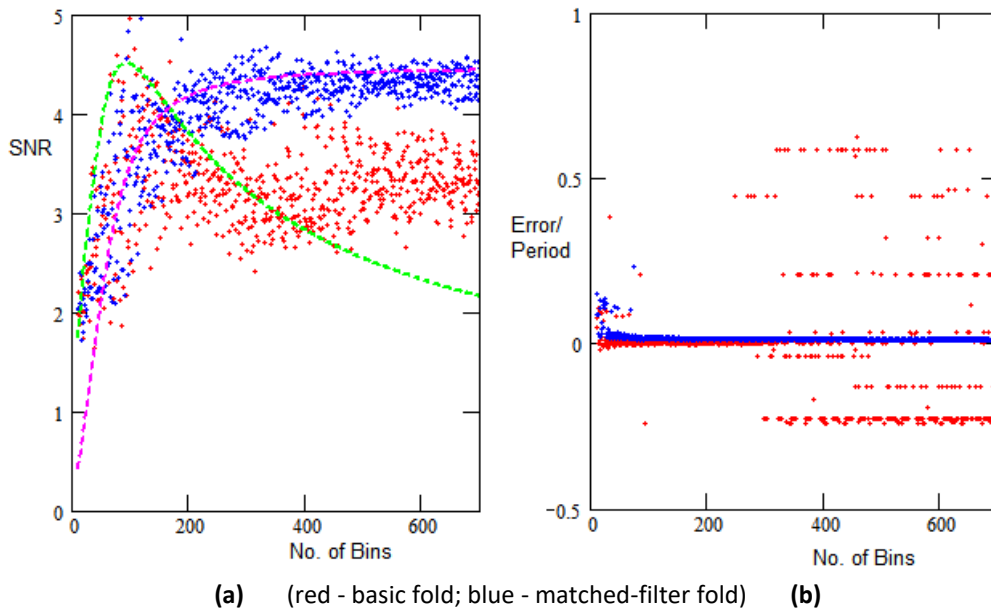


Figure 5. 4.4:1 SNR, B0329+54 Pulsar Data Result.

The bin errors in Figure 5(b) indicate a number of consistent error values. Basically, what is happening here is the noise level is rising above the pulsar level and certain bin noise peaks are capturing the peak detection function. Some actual folding plots are presented in Appendix 3 to support this conclusion.

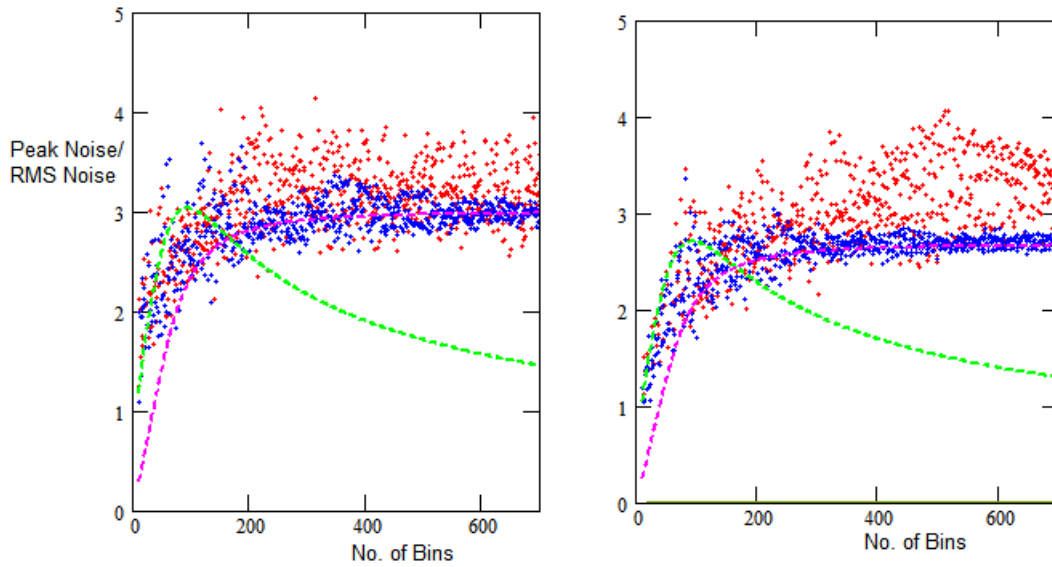
Effects of RFI and Low SNR

In general, the folding algorithm can cope quite well with low-level RFI, slightly raising the noise floor and similarly reducing the achievable SNR. Transient RFI and spectral lines should always be removed prior to folding.

In general, noise alone does not track the expected pulsar present theoretical curves.

The algorithm response to just noise is investigated in Figure 6. This plots the recorded data but with the period adjusted such that the pulsar pulse is spread out, effectively reducing the pulsar amplitude below the background noise rms level without significantly changing the folded noise statistics. Changing the B0329+54 search period by $4W/T \times 10^6$ parts per million, reduces the folded amplitude by a factor of 4; making it about equal to the noise rms level⁽²⁾.

It is evident from these entirely different data sets that there is a lot of similarity in the noise-only responses showing that the regular pulsar pulse has been effectively removed. What now is being indicated as SNR is actually, peak noise-to-rms noise ratio. Noise peak-to-rms noise ratio of between 2.5:1 to 3.0:1 is expected for Gaussian noise. Deviation from this range at low bin numbers, is probably due to the noise statistics varying from Gaussian to Binomial.



(a) Vela Data Noise (b) B0329+54 Data Noise
Figure 6. Noise-only Folding (red - basic folds; blue - matched-filter folds).

Considering the data medians, there is little evidence of the data following the green curve or its predicted peak and there is no sign of the basic fold data (red dots) undergoing any reduction in SNR. Indeed, over this region the SNR data is significantly different to the low real pulsar SNR plot of Figure 5(a). The reduced SNR uncertainty shown by the blue dot matched fold algorithm is due to the noise bandwidth reduction of the latter algorithm with increasing fold bin numbers and its more effective removal of quantization noise spikes (as evidenced by the increased noise spikes in the plots of Appendix 3).

The differences with pulsar present (Figure 5(a) - red dots) and absence (Figure 6(b) - red dots) for the basic algorithm are highlighted in Figure 7 (Figure 6(b) red dot noise-only data is now plotted as blue dots).

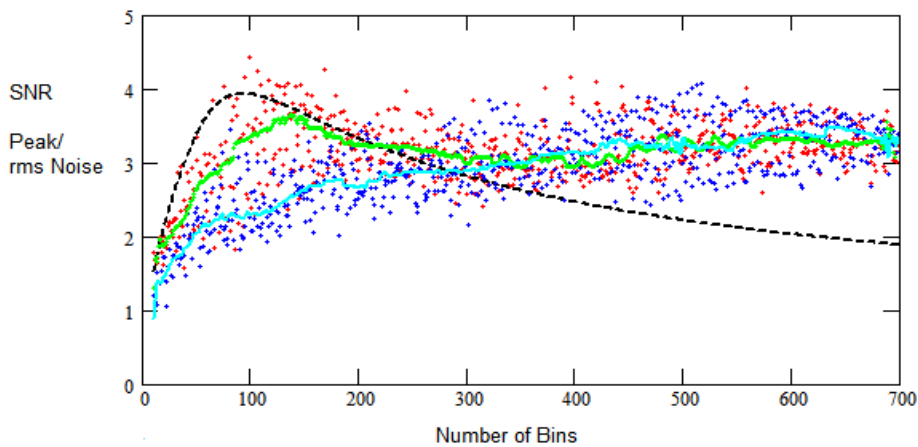


Figure 7. Basic Folding Only: red - 4.4:1 SNR B0329+54 pulsar data; blue - noise only; black- theory; green - pulsar data median; cyan - noise data median.

The red dots now show the actual SNR reported as a function of bin number with a 4.4:1 SNR pulsar pulse present and the blue dots peak noise-to-rms noise reported for the same data for noise only. As noted, to simulate noise only using the same data, the fold period is adjusted to spread the pulse out so reducing the pulsar amplitude below the background noise rms level.

Figure 7 shows that above 300 bins the statistics of both data sets are very similar. But below this bin number the pulse-present median data is somewhat larger. The differences are highlighted in the green and cyan curves which plot the computed data medians of the two data sets. These obvious median differences which follow the predicted curve suggest it might be useful as an added indicator for recognizing that a pulsar pulse train is actually present in the data.

Conclusions

This article has examined the folding algorithm and shown that the limitations of the basic folding concept can be overcome by matched filtering. Matched filtering as described here, operates on the basic fold algorithm output to limit the fold data spectrum to just pass the integrated pulsar pulse spectrum. This procedure is implied by the published pulsar radiometer equation. The theoretical SNR performance has been derived for both methods and are shown to prove reasonable matches to the two high and low SNR data examples tested.

The surprise bonus in doing this study was the unexpected capability of the basic folding method to show up the possible presence of a low level SNR pulsar, from plotting the data medians as seen in Figure 7. In addition, by indicating noise peaks in the correct range for Gaussian noise, it can be concluded that RFI is within acceptable limits.

Other articles on recognizing and validating low SNR pulsar detections can be found by following the link in Reference 3. Reference 4 links to the multiple bin folding software developed for this article.

References

1. D. Lorimer, M. Kramer. Handbook of Pulsar Astronomy. Cambridge University Press, 2005.
2. East PW. An Analytical Method of Recognizing Pulsars at Moderate SNR. Journal of the Society of Amateur Radio Astronomers. November-December 2018. p17.
3. Pulsar Astronomy Website. <http://www.y1pwe.co.uk/RAProgs/Pulsars.html>
4. Multifold Software. <http://www.y1pwe.co.uk/RAProgs/MultiFold.zip>

Appendix 1. Folding Integration Analysis

As shown previously, the indicated SNR is the ratio of the pulsar DC and the system noise AC terms, or

$$SNR = \frac{T_p}{T_{sys}} \cdot \sqrt{\frac{RP}{Nt_c}}$$

This equation is exact only when the pulsar pulse lies centrally in and fills a bin.

To take account of the pulse shape and effect on filling or not filling a bin, we need to integrate the samples within the bin where the pulse shape lies centrally.

If $p(t, W)$ describes the pulse, width W , shape, then the SNR contribution of the pulsar power in the bin is calculated

using the factor, $\frac{N}{P} \int_{-\frac{2N}{P}}^{\frac{2N}{P}} p(t, W) dt$ and the SNR for all bin numbers with no data filtering is given by,

$$SNR = \frac{T_p}{T_{sys}} \sqrt{\frac{RP}{Nt_c}} \frac{N}{P} \int_{-\frac{2N}{P}}^{\frac{2N}{P}} p(t, W) dt$$

As before, $1/t_c = \Delta f$, $t_{int} = PR$, this equation can be rewritten so that the predicted SNR for the basic folding algorithm now becomes...

$$SNR_{pred} = \frac{S_p A_e \sqrt{t_{int} \Delta f}}{2k_b T_{sys}} \frac{P-W}{W} \frac{\sqrt{N}}{P} \int_{\frac{P}{2N}}^{\frac{P}{2N}} p(t, W) dt$$

Assuming the pulse shape $p(t, W)$ takes a Gaussian form, $p(t, W) = e^{-4 \ln(2) \left(\frac{t}{W}\right)^2}$, using this approximation, calculation results in the green SNR curve in Figure 3; the tail-off at higher bin numbers is as expected, with no extra filtering or integration save provided by the basic folding algorithm.

The analysis of the matched filtered version is similar and using the same scaling factor is plotted as the magenta SNR curve in Figure 3. This relationship is set for equal response when $N = (P-W)/W$.

The predicted SNR for the enhanced folding algorithm now becomes...

$$SNR_{pred} = \frac{S_p A_e \sqrt{t_{int} \Delta f}}{2k_b T_{sys}} \sqrt{\frac{P-W}{W}} \frac{N}{P} \int_{\frac{P}{2N}}^{\frac{P}{2N}} p(t, W) dt$$

Digital integration of the term $\frac{N}{P} \int_{\frac{P}{2N}}^{\frac{P}{2N}} p(t, W) dt$, where $p(t, W)$ is the preferred Gaussian function

$p(t, W) = e^{-4 \ln(2) \left(\frac{t}{W}\right)^2}$. Computation can be made faster and easier using a numerical approximation function. A useful substitution in the present instance is Bell's approximation,

$$\frac{N}{P} \int_{\frac{P}{2N}}^{\frac{P}{2N}} p(t, W) dt \rightarrow \frac{\sqrt{\pi} 0.6 W N}{P} \sqrt{1 - e^{-\left(\frac{P}{\sqrt{\pi} 0.6 W N}\right)^2}}$$

Appendix 2. Matched Fold Filtering

Figure A1 lists the MathCad code to apply matched filtering to the data to optimize detection of a pulsar in the final data fold. The displayed signal-to-noise ratio is then no longer dependent upon the number of fold bins.

```

M_Fil(P, W, Fold_Dat, N) :=
  for n ∈ 0.. N - 1
  |
  | dat_n ← Fold_Dat_n
  |
  | gau_n ← exp [ -4 · ln(2) ·
  |               ( (n - N/2) / (W · N/P) )^2 ]
  |
  | fdat ← cfft(dat)
  | fgau ← cfft(gau)
  | for n ∈ 0.. N - 1
  |   mfdat_n ← fdat_n · ( fgau_n / fgau_0 )
  | tdat ← icfft(mfdat)
  | Re(tdat)

```

Figure A1. Matched Pulse Filtering MathCad Code.

Appendix 3. B0329+54 Low SNR Folding Results

Figure A2 illustrates the folding results with various bin numbers. Red plots are the basic fold results and blue the matched filtered results. Note the increase in noise for the basic method and the gradual SNR improvement and increased resolution with matched filtering. Near identical performance is observed for 108 bins, as at and below this number the folded spectrum is controlled more and more by increased bin averaging. Data has not been bin-centered.

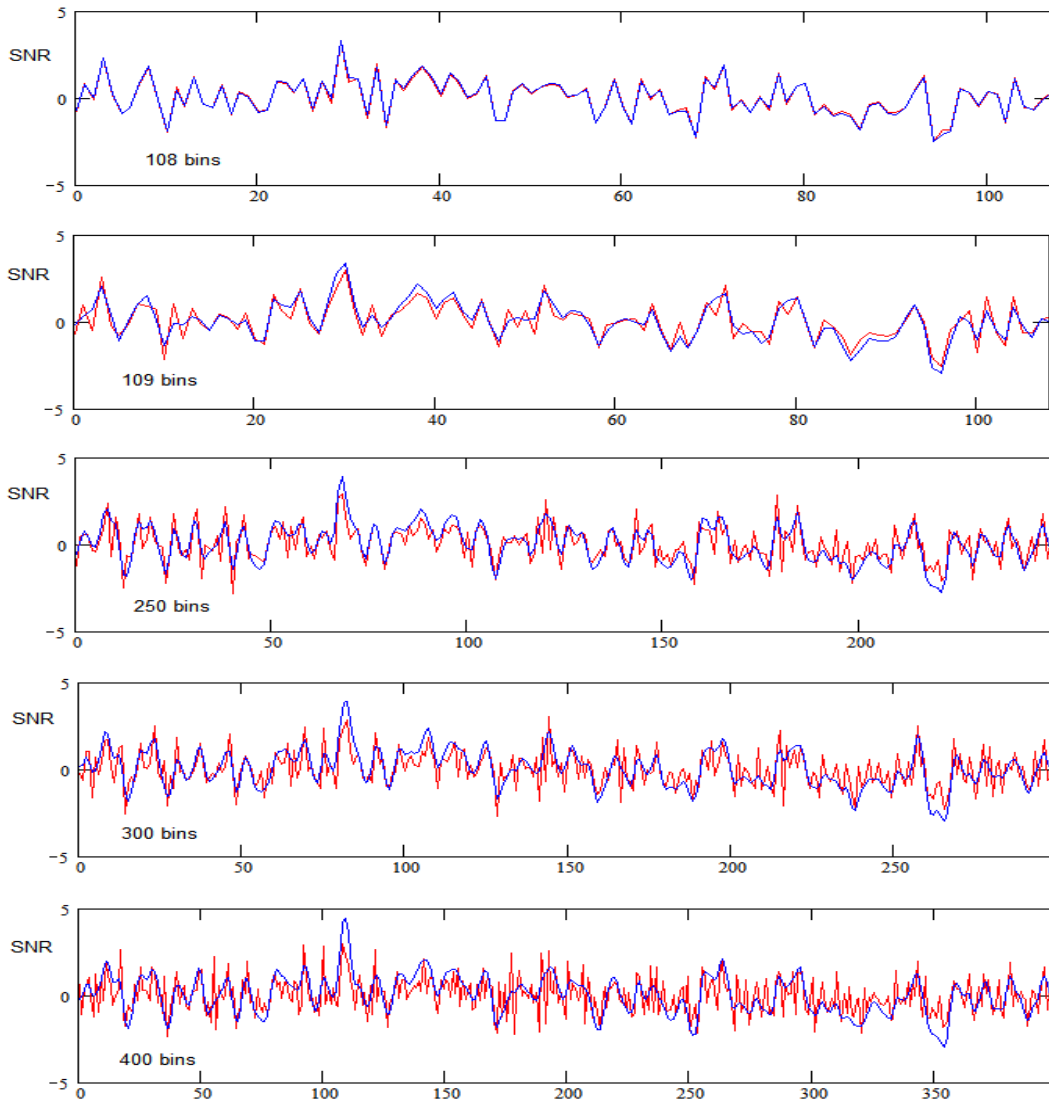


Figure A2. B0329+54 Comparison of Fold Methods Responses for Various Bin Numbers.
red - basic fold method; blue - matched folding method



Peter East, pe@y1pwe.co.uk is retired from a career in radar and electronic warfare system design. He has authored a book on Microwave System Design Tools, is a member of the British Astronomical Association since the early '70s and joined SARA in 2013. He has had a lifelong interest in radio astronomy; presently active in amateur detection of pulsars using SDRs, and researching low SNR pulsar recognition. He encourages free information exchange in the amateur community and is keen to widen interest in radio astronomy generally. He maintains an active RA website at <http://www.y1pwe.co.uk>

P W East June 2021

Observation of HF Sudden Frequency Deviation on 22 May 2021 Whitham D. Reeve

A Sudden Frequency Deviation (SFD) is a change in the received frequency of a fixed carrier caused by rapid changes in Earth's ionosphere from a solar flare. SFD concepts are discussed in detail in {Reeve15}. In the observation discussed here (figure 1), the carrier was from the WWVH 15 MHz time-frequency transmitter located approximately 4 km up the beach from Kekaha, Hawaii. The receiver station includes an Icom R-8600 wideband receiver connected to an 8-element KMA-1832 log periodic dipole array in Anchorage, Alaska. Argo software captured the demodulated carrier and showed a +2, -10 Hz deviation over a period of about 6 min.

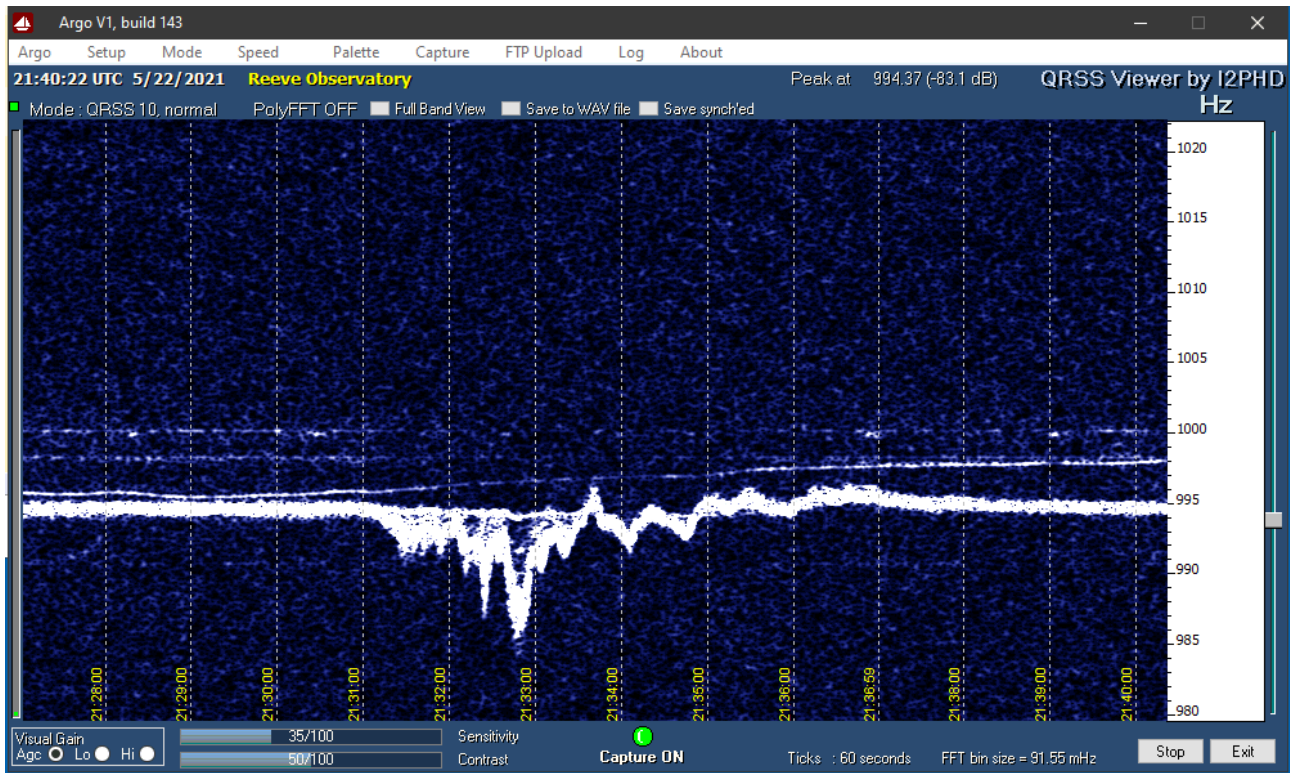


Figure 1 ~ The thick white trace is the WWVH carrier demodulated to 995 Hz over the time period 2127 to 2140 UTC. Frequency is shown on the right vertical scale. The signal shows several cycles of rapid frequency change with the largest negative peak of 10 Hz just before 2133. The faint traces are spurious signals.

The SFD likely was caused by a solar x-ray event in active region 2824 that produced an M1.4 flare observed from 2130 to 2136 UTC. See {SWPC-FCST} and {SWPC-EVNT} for 22 May 2021. The effects can be seen in the SFD trace from 2131 to 2136. Radio effects of the flare also were observed at Anchorage during this time period up to 415 MHz.

References & Weblinks:

- {Reeve15} http://www.reeve.com/Documents/Articles%20Papers/Propagation%20Anomalies/Reeve_SuddenFreqDevConcepts_P1.pdf
- {SWPC-FCST} <ftp://ftp.swpc.noaa.gov/pub/forecasts/discussion/>
- {SWPC-EVNT} <ftp://ftp.swpc.noaa.gov/pub/indices/events/>

Sky raster fly map with satellite rotors, DiSEqC-controller and CALLISTO

Christian Monstein

The goal of this project was to find a cheap and easy solution to map the sky, based on low-cost hardware and home brewed software. The basic idea was born with the previous article, published in the SARA journal [1]. For purely demonstration purposes, the plan was to map an area of several thousand square degrees on the sky where geostationary satellites are located and are transmitting in the Ku-band 10.7 GHz to 12.75 GHz. The system uses inexpensive components such as a low noise block down-converter (LNB) with a noise figure < 1dB and a small offset-dish antenna. My antenna was only 37 cm diameter and was mounted on top of two custom-mounted TechniSat DiSEqC (Digital Satellite Equipment Control) [2] satellite dish rotators (figure 1).



Fig. 1: Small 37 cm diameter offset dish antenna with a Ku-band LNB attached to two orthogonally mounted satellite dish rotators.

Modern professional radio telescopes provide many beams in parallel (opticians would say pixels) while an amateur radio-telescope like the one shown in figure 1 provides only one beam or one pixel. Therefore, the only way to image an area of the sky is to scan the area of interest, hoping that neither the image nor the background change too much during the observation time, which in my case is more than two hours.

An annoying problem is the antenna angle calibration because one cannot 'see' anything through such a telescope. The easiest procedure in my case was to calculate the position of the Sun in azimuth and elevation and then to manually adjust the whole antenna assembly so that the sunlight is projected to the cover of the LNB. The LNB was covered with a white paper while a small mirror was taped to the dish centre. When the antenna is adjusted so the sunlight is centred on the LNB, I know that both the azimuth and elevation angles are calibrated and measurement of the to-be-scanned area can start.

The scanning is controlled by a Python [3] script running on a PC that calculates the scanning positions, sends the angles to the rotors and collects measurements of the radio intensity from the CALLISTO spectrometer. The script sequence is to scan in elevation in 1° increments from about 10° to 70°, stop the elevation scan, increase the azimuth by 1° and then scan from 70° to 10° elevation; this process is repeated from an azimuth of 130° to 200°. The spectrometer in this experiment was set to a fixed frequency of 10385.75 MHz with support from a heterodyne down-converter (figure 2).

The measurement parameters of the spectrometer were as follows: Integration time 1 ms and observation bandwidth 300 KHz. To stabilize the whole setup with respect to vibration, each angular pixel was delayed by two seconds before a measurement was taken.

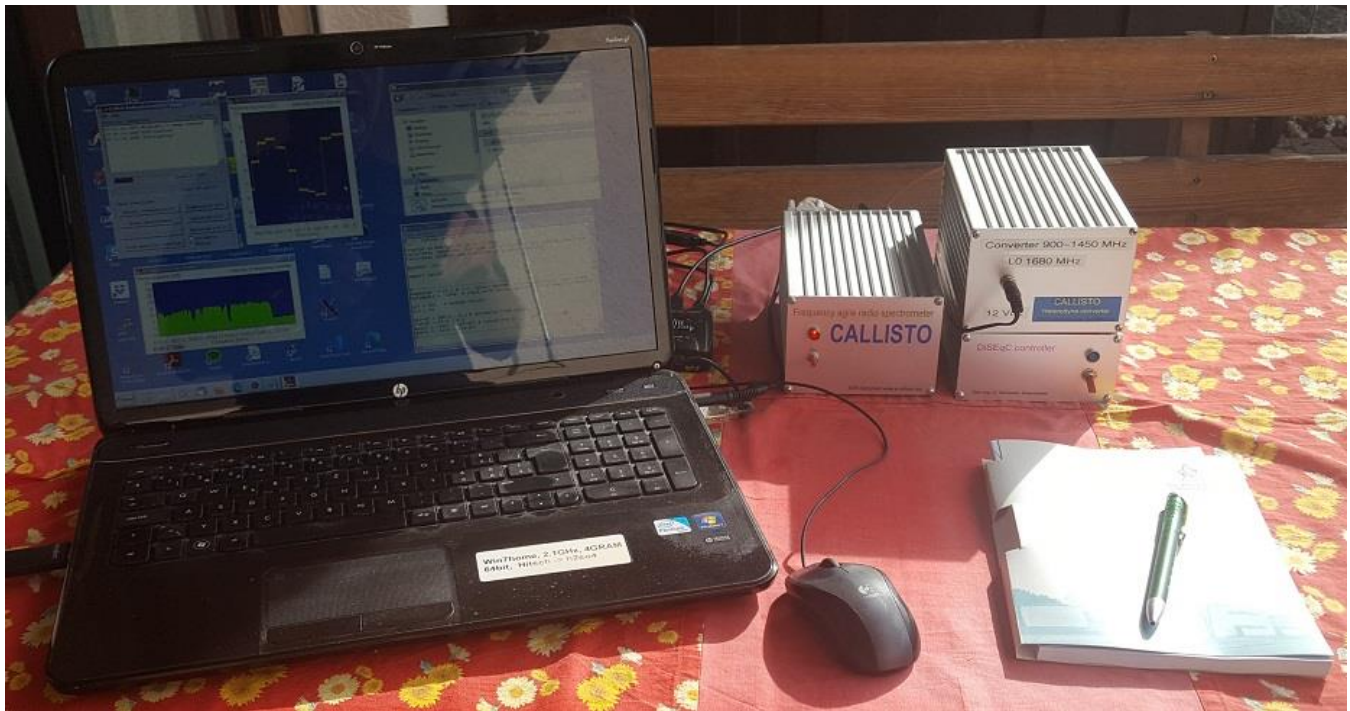


Fig. 2: Notebook (left) to control the spectrometer and satellite rotors. In the centre is the CALLISTO frequency agile spectrometer and on the right side is a heterodyne frequency down-converter (upper unit) to shift the LNB intermediate frequency (IF) output from the L-band down into VHF/UHF range for the CALLISTO. Below the converter is my DiSEqC control unit, which control the two satellite rotors in azimuth and elevation.

Once the script is started, operation is fully automatic, and I just need to wait for the end of the scanning process which required more than two hours. After that, the comma separated variable (CSV) compatible data file produced by the control PC was transported to another PC in the office running a dedicated Python script. This script reads the CSV-file and generates a two-dimensional matrix out of the one-dimensional file and also

generates the plots shown in figures 3 to 5. The plots in figure 3 and 4 are quality control plots that show the raw data as read from the CSV-file. These are used to determine if data are possibly missing or wrong. Plot 3 shows an xy-plot of elevation as function of azimuth for the scanned area while figure 4 shows the individual angles for quality control.

In figure 5 we get the final result, a raster fly map of the southern sky at my location in Freienbach, Switzerland (Grid Locator JN47je). It is interesting to see that individual satellites show differences in radio brightness or intensity. There may be several reasons for this. For example, the polarization of the LNB feed was fixed for all measurements while the polarizations of the satellites may be different. Another reason might be unequal transmission power of the satellites. In fact, there are more satellites inside the bright spot in the centre of the image than labelled. It also is interesting to see the hot house of my neighbour which radiates on the order of 300 kelvin, much more than the radiation temperature of the so-called cold sky, which is just a few kelvin.

To avoid any interference from the Sun, the observations started after transit of the Sun, otherwise I would expect a smeared area where the sun is moving while the scanning process is taking place. Another detail is the processing of the plot. Intensities are plotted on a logarithmic scale; otherwise, it would be difficult to see the hot satellites on the same plot with the neighbour's warm home.

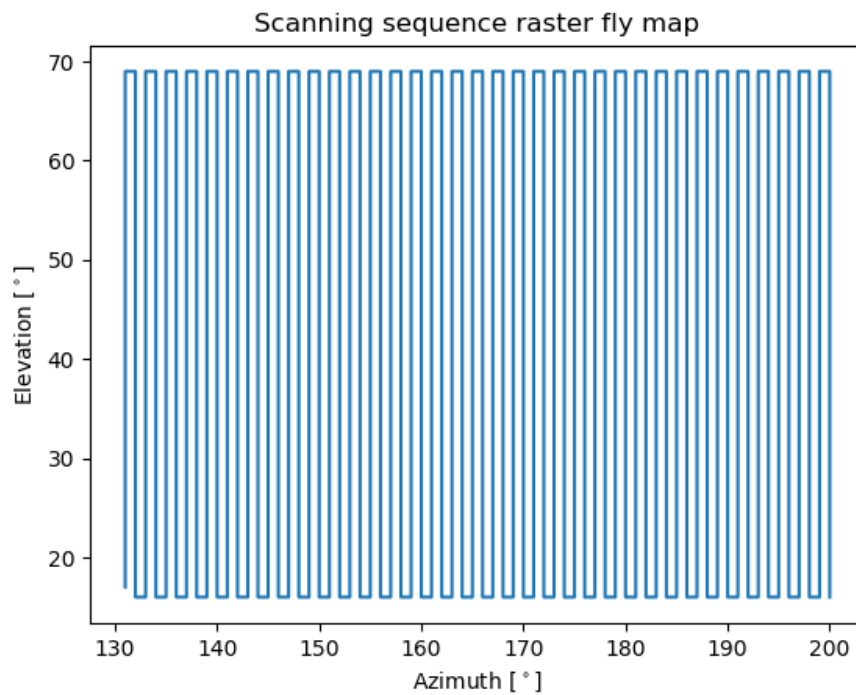


Fig. 3: Scanning strategy to map a sky area of ~3850 square degree. Start bottom left, end of the scanning process bottom right. Resolution in both angular directions is 1°, as determined by the resolution of the satellite rotors.

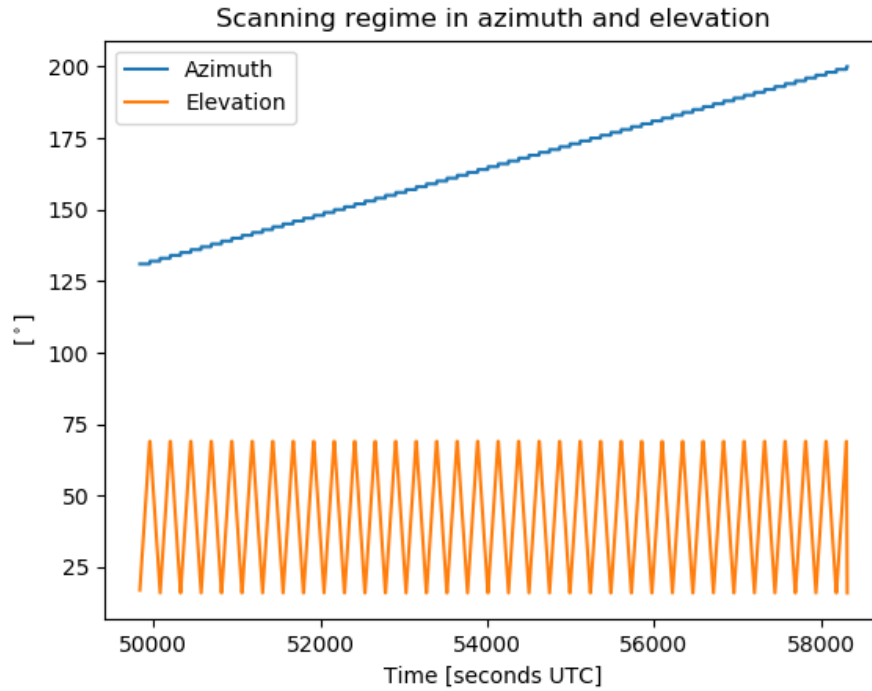


Fig. 4: Azimuth and elevation as function of time. From the x-axis we can derive the total measurement time of about 8100 s = ~2.25 hours.

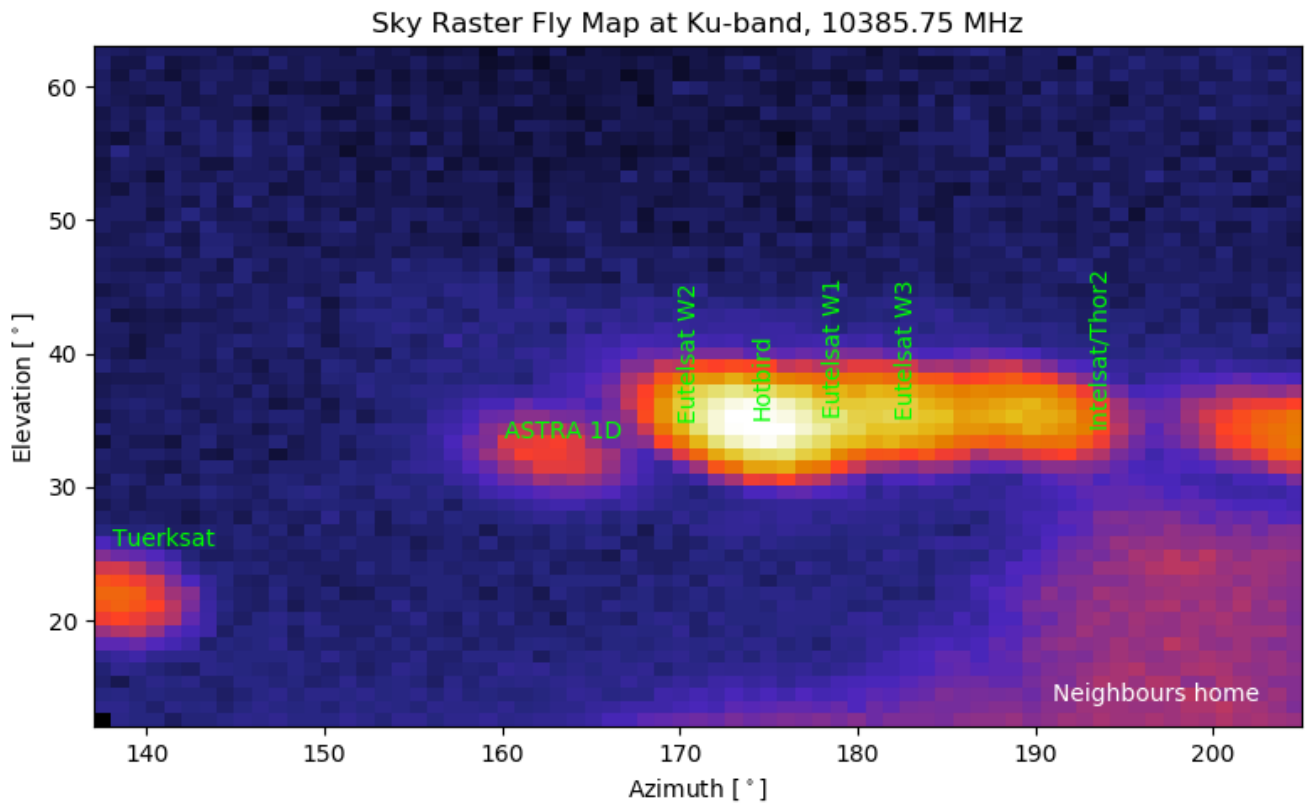


Fig. 5: Resulting map generated with Python showing several satellites and our neighbours home radiating with an equivalent temperature of about 300 kelvin. Spot size of a satellite corresponds nicely with the main beam size

given by the equation $70^\circ \lambda/D = 5.5^\circ$. Satellites at the distance of geostationary orbit can be seen by radio astronomers as point sources. Therefore, such plots show the antenna beam pattern. In fact, it is the convolution of the real beam pattern with a point source.

References:

- [1] Monstein, C., DiSEqC Low Cost Antenna Tracker, Radio Astronomy, Society of Amateur Radio Astronomers, November-December 2019
- [2] DiSEqC: <https://en.wikipedia.org/wiki/DiSEqC>
- [3] Anaconda/Spyder: <https://www.anaconda.com/>



Christian Monstein is a native of Switzerland and lives in Freienbach. He obtained Electronics Engineer, B.S. degree at Konstanz University, Germany. Christian is a SARA member and is licensed as amateur radio operator, HB9SCT. He has 21 years of experience designing test systems in the telecommunications industry and is proficient in several programming languages including C++, IDL and PYTHON. He has worked at ETH-Zürich on the design of a noise transmitter as payload on a drone and is responsible for the hardware and software associated with the e-

CALLISTO Project. He plays also the role of a coordinator of SetiLeague in Switzerland and he is also representing Switzerland within CRAF. He is a member of the ISWI steering committee at UN office for outer space affairs in Vienna (UNOOSA) and has just been nominated as member of ITU. Email contact:

christian.monstein@irsol.usi.ch

Observation of VHF Type II Solar Radio Burst on 28 May 2021

Whitham D. Reeve

Compared to a year ago, the Sun was very active throughout May 2021, when numerous solar radio bursts were observed around the world by the e-CALLISTO solar radio network {[e-CALLISTO](#)}. Type II bursts were observed at Cohoe Radio Observatory in Cohoe, Alaska late in the UTC day on 28 May (figure 1). Type II slow-drift radio emissions quite often accompany coronal mass ejections (CME), which, if directed toward Earth, can cause geomagnetic disturbances. For a more comprehensive discussion of Type II bursts, see {[Reeve18](#)}.

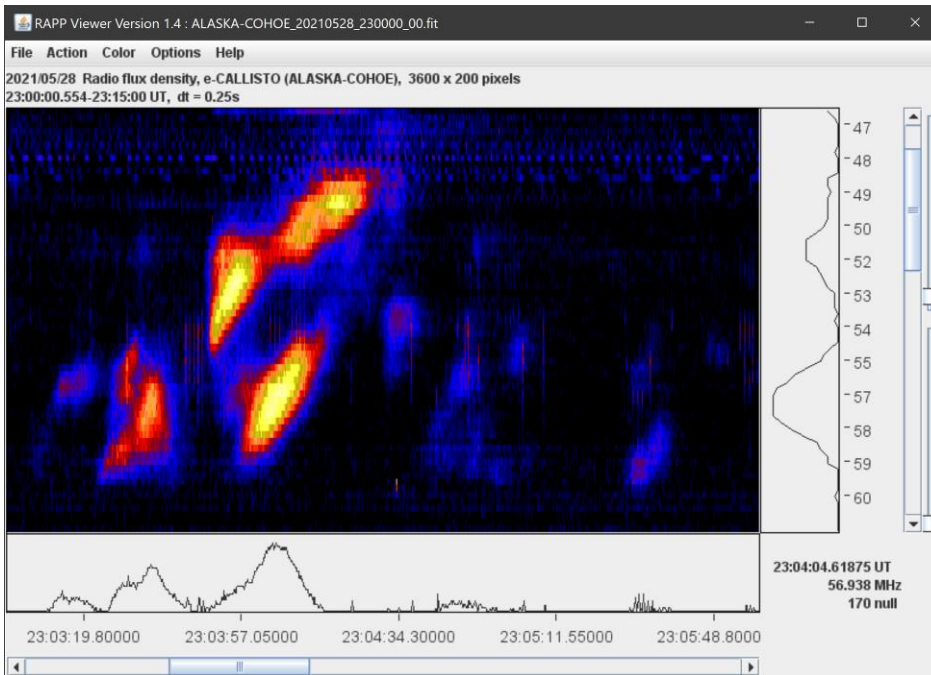
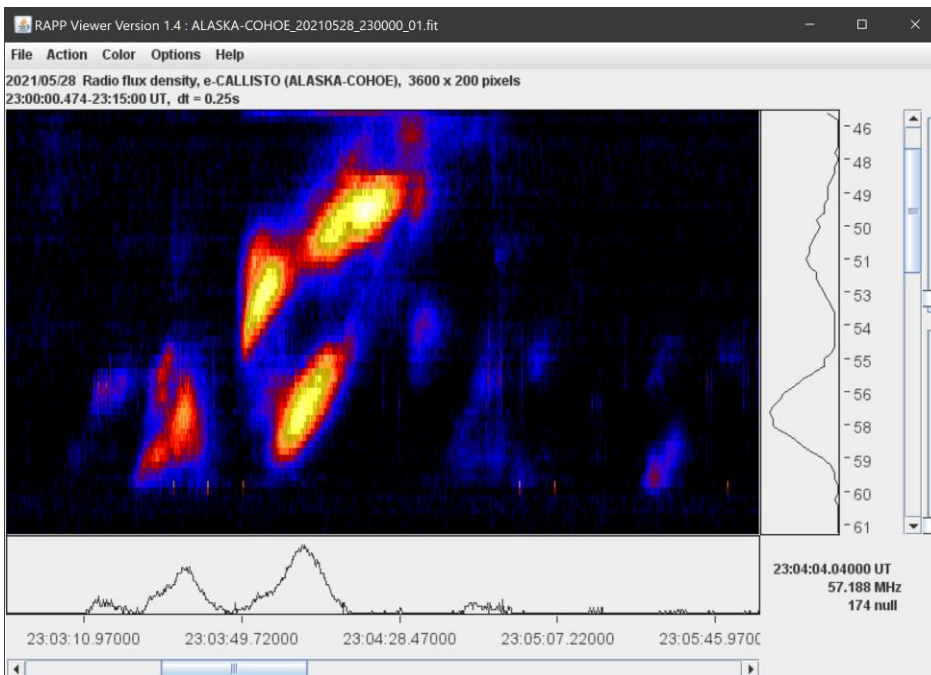


Figure 1 ~ Type II slow-drift radio bursts between 47 and 62 MHz. Upper: Right-Hand Circular Polarization (RHCP). Lower: Left-Hand Circular Polarization.

Absorption is seen as dark regions in the Type II burst on the left side of the image. The spectrograms indicate that both polarizations have approximately the same intensity. Band-splitting was present, but no harmonic structure is seen in the observed frequency range of 45 to 92 MHz (only a portion of the frequency range is shown here).



Frequency in MHz is shown on the right vertical scale and time in UTC is on the horizontal scale at the bottom. The colors indicate relative intensity with black being lower and yellow being higher. The text in the lower-right corner indicates the time, frequency and relative power of the cursor location when the image was taken (the cursor is not visible in these images).

The faint blue band near the top of the upper image is interference.

These images are screenshots of the RAPP Viewer software.

According to Space Weather Prediction Center {[SWPC-EVNT](#)}, the event involved solar active region 2824 and also produced Type IV radio continuum and Type VI radio emissions (series of Type III fast-drift bursts), a coronal mass

ejection (CME) and a proton event. The CME was observed as a transient on the Anchorage SAM-III magnetometer at 1332 UTC on 2 June. The initiating agency was a long-duration C9.4 x-ray event with optical flare observed in Hydrogen- α . Although not shown in the truncated spectrograms above, the 2300 to 2315 time period included Type III bursts and some weak polarized continuum (probably the Type IV mentioned by SWPC). See {SOLAR} for information on the types and characteristics of solar radio emissions.

An LWA crossed-dipole antenna and two Callisto instruments were used for these observations (figure 2). The Callistos have an observation bandwidth of 300 KHz and an integration time of 1 ms per pixel. The Callisto software collects data as Flexible Image Transport System (FITS) files, which are stored locally. The files also are uploaded automatically to Fachhochschule Nordwestschweiz (FHNW) University of Applied Sciences & Arts website {FHNW} for permanent storage.

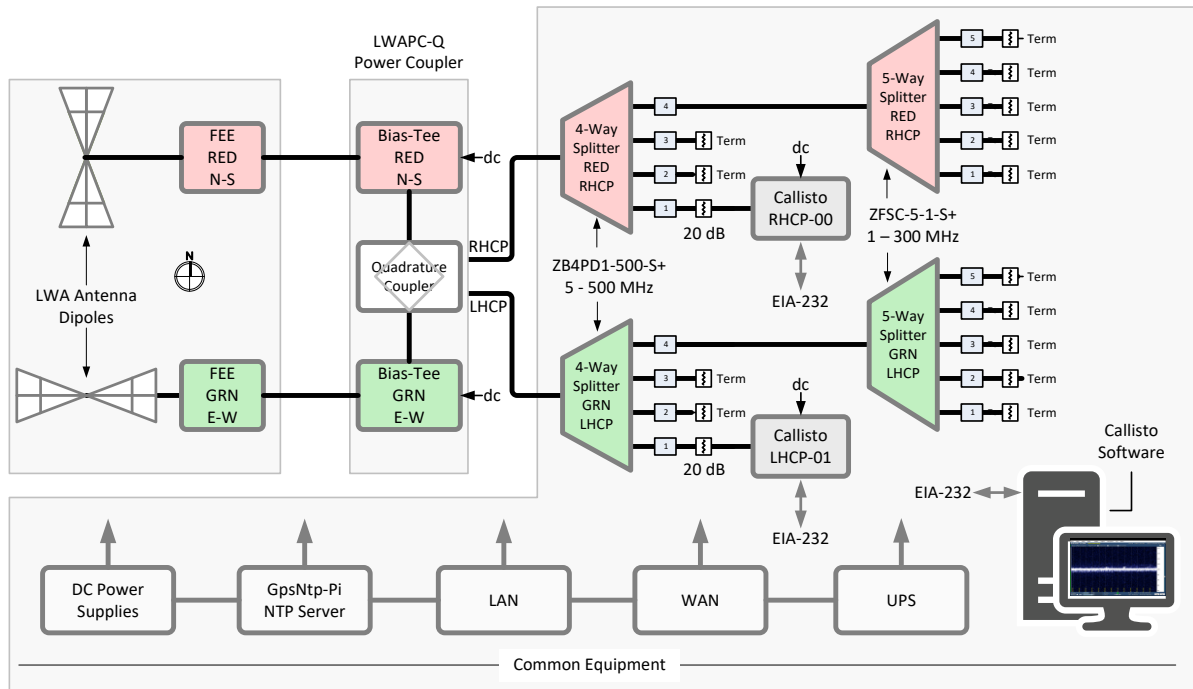


Figure 2 ~ System block diagram shows the components associated with the LWA Antenna and Callisto instruments and the common equipment shared across the observatory. Polarizations are color-coded. The Callistos are frequency agile and programmed to sweep through 200 channels between 45 and 92 MHz every 250 ms; the channel resolution is 250 kHz. The data are collected by the Callisto software through EIA-232 serial interfaces and formatted as FITS files for archiving.

References & Weblinks:

- {e-CALLISTO} http://soleil.i4ds.ch/solarradio/data/BurstLists/2010-yyyy_Monstein/2021/e-CALLISTO_2021_05.txt
- {FHNW} <http://soleil.i4ds.ch/solarradio/callistoQuicklooks/>
- {SWPC-EVNT} <ftp://ftp.swpc.noaa.gov/pub/indices/events/>
- {Reeve18} http://www.reeve.com/Documents/CALLISTO/Reeve_Typell-Burst.pdf
- {SOLAR} <http://www.reeve.com/Solar/Solar.htm>

Poor man's amateur radio astronomy with small dishes.

Job Geheniau

Abstract

The JRT (Job's Radio Telescope) is a 1.5-meter dish for the 21 cm band detection of neutral hydrogen. Recently, a 1.25-meter satellite dish for the 2 cm KU band 12 GHz has been added to the arsenal.

In my article I will describe highlights, but also problems that can (and will) occur with small radio telescopes.

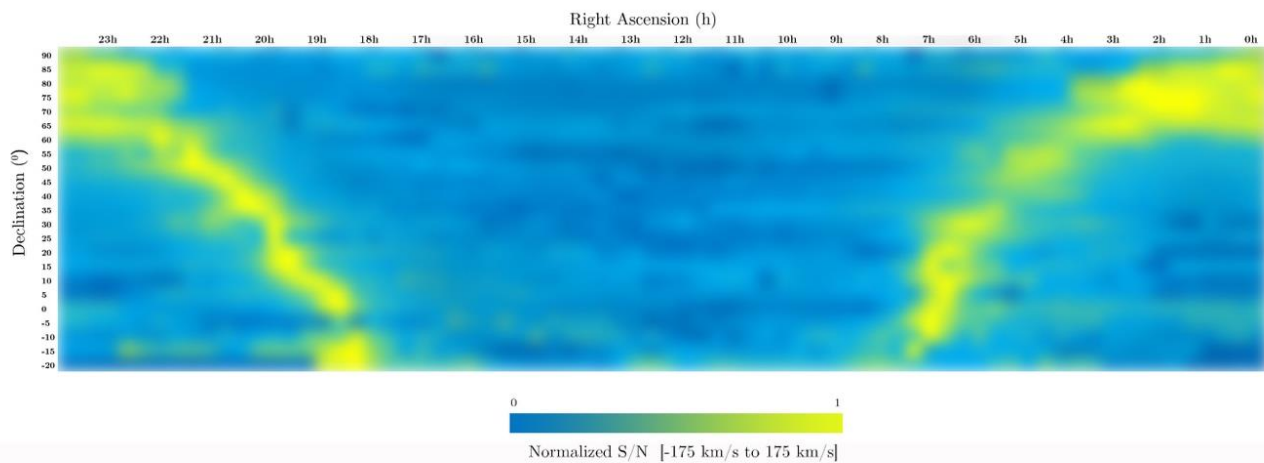
Because the telescopes are relatively small and fully remote controlled (50 km away) and placed on a rotator, you can imagine that it is quite a challenge to get to reasonable results.

I will write about my biggest project, The Northern Hemisphere Survey at 21 cm and the Milky Way rotation curve, the Milky Way in 3D with the JRT, but also Maser detection and what can go wrong, as well as meteor scattering, moon bounces, sun eclipses and much more.

A few important formulas and of course some nice results (Figure 1).

By the way, I am Dutch and English is not my native language. I am an radio astronomy amateur and not a scientific publisher, so sometimes the English is not perfect in this article.

JRT - Job's 1.5 meter Radio Telescope - Northern Sky HI (Neutral Hydrogen) Survey
derived from 1656 spectra 5 minutes each.



Job Geheniau, The Netherlands - October/November 2020

Figure 1: Northern Sky HI Survey with JRT

Introduction

My name is Job Geheniau, 55 years old and I live in the Netherlands.

After throwing in the towel a few years ago regarding visual perception and recording, I have been pleasantly surprised with the possibilities of radio astronomy for several months.

As a young student I was sometimes involved with the "illegal" 3-meter band, building transmitters and using them and I studied electrical engineering for a while. So I have some knowledge of things such as transmitters, receivers, antennas, etc. For example, in addition to radio astronomy, I started receiving weather satellites on the 2-meter band - 137 MHz (NOOA, MeteorM2 and Fengyun 3B) and the space station ISS with its ISS SSTV broadcasts with a self-built QFH antenna. Figure 2,3 and 4.



Figure 2: Several antennas I use beside my dish



Figure 3: ISS SSTV received

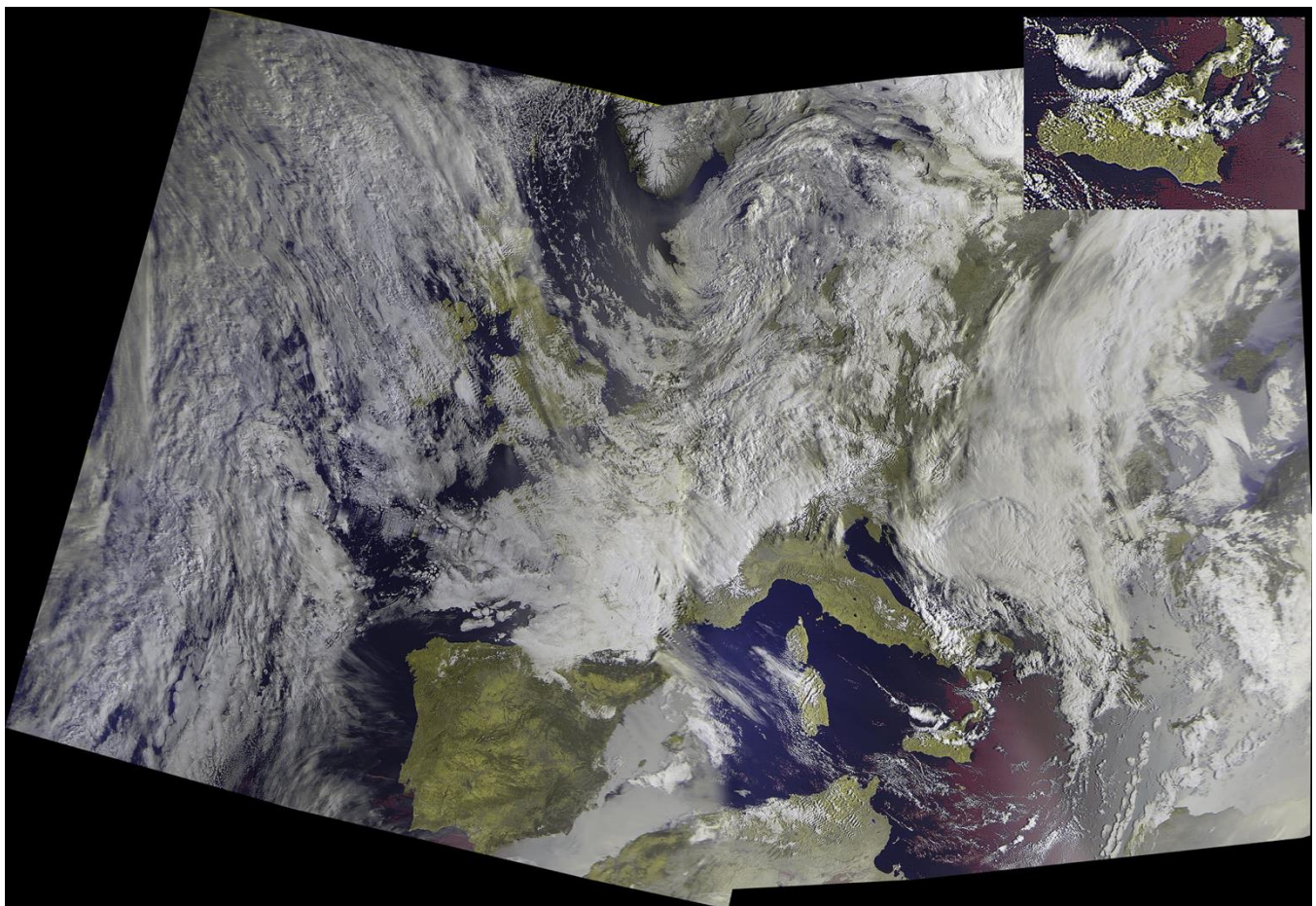


Figure 4: Recording of 3 Russian weather satellite Meteor M2 passes

Then I started to try to receive Meteor Scatter (ionization traces) (Figure 5) on the 2-meter and 6-meter band. 143 MHz and 50 MHz. For this I use two 4 elements Yagi Antennas. These capture the reflection of a meteor ionization trace from 2 well-known beacons, namely GRAVES (> 40 KW) in France and BRAMS/Dourbes in Belgium (150 Watt). I won't go into too much detail about that, but a nice extra is that it is possible to receive an EME (Earth, Moon, Earth) reflection from the GRAVES transmitter. GRAVES emits pulses of about two seconds and you can clearly see the pulses and the associated Doppler effect in the spectrum because the moon moves in the recorded time. In the Figure 6 you can see the moon reflective, some planes (oblique lines) and some small meteor ionization traces (vertical lines).

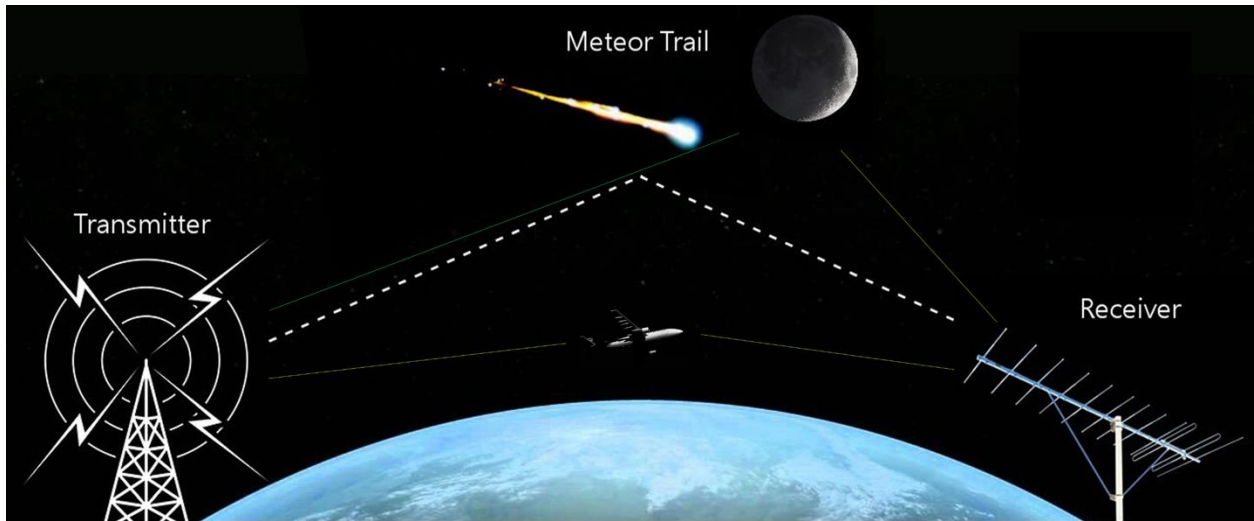


Figure 5: Principle of meteor scatter, moon and airplane reflection

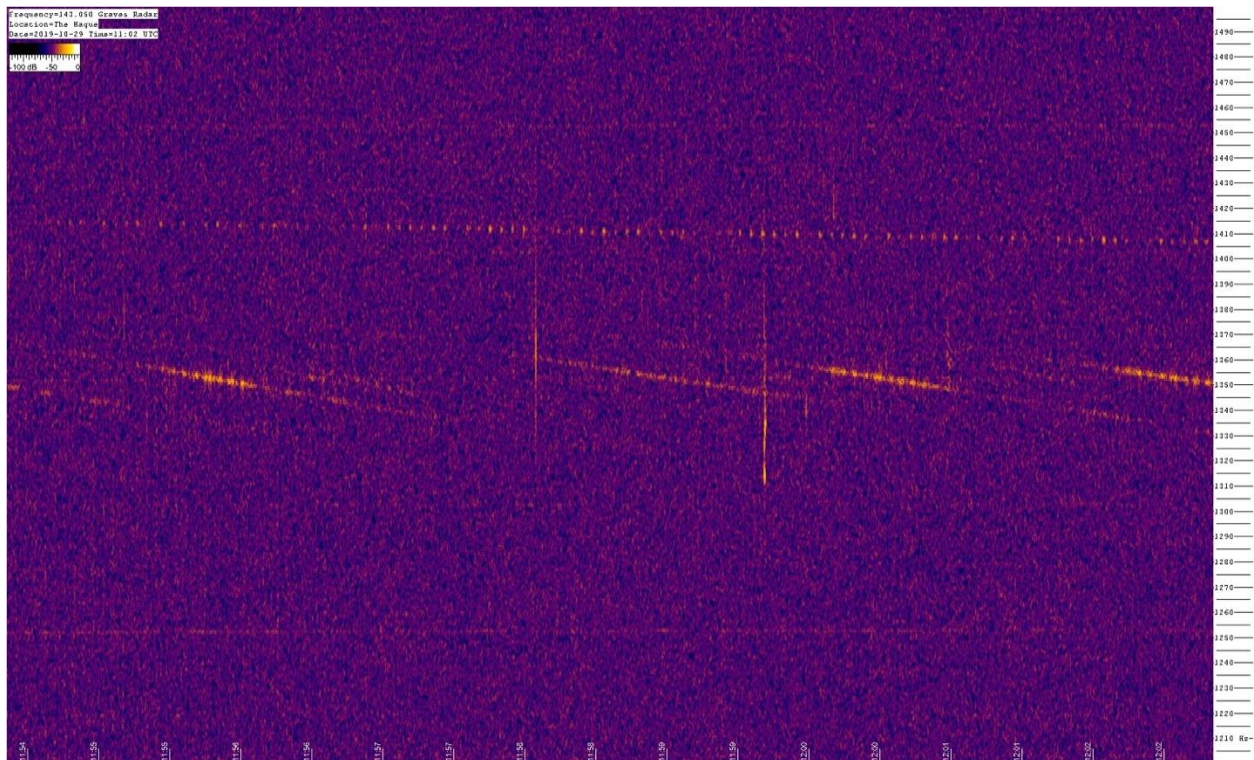


Figure 6: Spectrum of meteor scatter and EME moon reflection.

But after that, a long-awaited dream came true. The purchase of a 1.5-meter RF Hamdesign radio dish with rotator.

Hardware



Figure 7: JRT, Job's Radio Telescope with extra mesh and rotator. Can feed and the LNA's/filters in black box

I started building that "small" radio telescope. My goal was to make everything work automatically, remotely and autonomously as much as possible (while I'm writing this article on vacation, I can view the status of the telescope online and start an observation via the laptop). I chose a 1.5-meter telescope from RF Hamdesign (a kit) because of the limited space on my roof. The receiver (Feed) is a so-called can feed with the 1420 MHz probe. Figure 7.

Since I am going to control everything remotely, I decided to add an Azimuth-Elevation rotator (SPX-02 from RF-Hamdesign). This rotor can track the object with an accuracy of 0.5 degrees. The more expensive one can track at 0.1 degrees. Then directly behind the feed (because the signal is extremely weak) the amplifiers and a bandpass filter must be placed. After a lot of experiments, I built the following construction:

A LNA (Low Noise Amplifier) from Mini Circuits (ZX60-P33ULN +), then a bandpass filter to filter out interference (1300-1700 MHz) and then a second LNA from Mini Circuits.

All this fed by a second bias-tee (which supplies the LNA's with voltage without disturbing the signal). The Mini Circuits LNA's operate on 3.3 volts so there is a second bias-tee with LM117 voltage regulator from + 5 Volt to +3.3 Volt. Figure 8.

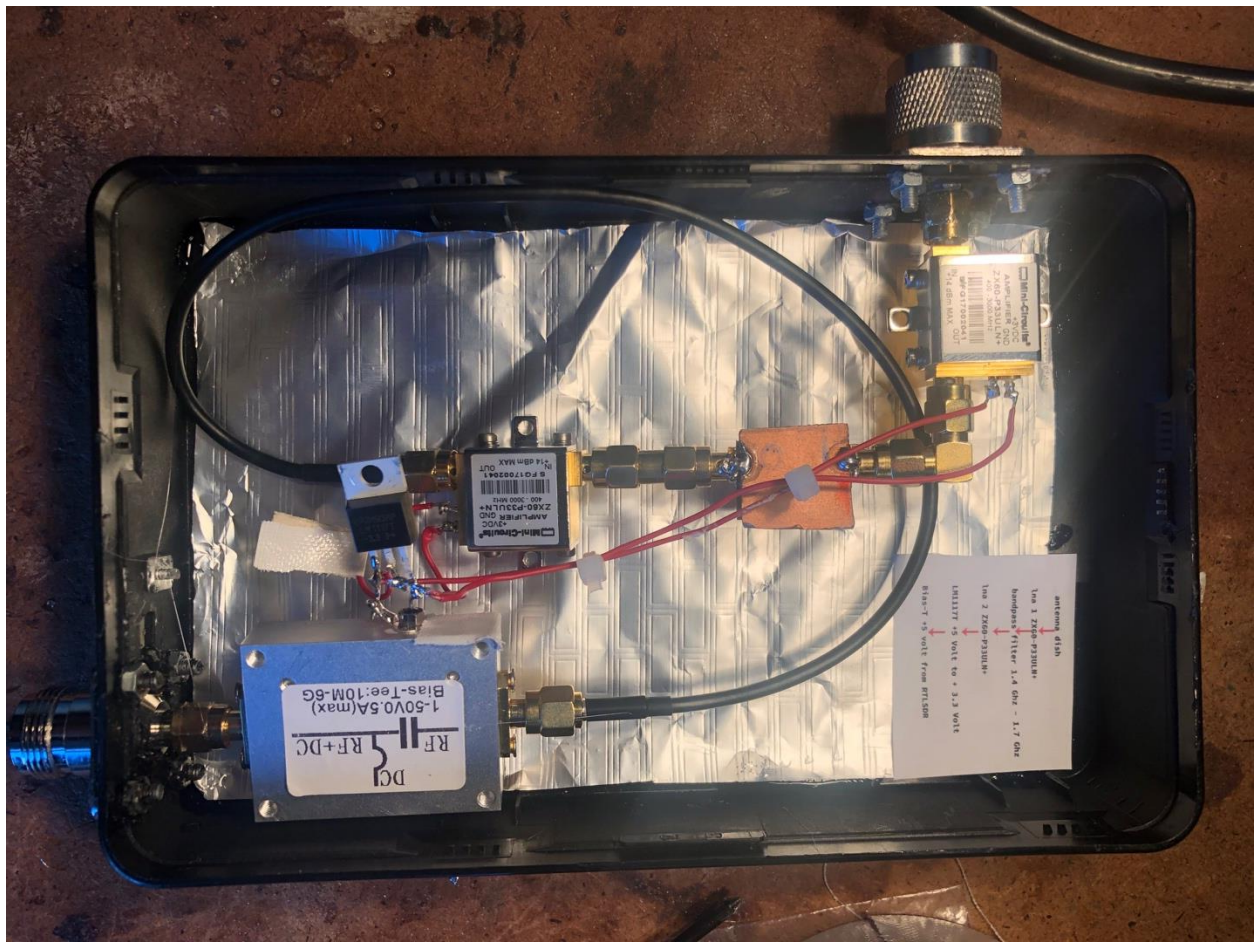


Figure 8: LNA's, bandpass filter and bias-tee

Via a 15-meter Coax cable, the signal enters the laptop to a RTL-SDR or Airspy Mini (a USB radio receiver).

Initially, I set up everything on the roof of my home in The Hague. It was a difficult job to walk with concrete blocks with a backpack over a roof edge of 12-meters high and 15-cm wide to reinforce the whole buildup for heavy winds. Unfortunately, it soon became apparent that the interference (RFI - Radio Frequency Interference) was so high that observations were impossible, and I had to remove the whole construction again!

Fortunately, my parents (80 years old) were willing to give up a place on their barn in the Haarlemmermeer for my dish (my father continues to call it 'Het Vergiet' 'The Colander').

The entire radio telescope and software can be operated fully automatically via Teamviewer/Chrome Remote and a resettable Internet repeater via WiFi. The computer can also be reset remotely, with an autostart when the power is switched on. To be less troubled by ground radiation and to improve the sensitivity, I managed to increase the dish diameter to about 1.9-meters with pieces of mesh.

Software

In radio astronomy, the final result is a file with collected data. This is usually the measured frequency versus the measured signal-to-noise ratio.

There are two main programs to make the signal visible. One method uses the program SDR# (SDR SHARP). My preference is the self-written program (in Python) of the Greek student Apostolos Spanakis Misirlis: VIRGO.

<https://github.com/OxCoto/VIRGO>

The disadvantage of this program is that it has proven impossible to use an Airspy Mini SDR under Windows 10, so the maximum bandwidth is 2.4 with a RTL-SDR. This because I need PsT Rotator and that application only runs under Windows.

So, when I want to use a bandwidth of 6 MHz I use SDR#, with my own Python scripts and an Airspy Mini.

Because I had a few extra requirements for the program, it has been adjusted over time and I later started programming in Python myself to make new adjustments. I have also written new Python programs in recent months to simplify and speed up the processing of data. Eduard Mol also helped me, among other things, with an explanation about data processing in Excel, a very handy tool for this type of data handling.

The dish is controlled with the PsTRotator program. This is an extensive program in which you can even control the dish with Python commands. The freely available program Cartes du Ciel or Radio-Eyes is linked to PsTRotator to allow the dish to track objects. It's a pity that Stellarium can't control PsT Rotator (yet).

Remote Control from The Hague, with webcam, Figure 9.

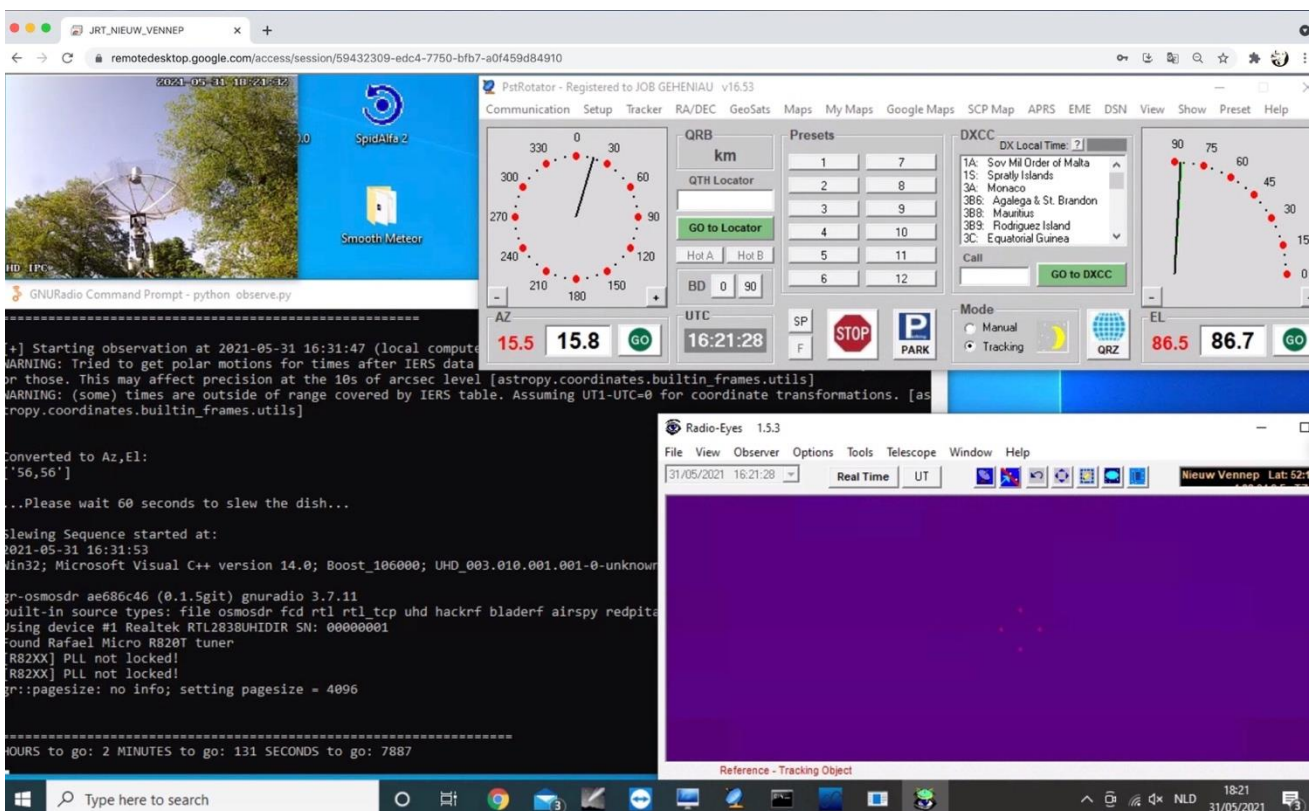


Figure 9: JRT Remote Control

Method

The starting point is to record the 21 cm hydrogen line. Because the signal is very weak, it is important to make a dark, just like in astrophotography. This is a measurement in which little / no hydrogen is present. This can be done on a frequency other than 1420 MHz (for example 1422 MHz) or by aiming the dish at a hydrogen-poor area (around Ursa Major). This signal is later subtracted from the official measurement so that you can remove radio noise and the specific disturbing characteristic of the SDR receiver.

If desired, you can compare the measurements with a simulation site:
<https://www.astro.uni-bonn.de/hisurvey/euhou/LABprofile/>

RESULTS

The following results are just a few of my observations the last year, but worth mentioning for such a small dish I think.

Standard measurement

There is a known reference point (HI Galactic Calibrator), 02h06m13s 60d32m52s called S7, in which we find a strong signal of neutral hydrogen.

When I make a measurement (around three minutes) and then plot the frequency against the SNR (Signal-to-Noise Ratio), I get the following graph (Figure 10).

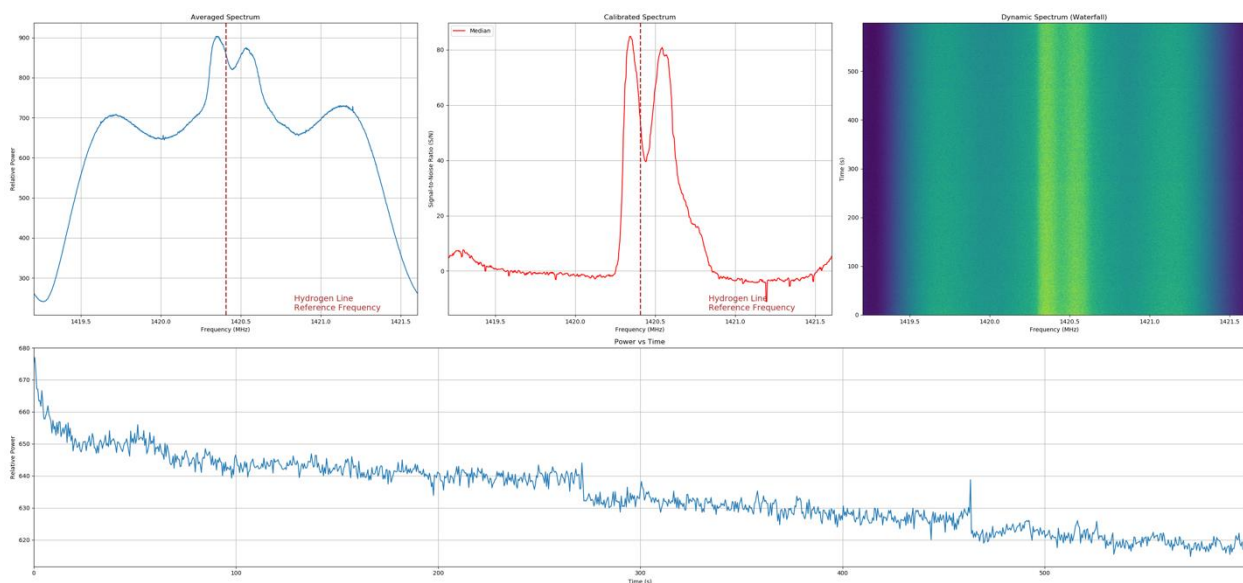


Figure 10: Calibrator S7 at 21 cm in HI

Sun drift scan

Another measurement method is the drift scan method. We fix the dish at 1 point and let the rotation of the earth do its work (also useful if you don't have a rotor).

Instead of frequency against SNR (Signal to Noise Ratio), we now plot the Power against Time. The sun generates many types of radiation, and we can also detect the sun at 1420 MHz (thermal radiation). In this graph, Figure 11, a drift scan of the sun.

The data generates a Gaussian Curve. A Gaussian curve is a curve with a classic bell shape that has a maximum around the average of the measured values and can be more or less narrow depending on the dispersion of the values around the average.

From the Gaussian curve we can calculate the effective dish beam.

I measure the time at 50% of slope 1 and measure the time again at 50% of slope 2. In this case 2070 seconds. The earth rotates at a speed of 15 degrees per hour. This gives a dish beam (effective beam size) of 8.6 degrees, which corresponds to a dish diameter of 1.9-meters.

A dish diameter of, for example, 25-meters has a beam of 0.6 degrees at 1420 Mhz. So, a much higher resolution.

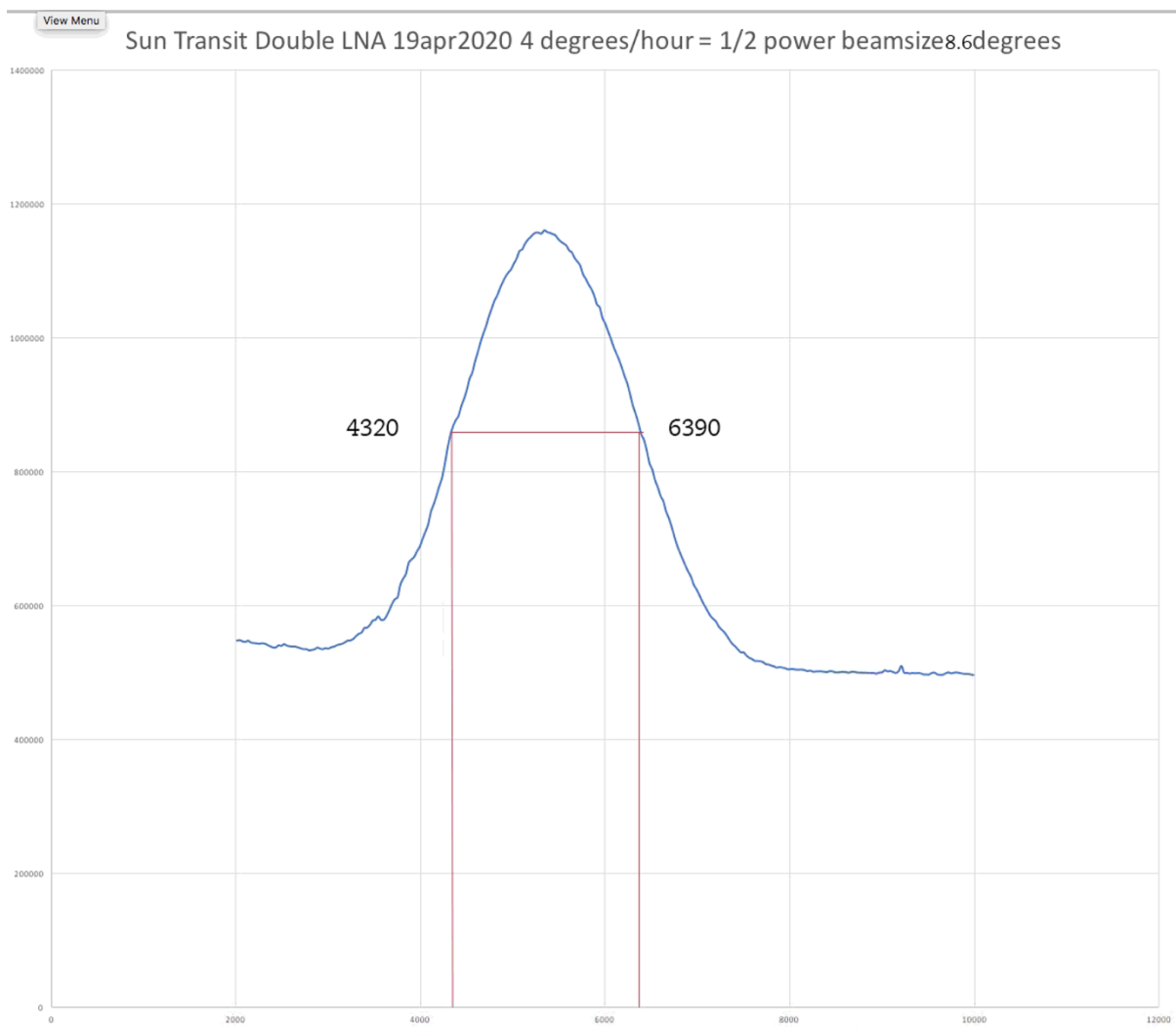


Figure 11: Driftscan of the sun with JRT

Milky Way drift scan

An interesting drift scan is the measurement of hydrogen emissions from our own Milky Way. We aim the dish at a fixed point in which the Milky Way passes twice within 24 hours. This is also clearly visible in the drift scan below. The color plot was created with a simple Python script. The black and white plot is a conversion of the data with Excel into color values (Conditional Format).

The sinusoidal structure is related to the Doppler effect. The Doppler shift is mainly due to the movement of the earth around the sun (30 km/s) and due to the rotation of the earth. We always look in different directions during the day with respect to this direction of movement.

The vertical axis is Time (total 24 hours). Figure 12 & 13.

Here a small movie from the Milky Way transit: https://youtu.be/aJnVMv_7o-k

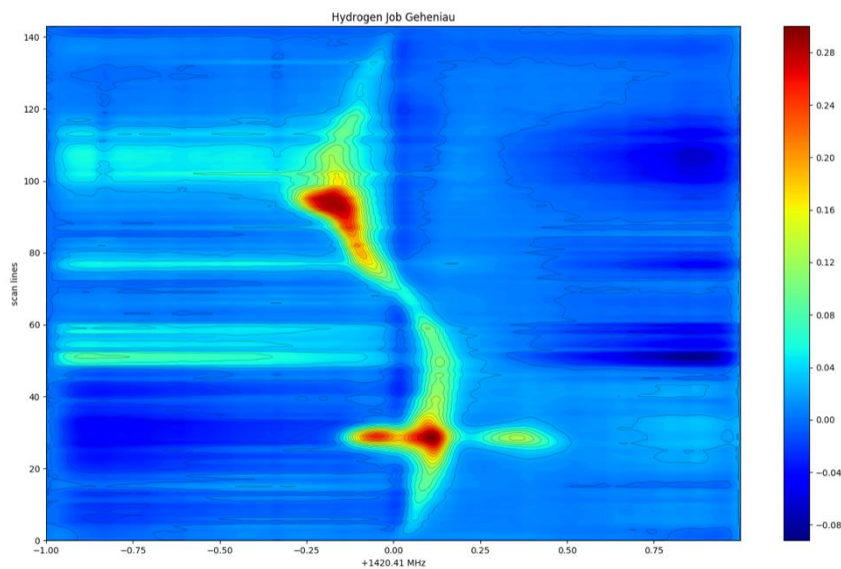


Figure 12: Python plot of Milky Way Galaxy driftscan

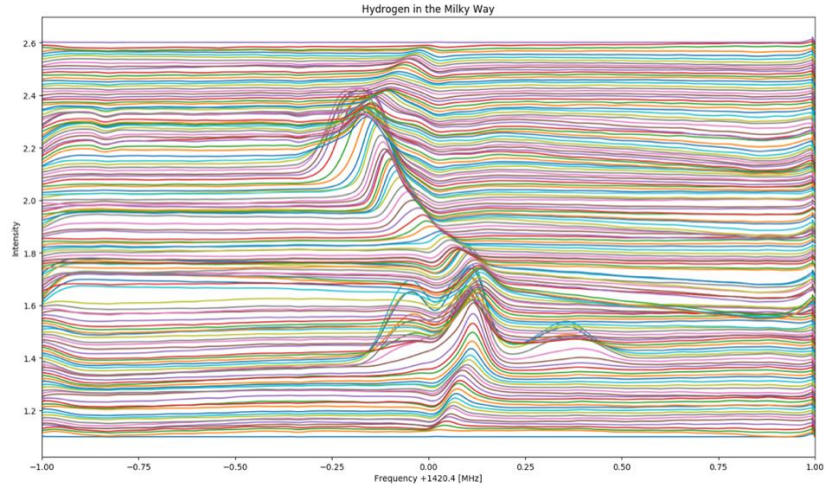


Figure 13: Python lineplot of Milky Way Galaxy driftscan

Hydrogen detection three spiral arms of the Milky Way (Deneb)

One of the most startling measurements was the discovery of the spiral arms of the Milky Way. For example, if the dish is pointed towards the star Deneb, the following graph (Figure 14) is created with JRT.

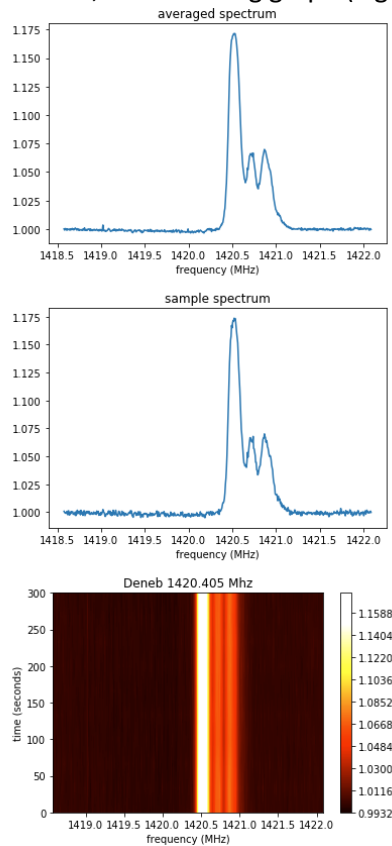


Figure 14: HI detection near the star Deneb

We see three times a hydrogen line detection with a small difference in frequency and intensity. This has to do with the Doppler shift of the three signals. Our own arm in which we (our solar system) are located is exactly 1420.406 MHz.

But the emission of hydrogen from the 2 other arms is also detected by the dish. These arms rotate around the core at the same speed as the Sun.

By the way, you would expect the outer regions to spin slower than the core (just like a vortex). However, this turns out not to be the case, which can also be measured with my radio telescope. It has to do with measurements of the rotation curve of the Milky Way showing that there is dark matter.

https://en.wikipedia.org/wiki/Galaxy_rotation_curve

See later in this article.

Because the arms are further out, they take longer than the Sun to make a circle around the core. The sun catches up with these arms, as it were, and thus we see a blue shift. Mind you, we detect HI from arms 15,000 to 30,000 light-years away. The moment HI emission took place there, we were still walking across the savannah with a bat.

Polar coordinates and formulas

Some essential formulas are needed to determine, for example, the position of the source. When we plot various positions (polar coordinates) in a graph, the spiral structure of our Milky Way becomes clearly visible.

A quite unique thing because we ourselves are in the Galaxy cloud. This is possible with a 1.5-meter radio telescope.

It took me quite a lot of calculations and research to get the most important formulas sorted out. So here they are for free ☺. These are, among other things, essential to the plot of the spiral arms of the Milky Way and to compute the rotation curve of the Milky Way.

In order, here are the formulas to determine the position of the measurement (polar coordinates). A number of details are fixed:

c : speed of light

l : longitude

f_0 : 1420.406

f_r : measured HI emission frequency (source)

V_0 : (speed of our solar system) 220 km/s

R_0 : distance Sun to center of our Galaxy 8.5 kpc

Speed of the measuring point

$$V_R = c * \left(\frac{f_0 - f_r}{f_0 - V_0} \right)$$

Distance from the measuring point to the center of the Milky Way

$$R = (R_0 * V_0 * \sin l) / (V_0 * \sin l) + V_r$$

Distance from the measurement point to the sun

$$r = \sqrt{R^2 - R_0^2 \sin^2 l} + R_0 * \cos l$$

Polar coordinates

$$X = r * \cos(l - 90^\circ)$$

$$Y = r * \sin(l - 90^\circ)$$

Rotation curve

$$X - axis = \sin l * R_0$$

$$Y - axis = V_r + (V_0 * \sin l)$$

Spiral arms of our own Galaxy, the Milky Way

One of my projects is to record 945 measurements of the entire Milky Way and its surroundings to detect the different spiral arms.

You can then record the required polar coordinates with the above formulas and then process them in a plot. You can also make a detailed overview of the Milky Way in HI.

From the plot below you can clearly see the spiral structure of our Milky Way measured with the 1.5 JRT radio telescope. Coordinate 0,0 is the Galaxy center and coordinate 0,8 our Sun position (8 kpc)

The red plane is the spiral arm in which our solar system is located.

The blue plane is the Perseus Arm.

The yellow plane is the Outer Arm.

The visibility of the arms (Figure 15) is thus formed by converting about 945 neutral hydrogen emission measurements into coordinates.

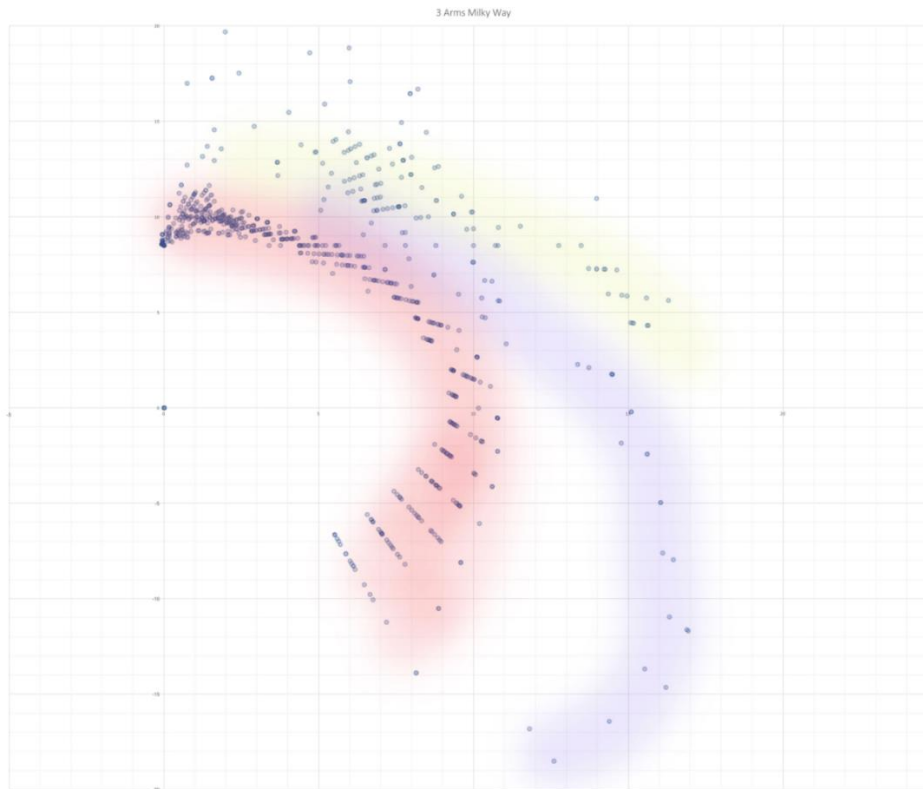


Figure 15: Spiral arms of Milky way Galaxy

Milky Way plot from longitude 20 – 230 and latitude 0

Another measurement that can yield interesting results is to measure the emission of hydrogen at different longitudes of the Milky Way where the latitude is 0 (Figure 16).

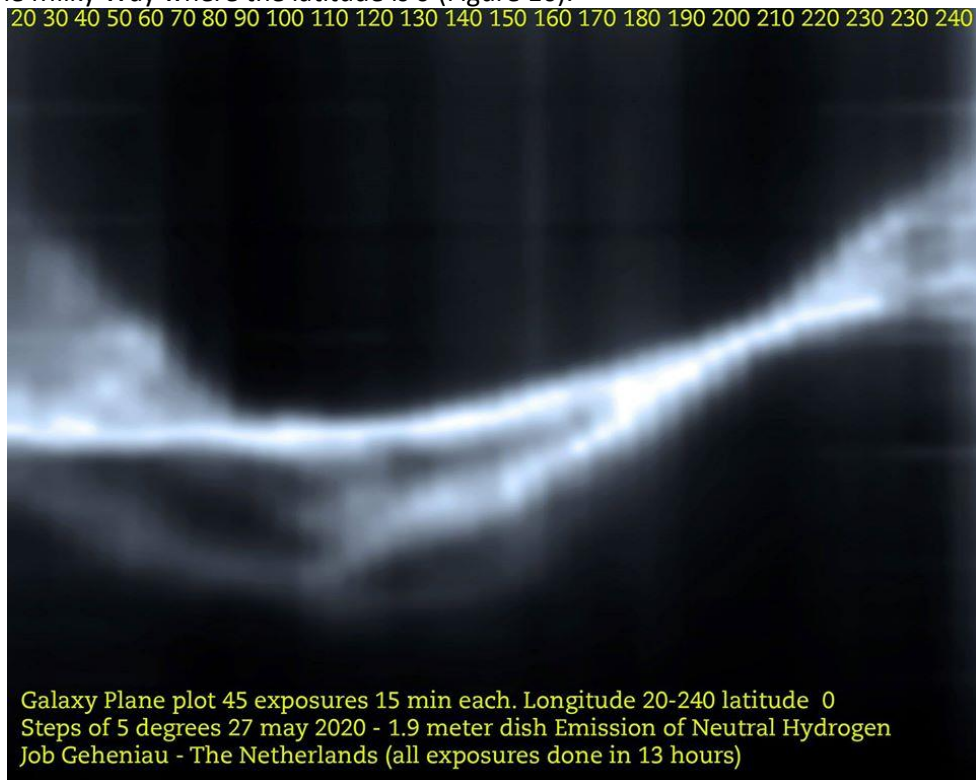


Figure 16: Milky Way Galaxy plot.

So, no drift scan, but track with the rotor per data measurement.

The above images have been a total of 45 recordings of 15 minutes each. It represents the distribution of HI (neutral hydrogen) in the Galaxy that is visible for my location (i.e. from longitude 20 to 240 in steps of 5 degrees). The collected data is put in an Excel sheet in which you generate 45 columns, then stitched them together in Photoshop with a little blur.

The highest and lowest values are converted into a color table (white is high, black is low).

A nice representation of the HI distribution of our Milky Way.

Galaxy Plane Milky Way in 3D

A nice experiment was generating 9 plots of the Galaxy Plane with 9 different latitudes and combine them in Touch Designer into a 3D plot/movie.

Of course, it's better to show the movie <https://youtu.be/Tg-td6FFNpk>

But here 2 screenshots (Figure 17a & 17b) from the movie to have an idea for a 3D plot of the Galactic Plane of Milky Way!

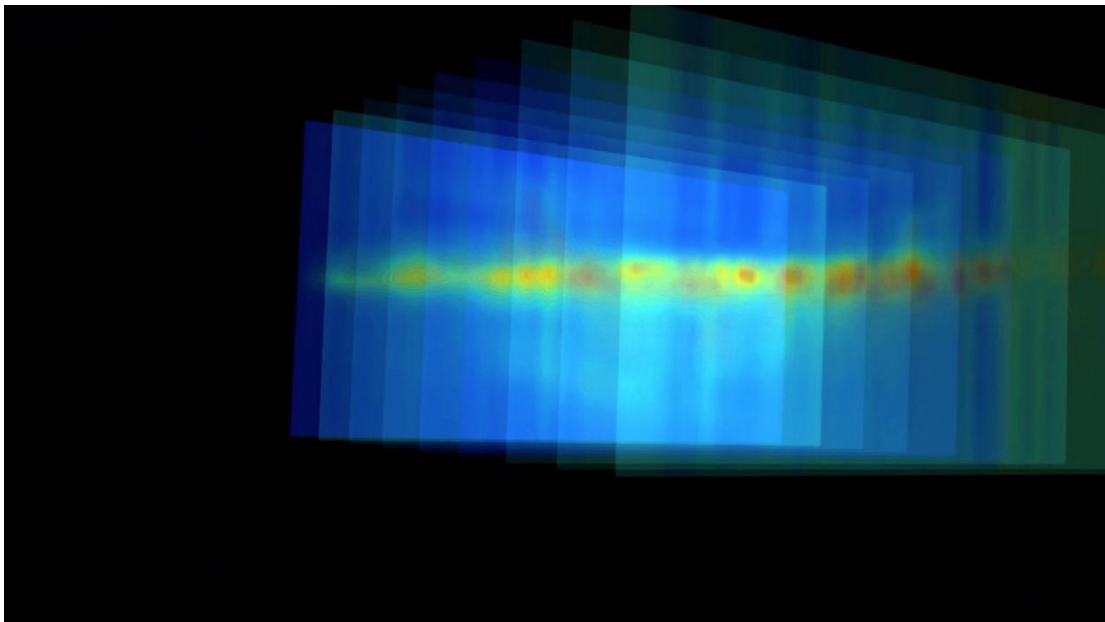


Figure 17a: Nine layers of Milky Way in 3D

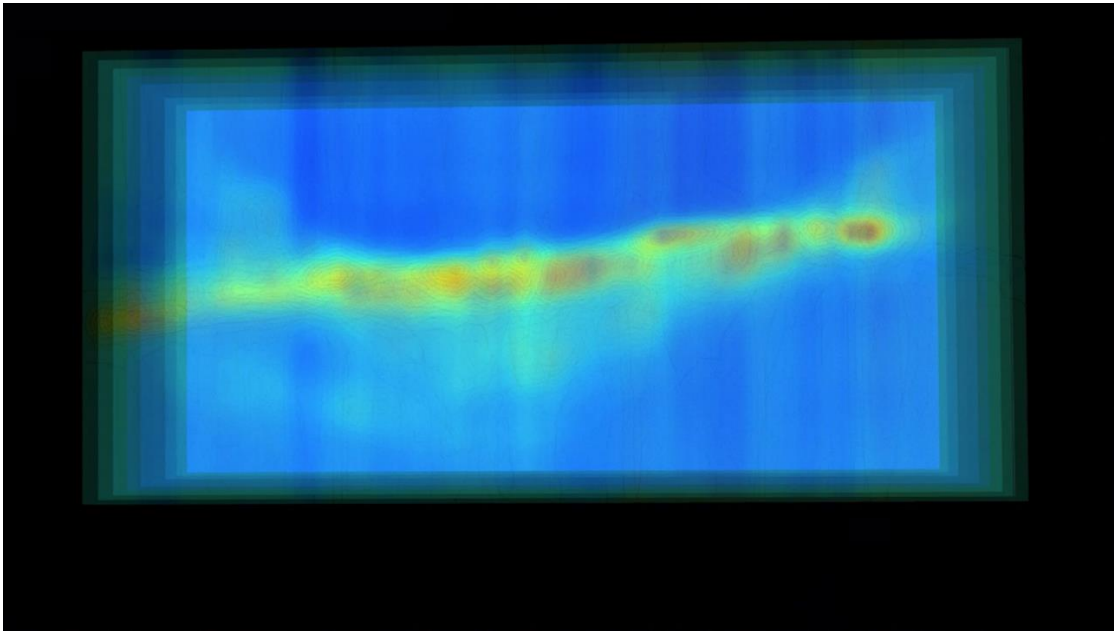


Figure 17b: Nine layers of Milky Way in 3D

Anti-Center Shell

If I want to work with long "exposure times", I choose objects that are difficult to detect at first. A real HI challenge are high velocity clouds, these are clouds of cold hydrogen that lie just outside the Milky Way and move at high speeds relative to us.

The ACS (Anti-Center Shell) is such an object. A large cloud located 180 degrees from the center of the Milky Way, 55,000 light-years away and a blue shift of -50 km/s.

Only discovered in 1979 but detectable with a 1.5-meter radio telescope! I am not sure but I hope to be the first who detected an ACS with a 1.5-meter dish in the amateur radio astronomy society. Would be an honor 😊. At this moment I am busy with new observations with even harder-to-detect high velocity clouds (A VI or A IV, A0, etc.)

In this case, the spectrum was monitored for 1 hour and then the hydrogen emission from the ACS becomes clearly visible as a small peak (Figure 18).

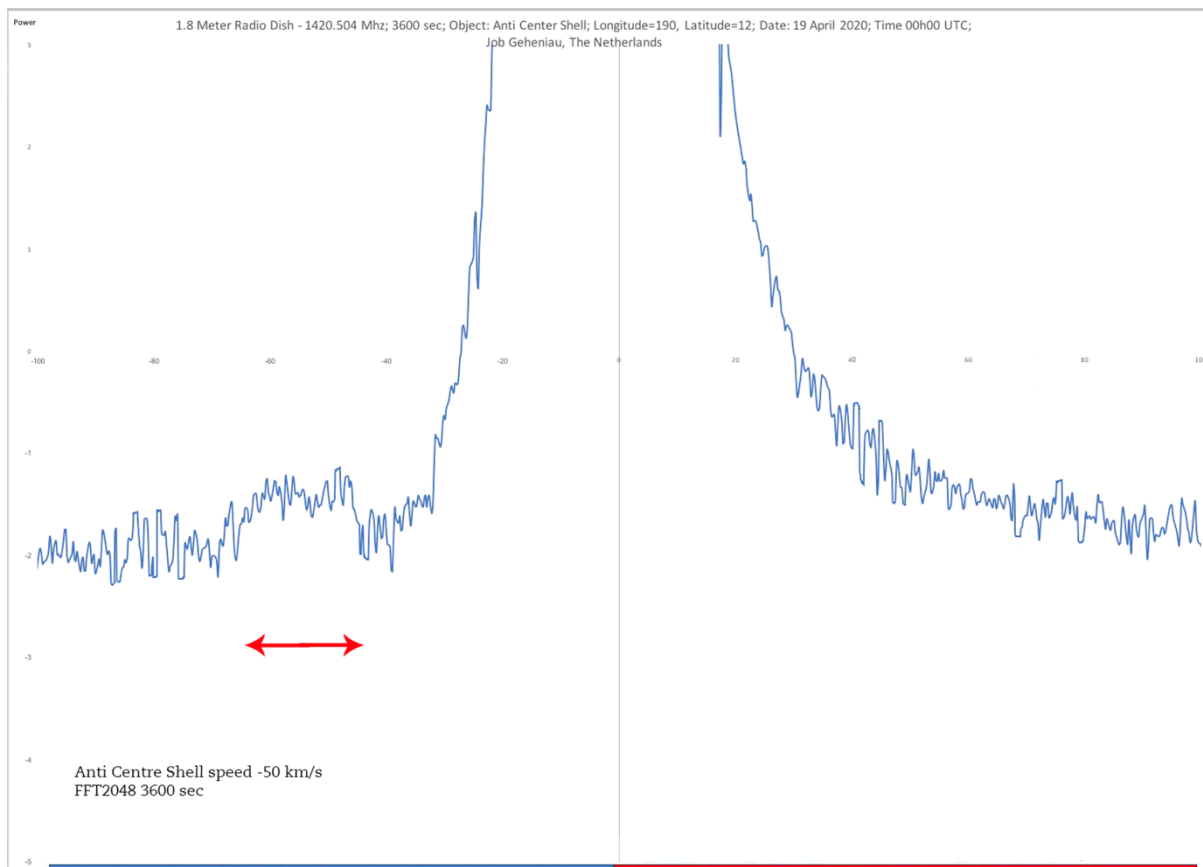


Figure 18: Anti Center Shell

The Big Galaxy

A bigger project that I have done with JRT.

The idea was to capture much of the visible Milky Way and its surroundings. I started with an array of 945 coordinates.

A lot has been programmed in Python to simplify things.

PSTRotator operates with ALT AZ input. That depends on place and time, of course. An adjustment in the VIRGO software now ensures that the ALT AZ is calculated for each new RA DEC coordinate. But entering 945 RA DEC coordinates by hand is asking for trouble.

So the following steps have been taken:

- Develop a measurement matrix
- Generate 945 longitude/latitude coordinates representing the matrix
- Generate 945 RA DEC coordinates
- Let JRT perform all measurements autonomously

Because I can only make a limited number of observations per 24 hours (the Milky Way which also rotates out of sight), I had to divide the number of observations over 8 days.

All observations over 8 days (150 seconds per observation) were carried out completely autonomously. VIRGO reads the RA DEC coordinates from the text file generated earlier by Python and sends the telescope to the correct ALT AZ point, takes a 150 second recording (non-tracked) and stores the data.

A custom Python script generates a color plot of the measures. I will not consider the technique behind this conversion in this article, but it did cause some headaches.

I also manually put the 945 values in Excel (the matrix) and converted them into color. Low HI value blue, high HI value red.

Finally, the values were converted into a Mollweide (elliptical) projection (Figure 20). The missing data is not visible from my location.

The result is an overview of the Milky Way and its surroundings between latitude -50 and +50 and longitude 20 to 230 in steps of 5 degrees. Every crossing from a red and yellow line is an HI observation (Figure 19).

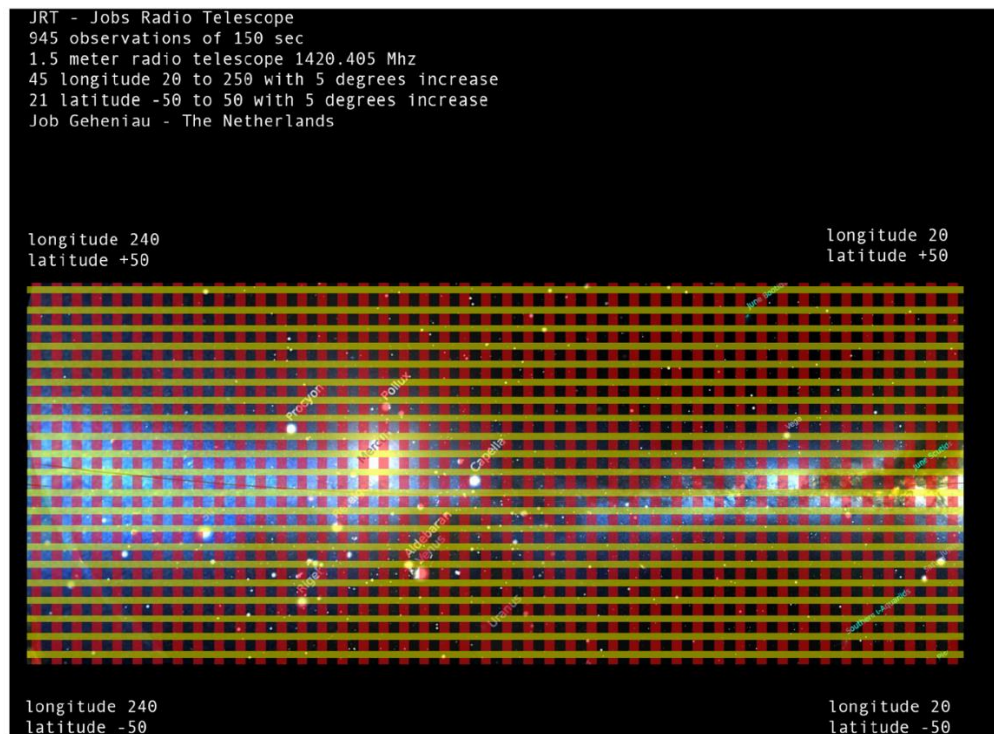


Figure 19: The matrix

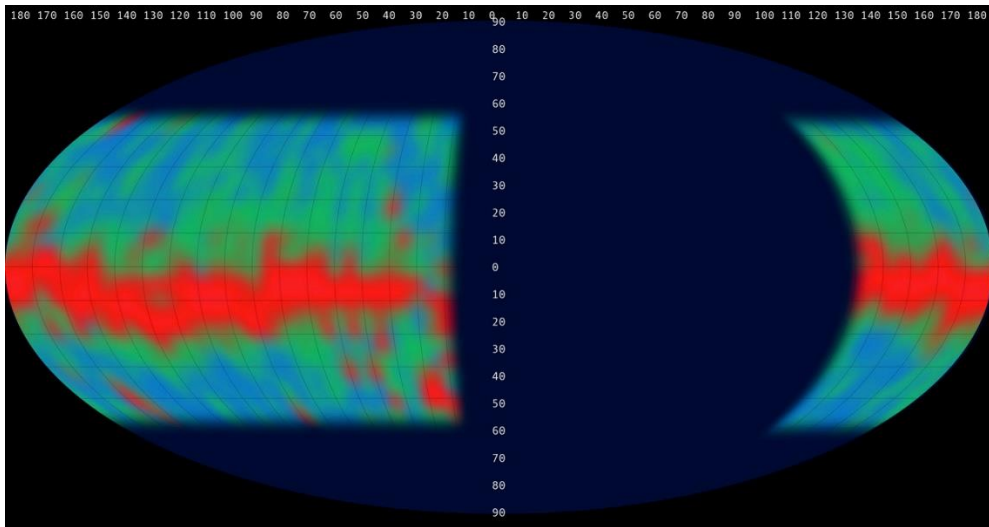


Figure 20: Mollweide projection of the Milky Way Galaxy with JRT

Northern Sky Survey

Of course, you can try to scan the entire Northern sky for HI and then plot the structure of the visible part in my region. This obviously takes a lot of time.

To avoid major problems with system temperature and RFI, I chose the drift scan method of 24 hours per 5 degrees. The lowest point in the Netherlands that can be registered is around -20 degrees latitude.

Because the dish has a beam of more than 8 degrees, a small overlap seemed okay to choose steps of 5 degrees. So -20, -15, -10.... +85, +90. That is a total of 23 observations of 24 hours.

A radio spectrum of 5 minutes is made every 20 minutes. That's three spectra per hour, 72 in total in 24 hours, so in the entire total of 1656 spectra! (Figure 21 & 22).

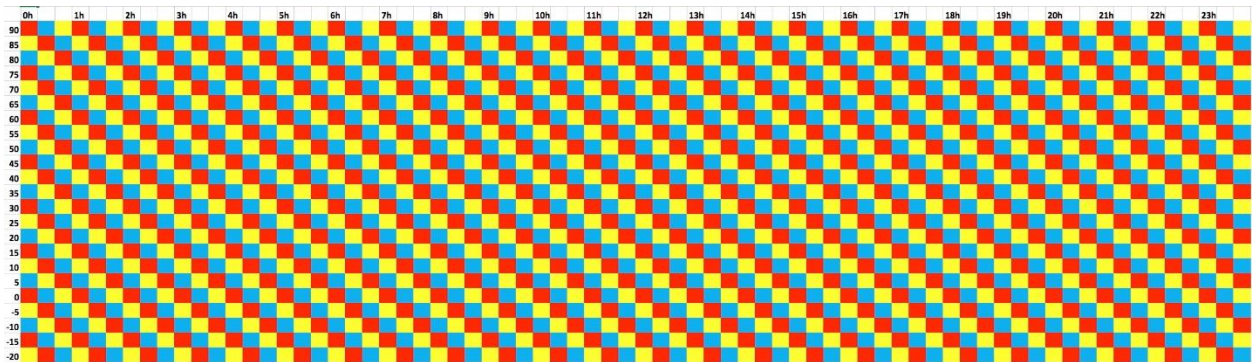


Figure 21: 1656 spectra needed for Northern Sky Survey

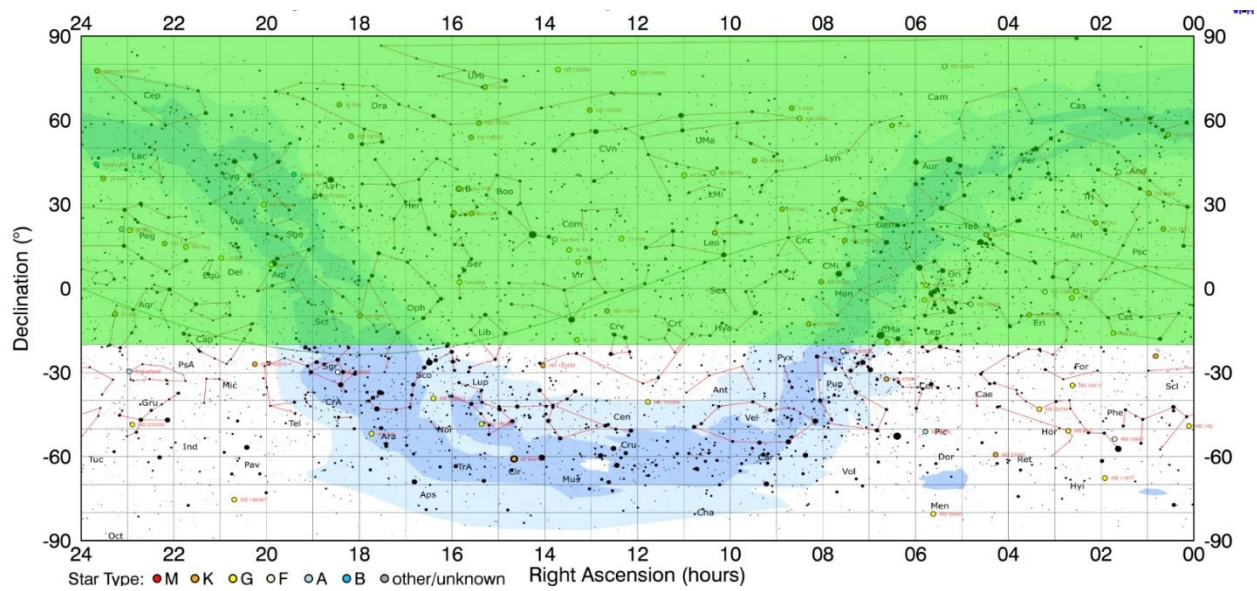


Figure 22: The visible part of the Northern Sky in my region

Each spectrum is a pixel, as it were. Replace the measured values with a color (high yellow, low blue) and you get a visible image. (Figure 23)



Figure 23: Every spectrum get's its own color (detected value)

After 30 days, the final result is The Northern Sky Survey in HI.

Compare the result (Figure 25) with an old (136 MHz) chart ☺. (Figure 24)

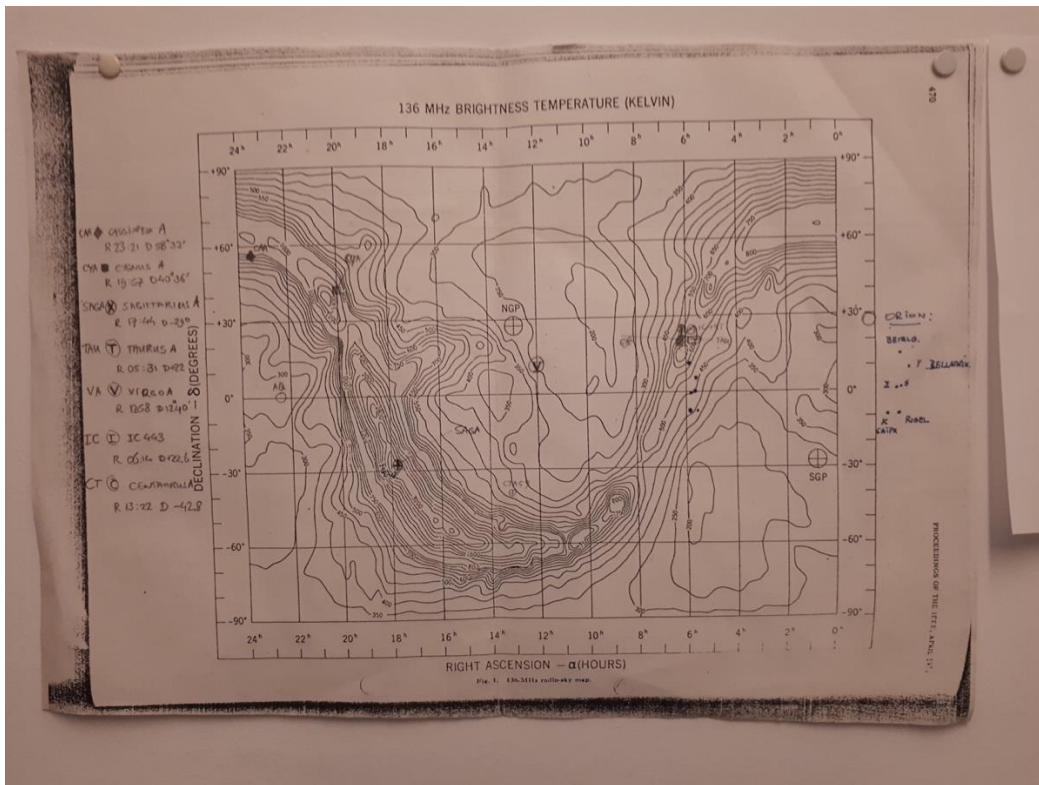
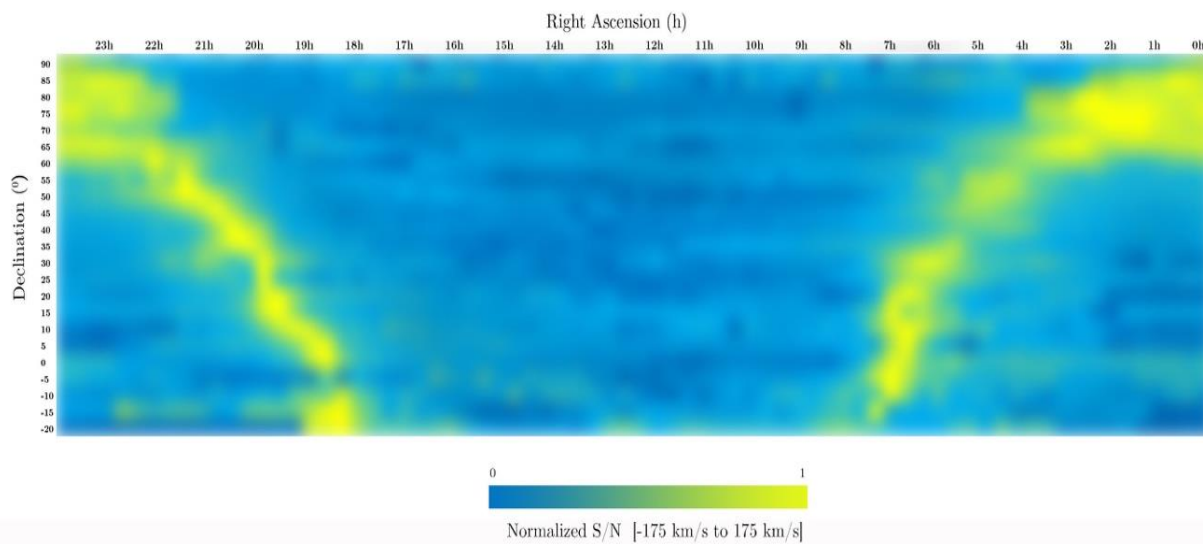


Figure 24: Chart of the Sky not in HI (but 136 MHz)

JRT - Job's 1.5 meter Radio Telescope - Northern Sky HI (Neutral Hydrogen) Survey
 derived from 1656 spectra 5 minutes each.



Job Gehenaui, The Netherlands - October/November 2020

Figure 25: Northern Sky Survey in HI with JRT

Rotation Curve

Finally, after some effort, I managed to capture the rotation curve of the Milky Way.

“For spiral galaxies like the Milky Way, we can derive the mass of the entire galaxy by observing the movements of stars and gas clouds in the disk as they rotate. The rotation curve of a galaxy shows how the speed of stars varies around the center as the distance from the center increases. It follows from Kepler's second law that the rotational speeds will decrease as the distance from the center increases, just like the planets in our Solar System. But that's not what we see. Instead, we see that the rotation curve is more or less flat. However, if more than ten times as much mass were present, this problem would not exist and the rotation curve as we perceive it could also be explained. The first proof that there must be matter that we don't see: dark matter. Figure 26.

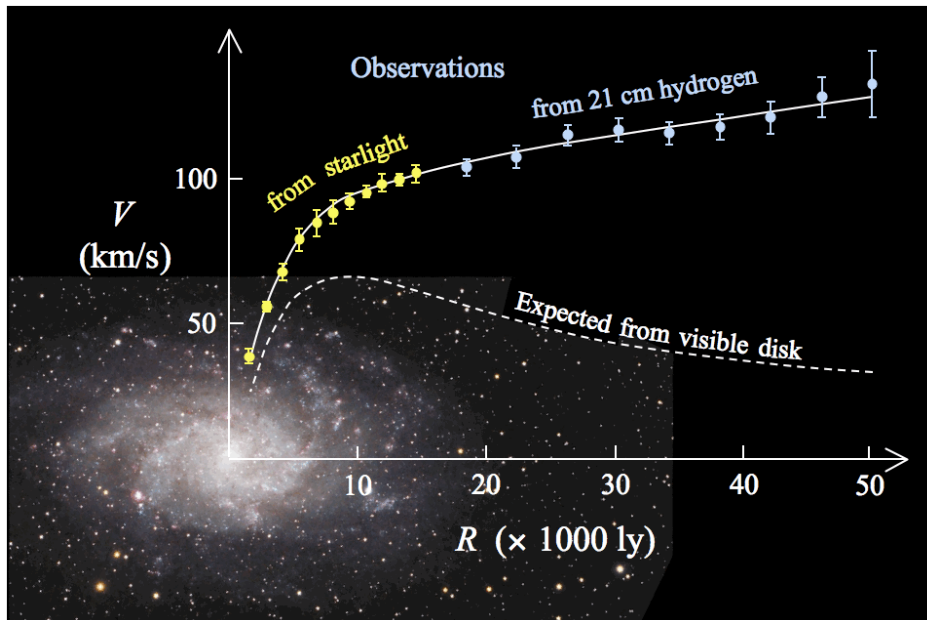


Figure 26: Expected rotation curve ([M33_rotation_curve_HI.gif \(963x639\) \(wikimedia.org\)](#))

In this situation (Figure 27a), the line of sight is tangent to the path of the cloud that we want to observe. R is therefore perpendicular to the line of sight.

We can easily calculate R with the sine ($R = R_0 * \sin(l)$).

Because the movement of that cloud is also exactly along the line of sight, the redshift is maximum. Suppose we choose another point that is further away (for example, the point where the line of sight in the diagram intersects the outer circle again), then the angle between R and the line of sight is not 90 degrees and our simple sine formula for R no longer applies.

Even at longitude > 90 degrees it no longer fits, then your line of sight cannot be a tangent line with a circular orbit around the center of the galaxy. Figure 27b.

The reason why results of longitude < 20 degrees are usually not useful is because around those galactic longitudes the redshift is very small, and the most redshifted peak is therefore indistinguishable.” (E.Mol)

From

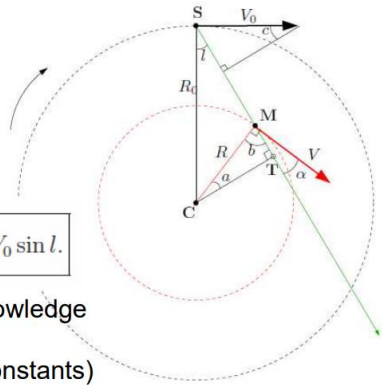
$$V_r = V \cos \alpha - V_0 \sin c.$$

with

$$CT = R_0 \sin l = R \cos \alpha$$

one gets:

$$V_r = V \frac{R_0}{R} \sin l - V_0 \sin l.$$



Most important is the knowledge of the Galactic constants R_0 and V_0 (called Oort constants) A good approximation is $V = V_0$ (flat rotation curve)

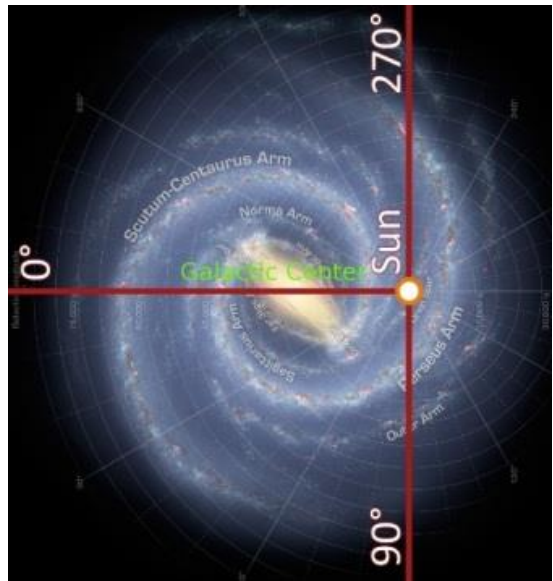


Figure 27a: Geometry for inferring the distance from galactic center (center (https://www.astro.uni-bonn.de/hisurvey/euhou/HI_Spirals_HowTo.pdf))

Figure 27b: Galactic longitude 0 and 90 degrees.

When I did have enough measurement points for spectra between longitude 0 and 90, I used my Polar coordinates and formulas.

And finally Excel to plot the computed rotation curve. Figure 28.

It is striking that a beautiful rotation curve also rolls out with the JRT 1.5-meter dish, which needed quite a lot of calculations. Here's why we need some formulas which I mentioned earlier. Figure 29.

Degrees Longitude	Sinus calculation	Higest redshift	Speed of cloud	Distance from Galactic Center	11 min per observation	sin l * 8.5 (kpc)	Vr+220 * sin l	GRAPH X	GRAPH Y
Rad	Frequency in Hertz	km/s	kpc	km/s	Rotation Curve X-axis	Rotation Curve Y-axis	Kpc	Column G as Value	Column H as Value
0	0	1420324000	1.7468686	0	15.56	0	1.7468686	0	35.7068686
2.5	0.087155743	1420330000	0.460512361	0.000543585	15.58	0.732108239	19.63477582	0.732108239	53.12477582
5	0.087155743	1420307000	5.334877943	6.649814313	15.56	0.732108239	24.50914135	0.732108239	57.54914135
7.5	0.130526192	1420304000	38.38805606	3.637408205	-16.86	1.096420015	67.10381835	1.096420015	67.10381835
10	0.173648178	1420303000	38.21911544	4.249081485	-16.48	1.458644692	76.42174552	1.458644692	76.42174552
12.5	0.216439614	1420303000	37.78911544	4.739045047	-16.05	1.818092757	85.4058305	1.818092757	85.4058305
15	0.258819045	1420250000	48.29526221	4.599130849	-15.37	2.174079979	105.2354521	2.174079979	105.2354521
17.5	0.3007058	1420123000	74.60980261	3.994736883	-14.88	2.525928716	140.7650785	2.525928716	140.7650785
20	0.342020143	1420100000	78.74416819	4.153409208	-14.16	2.872969204	153.9885997	2.872969204	153.9885997
22.5	0.382639432	1420058000	87.0886186	4.178083405	-13.64	3.214540832	171.279017	3.214540832	171.279017
25	0.422618262	1419955000	107.9877773	3.932529886	-12.8	3.549993399	200.9637940	3.549993399	200.9637940
27.5	0.461748613	1419973000	103.6287086	4.207668174	-12.24	3.878688351	205.2134035	3.878688351	205.2134035
30	0.5	1419928000	112.2263804	4.207421272	-11.34	4.2	222.2263804	4.2	222.2263804
32.5	0.537299608	1419889000	98.21175861	4.642644273	-10.2	4.51331671	216.4176724	4.51331671	216.4176724
35	0.573576436	1419968000	102.2640054	4.695049592	-9.82	4.818042065	228.4508214	4.818042065	228.4508214
37.5	0.608761429	1419980000	99.10129297	4.885163707	-9.19	5.113596004	233.0288074	5.113596004	233.0288074
40	0.64278761	1420000000	93.90010551	5.108136358	-8.21	5.399415921	235.3133796	5.399415921	235.3133796
42.5	0.675950208	1420000000	93.25010551	5.223067877	-7.56	5.674957744	241.8799512	5.674957744	241.8799512
45	0.707106781	1420036000	84.63196807	5.505056928	-6.54	5.939696962	240.1954599	5.939696962	240.1954599
47.5	0.737277337	1420058000	79.30866186	5.709709659	-5.86	6.193129629	241.509676	6.193129629	241.509676
50	0.76604443	1420034000	83.33408682	5.687638711	-4.82	6.434773322	251.8638643	6.434773322	251.8638643
52.5	0.79335334	1420065000	76.09124625	5.913930247	-4.12	6.664168058	250.6289811	6.664168058	250.6289811
55	0.819152044	1420075000	72.92065252	6.051394534	-3.06	6.880877172	253.1341023	6.880877172	253.1341023
57.5	0.843391446	1420082000	70.73323691	6.153995525	-2.35	7.084488145	256.279355	7.084488145	256.279355
60	0.866025404	1420105000	64.80887132	6.34253404	-1.28	7.274613392	255.3344602	7.274613392	255.3344602
62.5	0.887010833	1420107000	63.6667258	6.409098984	-0.56	7.450809999	258.8091359	7.450809999	258.8091359
65	0.906307787	1420112000	58.8656511	6.575262876	0.52	7.612985411	257.7532783	7.612985411	257.7532783
67.5	0.923879533	1420132000	56.59026825	6.64882116	1.24	7.760588073	259.8437654	7.760588073	259.8437654
70	0.93962621	1420144000	52.98755577	6.765846522	2.31	7.893418015	259.7199323	7.893418015	259.7199323
72.5	0.953716951	1420193000	41.93564648	7.084118309	3.02	8.011222386	251.7533756	8.011222386	251.7533756
75	0.965923826	1420198000	39.81034962	7.158861856	4.09	8.113776941	252.3140314	8.113776941	252.3140314
77.5	0.976296007	1420210000	36.57783714	7.263102707	4.79	8.20088646	251.3627587	8.20088646	251.3627587
80	0.984807753	1420184000	41.02518084	7.146731873	5.83	8.272385125	257.6828865	8.272385125	257.6828865
82.5	0.991444861	1420186000	39.9130621	7.185192408	6.52	8.328136836	258.0309316	8.328136836	258.0309316
85	0.996194698	1420189000	38.25988398	7.23673216	7.54	8.368035464	257.4227176	8.368035464	257.4227176
87.5	0.999048222	1420173000	40.98683395	7.164040551	8.19	8.392005061	260.7774427	8.392005061	260.7774427
90	1	1420179000	47.13047771	7.000324396	0.78	8.4	267.1304777	8.4	267.1304777

Figure 28: A lot of Excel calculations for the rotation curve

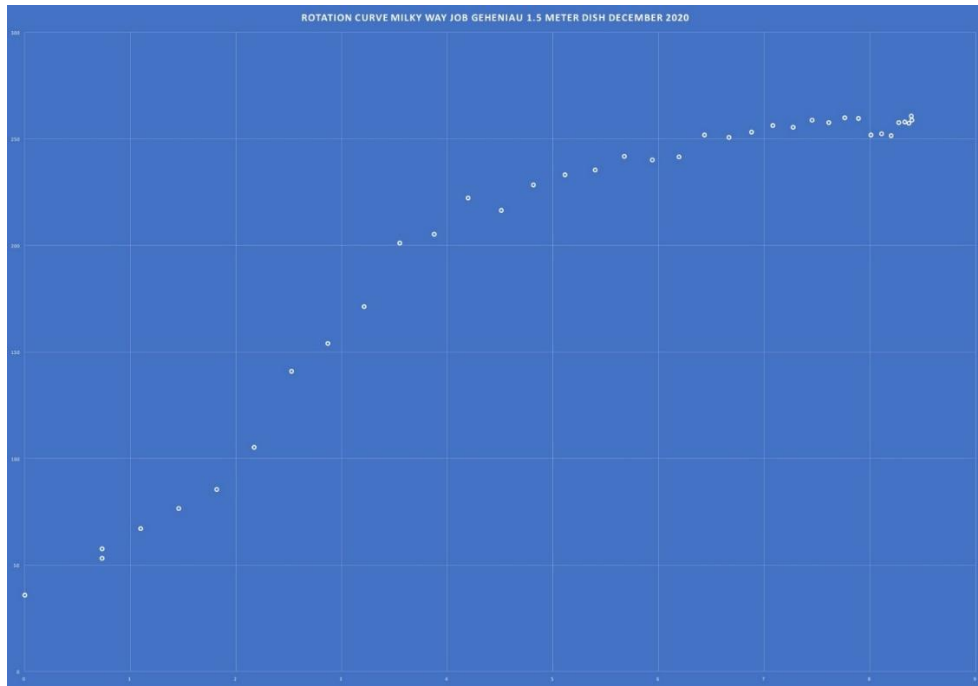


Figure 29: The rotation curve of the Milky Way Galaxy with JRT

12 GHZ.

Because a sun drift scan is no problem with the 1.5 dish, but a moon drift scan did not work, stimulated by Eduard Mol, I started working with a dish that is suitable for 12 GHz. Figure 30.



Figure 30: author with his 12 Ghz 1.25 meter dish.

I opted for a 1.25-meter satellite dish (beam size 1.2 degrees @ 12 GHz), with a normal KU Band LNB (\$ 14,-)

This LNB has a two-band conversion of 12 GHz to a workable frequency for the RTL-SDR or Airspy Mini.

For the LNB to work at 12178 MHz i.e. Maser (W3(OH), it must be powered with 13.8 volts and it must have a control signal sine wave of 22 KHz, 0.6 volts.

I already had a simple sine wave generator and with the help of Michiel Klaassen, I was able to make a simple filter to activate the LNB at the second band. Figure 31.

The LNB down converts the signal 10600 MHz when triggered with 22 KHz. So $12178 - 10600 = 1578$ Mhz. A good frequency for the SDR.

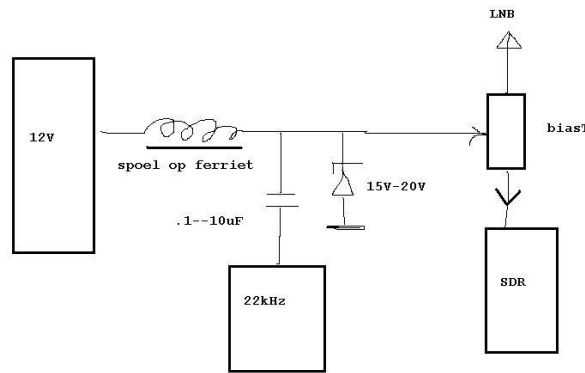


Figure 31: filter for 22 KHz (M. Klaassen) “spoel op ferriet” means “coil on ferrite” 1 mHenry.

In this area there is not much to receive with a 1.25-meter dish, but the following 3 objects were on my list. Sun, Moon and W3 (OH) maser, so definitely worth a try and the investment.....

Masers: “After the discovery in 1963 of OH in the interstellar medium at a wavelength of 18 cm, the relative intensities of the four spectral lines of OH (at 1612, 1665, 1667, and 1720 MHz) were found to be very different from the expected values. For a short time, these lines were attributed to an unknown element called mysterium. After more measurements of, among other things, the polarization of the lines, it was recognized that the observed intensities must be caused by anomalous excitation of the energy levels of OH. In all cases, these sources showed a combination of small linewidths and very high effective temperatures, which could only be explained by a mechanism in which microwave radiation was amplified. By analogy with laboratory masers, these sources were also called masers. These masers were found near young H-II regions and other star formation sources.” Wikipedia

W3 (OH) is a maser at 12,178 GHz. Subtract 10,600 GHz from the LNB converter and you can measure at 1578.5 MHz with a normal USB sdr.

My main problem is the relatively narrow beam of 1.2 degrees with a rotator accurate to 0.5 degrees. This is no problem for a sun or moon drift scan:

A moon drift scan (Figure 32) is doable at 12 GHz and it was good to see that the moon can be detected very well with this dish and setup. Because the thermal radiation from the Moon is much lower than the Sun.

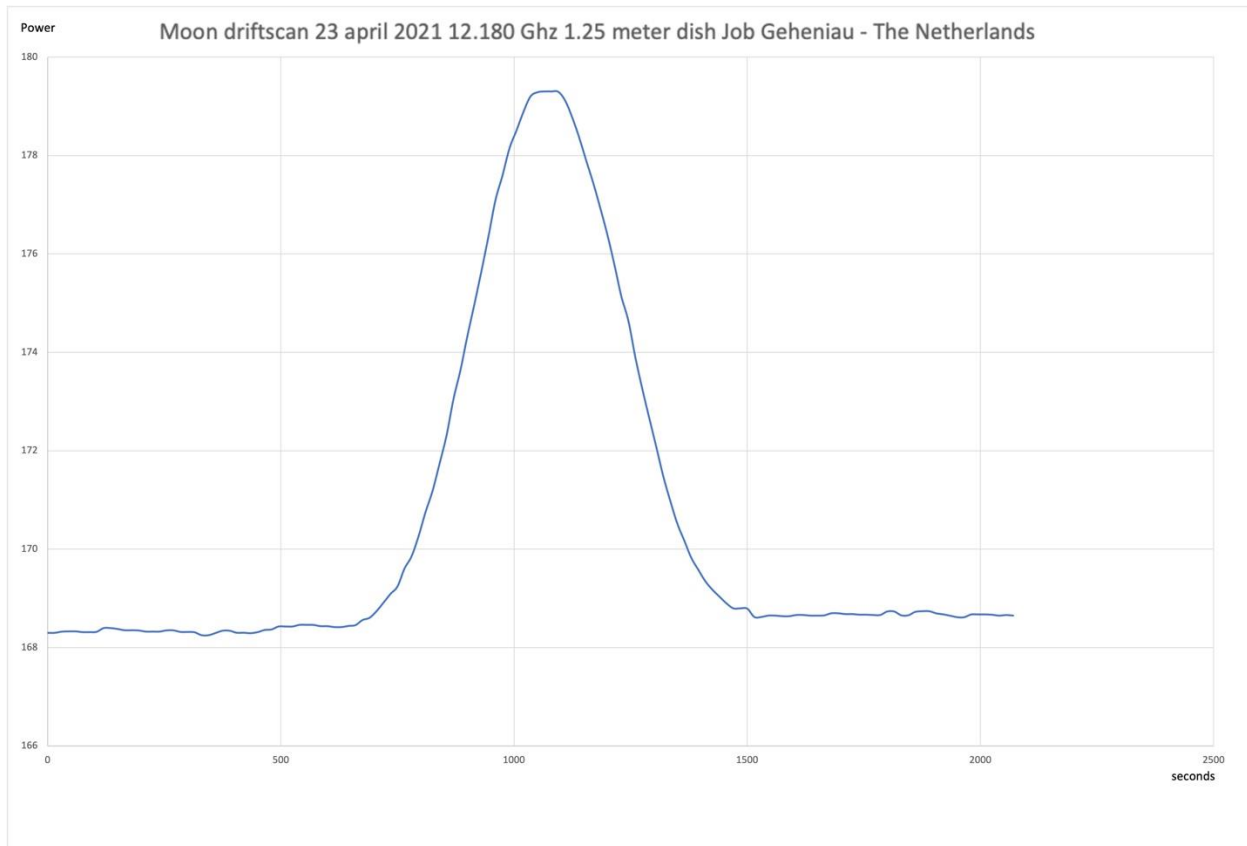


Figure 32: Moon driftscan at 12 GHz

But I must admit that till today I didn't manage to record W3(OH) at 12 GHz.

Did try about more than 30 times, different offsets with altitude and azimuth, new balancing of telescope at exact 0 degrees, 3 MSPS bandwidth, 6 MSPS bandwidth, etc. None. Not even a little increase in data energy visible.

I recorded a drift-track-drift scan of the sun. This soon showed that with this rotator the chance is almost nil that W3 (OH) can succeed. There are too many fluctuations in the signal strength, because of the 0.5 degrees offset of the rotator.

The 12 GHz dish will be exchanged for the 1.5-meter 1420 MHz dish again because on June 10th 2021 there is a partial solar eclipse (17%) that I want to capture with a drift-track-drift scan.

The 12 GHz dish was a nice experiment but a bit too high as an investment to capture thermal radiation only for the moon.... :(You never know what the future will bring. Masers are patient. But since the dish is temporarily stored, there is a good chance that in near future I will try again to detect the 12 GHz maser, maybe even with a smaller dish (1-meter) which has a wider beam.

Solar eclipse June 10, 2021

Finally, just 2 days before I could post the final version of this article, I tried to record a partial solar eclipse on 1422 MHz.

On June 10, 2021, I observed the partial solar eclipse with the 1.5-meter dish at 1422 MHz and an ETX90 optical telescope.

The idea is to record the whole eclipse while tracking the Sun. By making observations of the eclipse, we can get an idea about the radio radiation from the Sun.

There were some tracking issues but after a median still a dip is visible (Figure 33) in the power graph. I would like to try this again, but unfortunately, I have to wait for the next eclipse.

Because it was a cloud free day, I was lucky to also get some visuals with my ETX90. Figure 34.

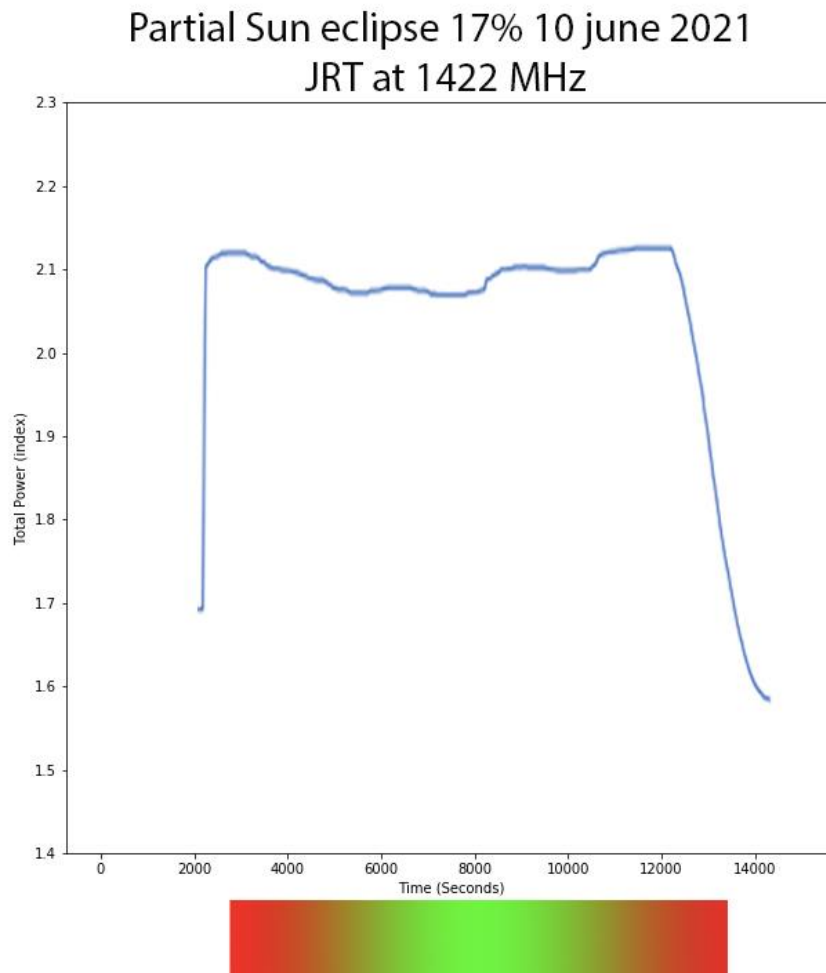


Figure 33: Solar eclipse tracked at 10th of June with JRT



Figure 34: Solar eclipse with Meade ETX90 telescope

Get started yourself, future projects

If you want to get started yourself, but you have a limited budget, you can use remote radio dishes. A good starting point are the two 2.3-meter dishes in Sweden from the SALSA project:
<https://vale.oso.chalmers.se/salsa/welcome>

Future projects:

High Velocity Clouds

Andromeda Nebula

Synchrotron radiation

Pulsars

Improve sensitivity

Interferometry

W3(OH)

And so on

In short, enough work to be done.

Acknowledgment

Thanks to Apostolos Spanakis Misirlis, Eduard Mol, Michiel Klaassen, Simon Bijlsma, Andries Boone, Jac de Bruijn, Lukasz Furman, Raydel Abreu, Rich Russel and many others. And my wife for her angelic patience and acceptance of equipment/cables on our rooftop.

If you have comments or questions, feel free to email me.

© Job Geheniau – The Netherlands

jobgeheniau@gmail.com

jgeheniau.nl

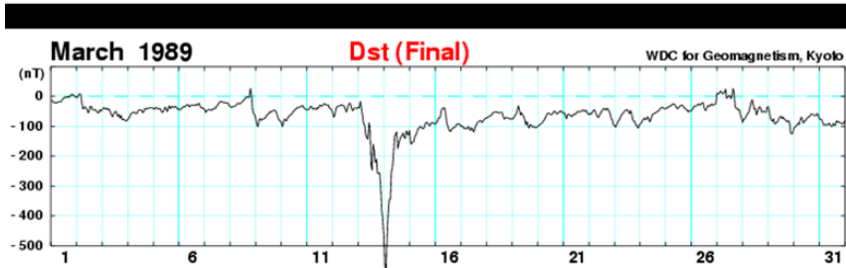
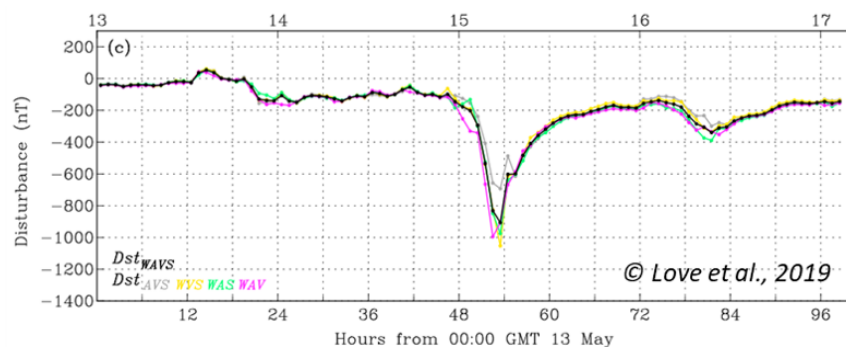
Some references in this article are from Eduard Mol, Wikipedia and AstroPeiler Stockert

The Great Storm of 15 May 1921



Reprinted with permission from Solar-Terrestrial Centre of Excellence newsletter for 10 – 16 May 2021: www.stce.be/newsletter/pdf/2021/STCEnews20210521.pdf)

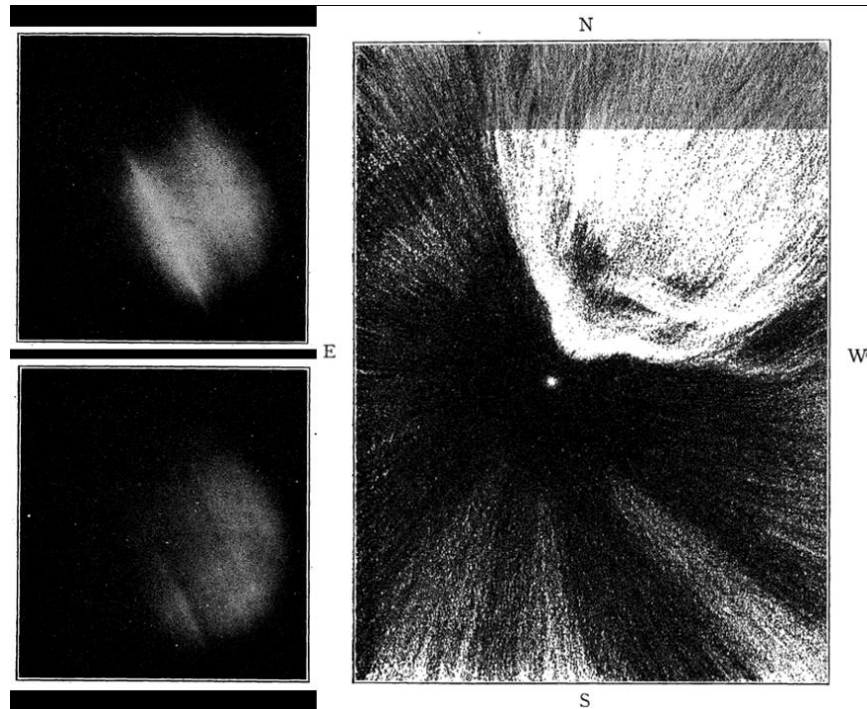
On 15 May 1921, the strongest geomagnetic storm of the entire 20th century took place. With a reconstructed Dst index of 907 +/- 132 nT (Love et al., 2019 - for links to the papers see the online version of this article at <https://www.stce.be/news/529/welcome.html>), it was significantly stronger than the March 1989 storm (-589 nT ; see the comparison underneath) and of comparable strength as the Carrington storm in 1859 (Dst between -850 (Siscoe et al., 2006) and -1050 nT (Gonzalez et al., 2011)). The Dst ("storm-time disturbance") index is calculated by 4 near-equatorial geomagnetic observatories and reflects variations in the intensity of the ring current. The stronger the disturbance, the more negative is the Dst index. Underneath a comparison of the storms from 1921 (black curve, Dst reconstructed from 4 observatories; from Love et al. 2019) and 1989 (from the Kyoto World Data Center for Geomagnetism). Mind the difference in scalings of both the horizontal (time) and vertical (Dst) axis.



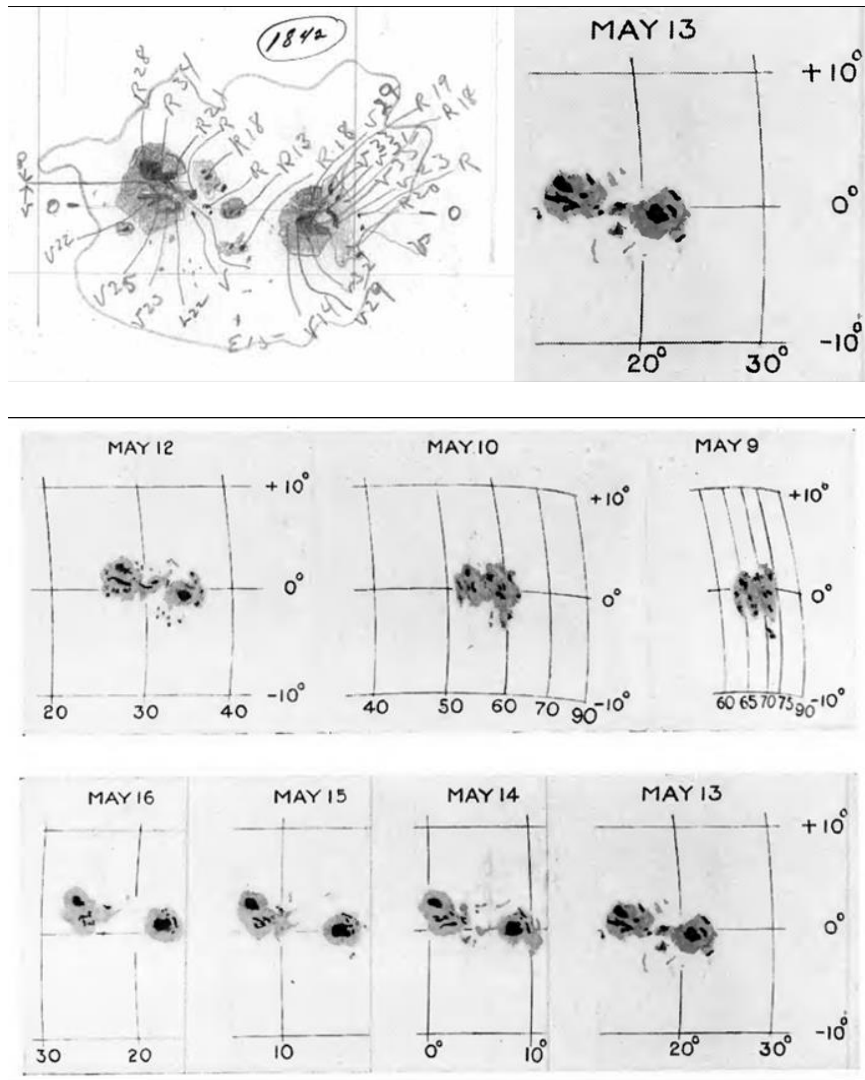
This strong geomagnetic storm induced electrical currents in the Earth's crust which found their way in telegraph/telephone systems, the key technologies at that time. Telegraph service was severely disturbed worldwide. Telegraph systems in Paris were unable to receive messages from the rest of Europe, or from the United States, during the night of 14/15 May. In Karlstadt (Sweden), currents were so strong they created a fire in the telegraph and telephone station. In Brewster (New York state), a railroad station got destroyed following a fire which was attributed to strong electrical currents in the telegraph system. Another fire destroyed a railroad control tower near New York City's Grand Central station, also and significantly delaying train traffic. However, recent research by Hapgood (2019) has indicated that the latter incident occurred well after the main storm phase and was probably due to technical failures. Nonetheless, the labelling of this geomagnetic storm as the "New York Railroad Storm" has remained, in view of the Brewster incident.

The polar lights were particularly bright, despite the first-quarter moon (Campbell, 1921). They were even seen from Samoa, which is only 14 degrees south of the Earth's equator, where intense red aurora were reported as high as 22 degrees in the sky (Hapgood, 2019). Other reports from southern locations were coming from Texas, Arizona, California, and Hawaii. In France, aurora were observed by Bernard Lyot and colleagues at Meudon. Three maxima of auroral intensity were reported (at 01:14, 02:10 and 03:05 GMT). The second maximum was most

intense, obscuring some second magnitude stars and providing enough light to read watches and make notes. In New York, visitors from movie theatres returning home were treated on an encore performance by the night sky theatre, where aurora were so brilliant they easily outshone the Broadway lights. The two pictures below left were taken from the Lowell Observatory in Flagstaff, Arizona (!), USA and reported by Truman in the Popular Astronomy magazine (1921). The aurora were about 10 to 20 degrees above the northwestern horizon, the pictures bringing out very well the auroral streamers. The drawing on the right was made by L. J. Wilson from New York City (published in Popular Astronomy (1921), who commented that the shining auroral cloud was moving to Arcturus (the bright dot near the middle) from the northwest, and that it had colors of pale green and lavender.



The source region of all this excitement was sunspot group Greenwich 933404, which rounded the Sun's east limb on 8 May. Its maximum area was reached on 11 May, and was about 10 times the total surface area of the Earth (see the Solar Cycle Science webpage), making it a large sunspot region, but not extremely so. Analysis of Mount Wilson drawings and magnetograms indicated that the sunspot group, here called Mount Wilson 1842, contained several magnetic delta's in its main portions. Delta's are spots of opposite magnetic polarity separated by less than 2 degrees and situated within the common penumbra. See the STCE Space Weather Classifications page for more information. These magnetic structures are known to increase the likelihood on very strong flares, which may be associated with solid coronal mass ejections. The figure below on the left is a Mount Wilson drawing of the group on 13 May, indicating the magnetic polarity and intensity of the sunspots. "V" means a direction of the magnetic field towards the Sun, "R" means away from the Sun, and the 2 numbers express the magnetic field strength in Gauss divided by 100. Typical values for sunspots are between 2600 and 2900 Gauss (Borrero et al., 2011). The drawing below on the right was made by projection with the 15-inch equatorial by the Rev. H. Macklin, S.J. from the Stonyhurst College Observatory on the same day (from Cortie, 1921).



The drawings above illustrate the development and evolution of the sunspot group, for the period of 9 till 16 May 1921. They are accurate copies of the drawings made by the Rev. H. Macklin, S.J. from the Stonyhurst College Observatory (Cortie, 1921).

Comparative Observations of the 12 May 2021 Geomagnetic Event

Whitham D. Reeve & Roger Blackwell (GM4PMK)

This report compares observations at three locations, two in Alaska and one in Scotland (table 1), of geomagnetic activity on 12 May 2021. One of the magnetometers in Alaska and the one in Scotland are SAM-III, whereas the other magnetometer in Alaska is a professional unit operated by University of Alaska Geophysical Institute [{UAF-GI}](#). A solar flare on 9 May produced a coronal mass ejection (CME) that intercepted Earth on 12 May, producing interesting geomagnetic and radio phenomena. Our report focuses only on the geomagnetic observations and uses additional information from Space Weather Prediction Center (SWPC).

Table 1 ~ Magnetometer locations and types

Station	Geographic Coordinates	Geomagnetic Coordinates*	Type
Anchorage, Alaska USA	61.199° N; 149.957° W	61.72° N; 94.50° W	SAM-III fluxgate
Gakona, Alaska USA	62.407° N; 145.157° W	63.64° N; 90.73° W	Narod ring core fluxgate
Isle of Mull Scotland	56.380° N; 6.001° W	58.85° N; 80.86° E	SAM-III fluxgate

* Coordinate transformation for 2021 using IGRF [{Kyoto}](#)

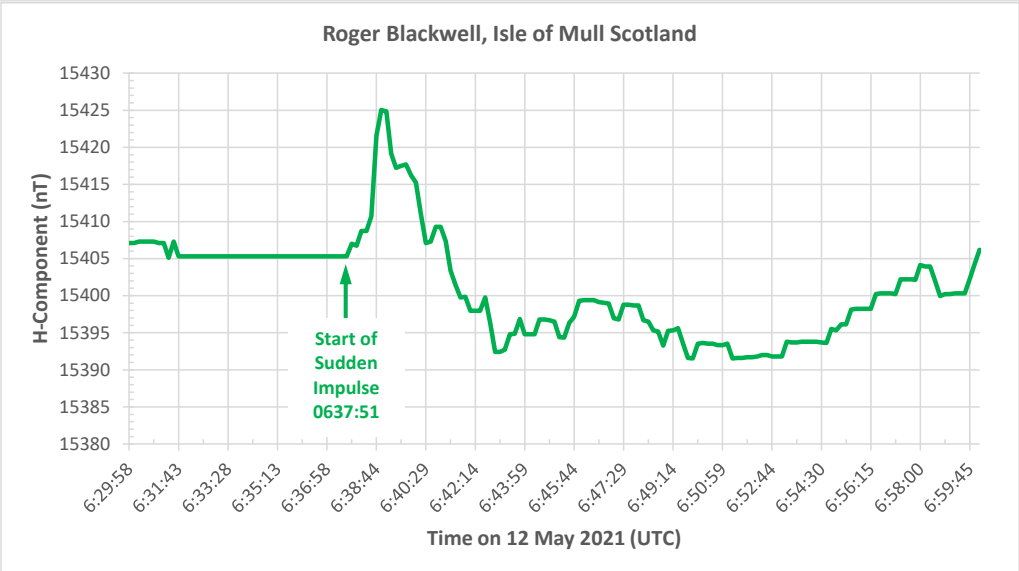
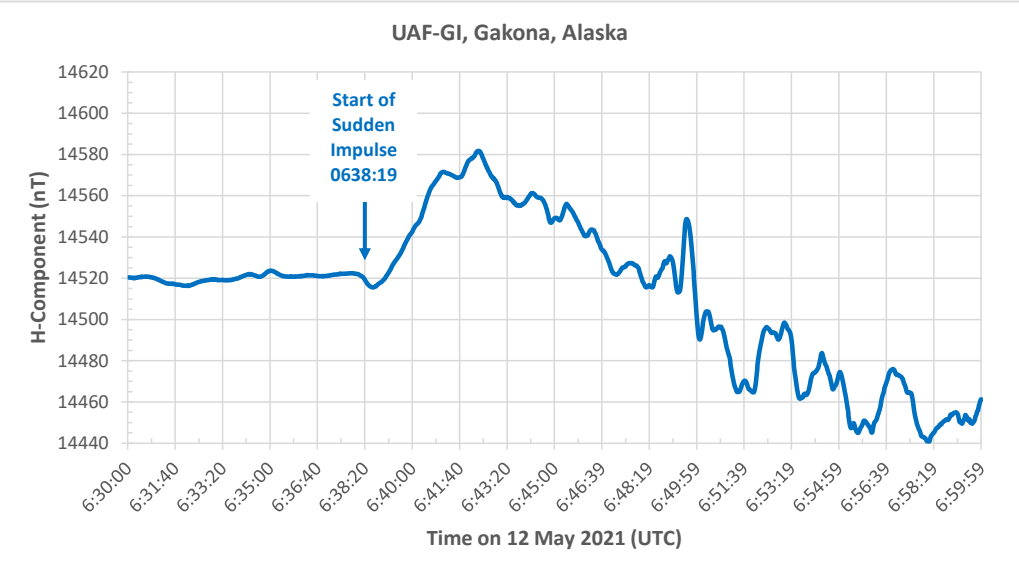
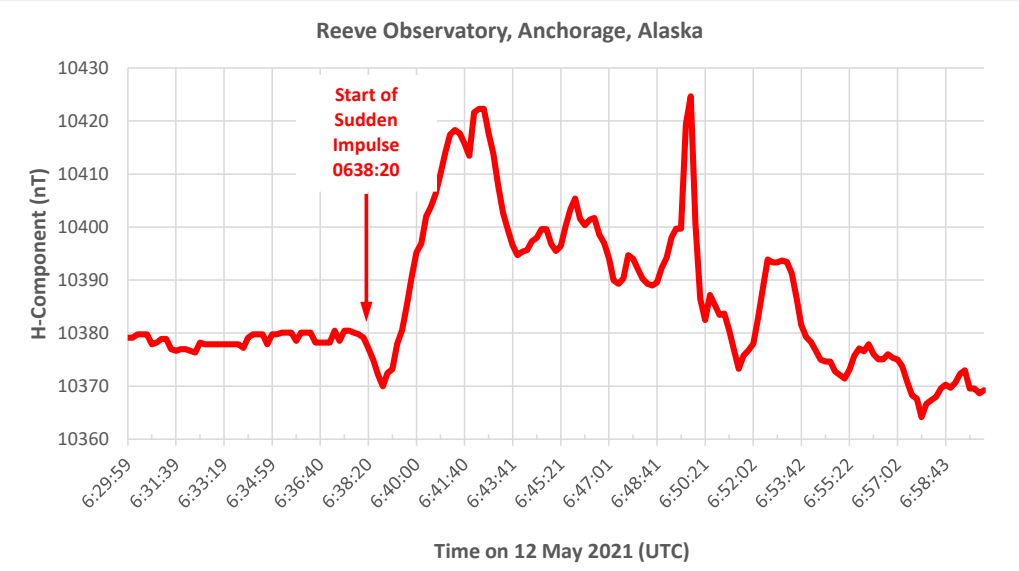
Event Description (based on SWPC *Forecast Discussions* [{SWPC}](#)): Solar active region 2822 produced a long duration C2/Sf flare at 1449 UTC on 9 May with an associated Type II radio sweep and a CME seen in STEREO A COR2 imagery beginning at 1538 UTC. An interplanetary (IP) shock was later observed at the DSCOVR spacecraft at 0547 UTC on 12 May. Solar wind speed at the spacecraft jumped from around 320 km s⁻¹ to 450 km s⁻¹ with similar jumps in density, temperature and magnetic field. The interplanetary magnetic field (IMF) associated with the CME showed only a short southward (negative) component immediately after shock arrival and was predominantly northward (positive) for the rest of the SWPC reporting period. Total IMF flux density reached 20 nT (the total magnetic flux density for background conditions is around 5 to 6 nT).

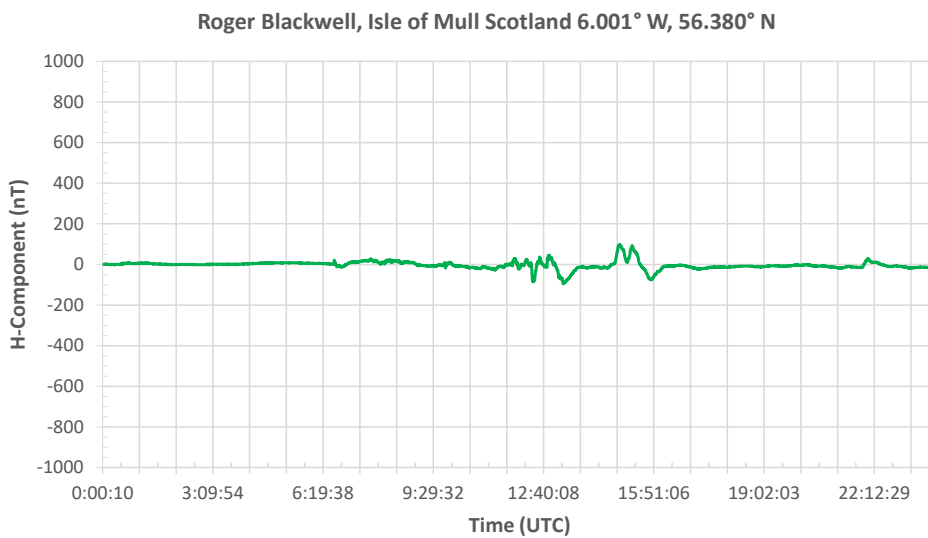
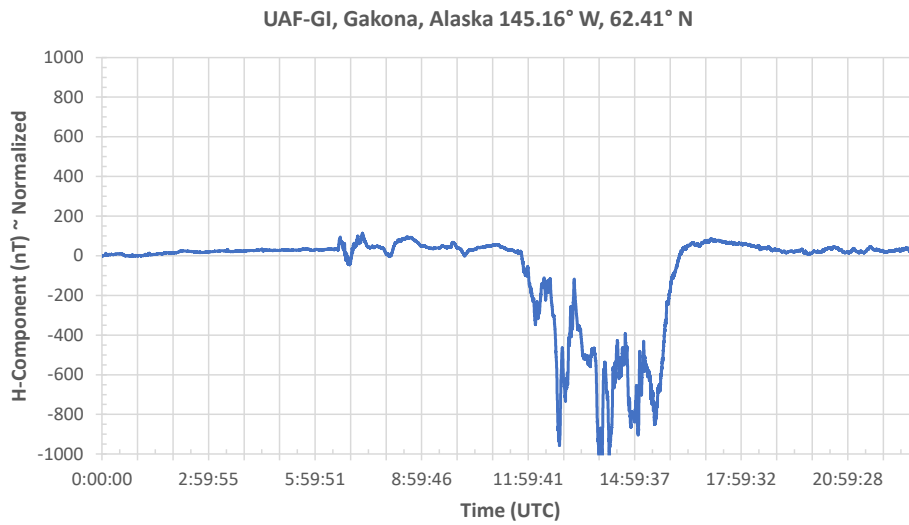
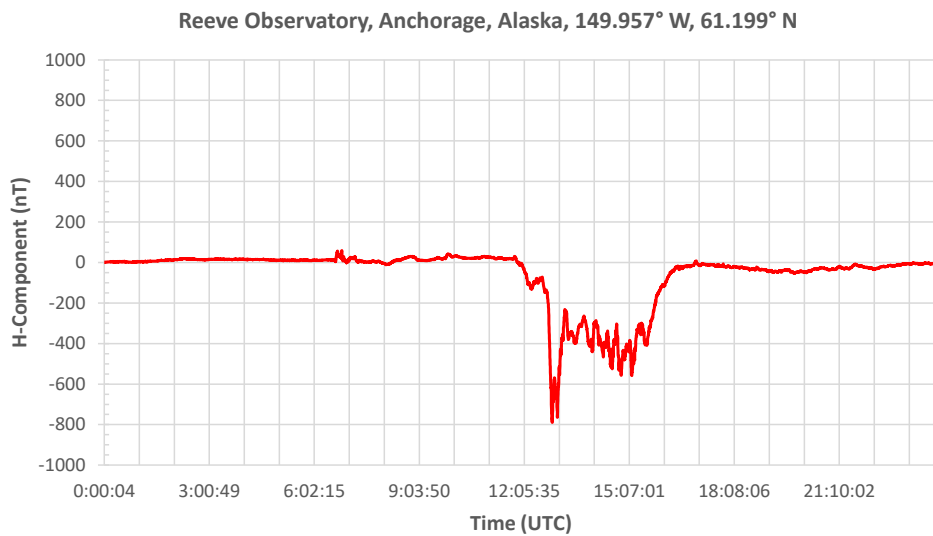
Ground magnetometers were quiet until the IP shock arrived at Earth’s magnetosphere. SWPC reported the shock arrival as a sudden impulse (SI) at 0643 UTC with an amplitude of 51 nT based on data from the USGS Fredericksburg, Virginia USA magnetometer. SWPC also reported that by 0711 UTC on 12 May, geomagnetic field activity had risen to *active* levels (Kp-index = K4), reaching K7 by mid-day.

Observations: Slight differences in SI time and amplitude were recorded by the three magnetometer stations (table 2). The differences in time with respect to SWPC may be due to the way they interpret their data. They “look for ‘a sudden perturbation, positive or negative, of several nT, in the H-component of the data’ ... contained in an ASCII text list of the one-minute readings.”[Reeve] The differences in amplitude are accounted for by the different locations of the magnetometer sensors and their sensitivities. The SAM-III magnetometer sensors are uncalibrated. Raw data produced by the three stations for the time period 0630 to 0700 UTC are plotted below.

Table 2 ~ Sudden impulse observations and magnetometer sample rates. Amplitudes are based on the H-component of the magnetic field (vector sum of local Bx and By measurements).

Station	SI time (UTC)	SI amplitude (nT)	Sample rate
Anchorage, Alaska USA	0638:20	52	0.1 Hz
Gakona, Alaska USA	0638:19	70	1.0 Hz
Isle of Mull Scotland	0637:51	20	0.1 Hz





24-h data: Plots of the data produced by the two SAM-III magnetometers and the UAF-GI Gakona magnetometer for 12 May are shown above. These plots show only the H-component of the magnetic field. The SAM-III magnetometers produce Bx-, By- and Bz-components (geographic coordinate system), so the H-component is

derived by calculating the vector sum of B_x and B_y . The data posted by UAF-GI already includes the H-component {UAF-GI}. The H-component is then normalized to its value at the beginning of the UTC day. The vertical scales in the three plots are set to the same value of ± 1000 nT. This setting compresses the Isle of Mull data so that many features seen in the Alaskan magnetograms are not obvious in the Isle of Mull magnetogram. The disturbance between 1200 and 1700 UTC measured at Isle of Mull had peak values of +98 and -95 nT, whereas the peak values for Anchorage were +59 and -789 nT and for Gakona were +114 and -1081 nT.

Discussion: The data produced by the two SAM-III magnetometers are time-stamped by the PCs that collect the data, and both PCs are synchronized by the Network Time Protocol (NTP) with GNSS-traceable time references. The Gakona magnetometer also uses a GNSS for time-stamping. Thus, it is believed that all data times are accurate to better than 20 ms. The slight differences in the times shown in the horizontal scale labels are due to missing data, but data timing errors are small compared to the overall time characteristics of the event.

There are two additional aspects of these observations that we mention. First, the 30-min plot for the sudden impulse from the relatively inexpensive SAM-III magnetometer in Anchorage compares very well to the far more expensive professional Narod magnetometer in Gakona. Many features in the 24-h data also are very similar. The stations are about 290 km apart and differ by 1° geographic latitude and 2° geomagnetic latitude. Some differences are expected simply because the magnetometers are in different magnetic environments but, in this case, they are relatively small.

Second, the data from Scotland shows similar feature timing aspects but much lower magnetic amplitudes, not only in the sudden impulse but also in the follow-on magnetically active conditions between 1200 and 1700. The time of the sudden impulse at 0638 corresponds to 10:38 pm local time at Anchorage (nightside) and 7:38 am at Isle of Mull (dayside). The great circle distance between the two stations is 6585 km and they differ by 5° in geographic latitude and 3° in geomagnetic latitude. Because of the different times, distance and geomagnetic latitude, it is expected that the current systems in the magnetosphere that produce varying magnetic fields on the ground, as well as the widely different ground magnetic environments, would lead to significantly different measurements. This appears to be the case with our observations. In particular, the Anchorage and Gakona stations are closer in latitude to the auroral electrojet than Isle of Mull and, thus, the former stations are more heavily influenced by geomagnetic variations produced by the electrojet current. Also, the shock occurred about 2.5 h after local sunrise at Isle of Mull, which explains why the shock was detected slightly earlier there than in Alaska.

Weblinks & References:

{Kyoto} <http://wdc.kugi.kyoto-u.ac.jp/igrf/gggm/index.html>

{SWPC} <ftp://ftp.swpc.noaa.gov/pub/forecasts/discussion/>

{UAF-GI} <https://www.gi.alaska.edu/monitors/magnetometer> : Magnetometer data, Geophysical Institute, UAF 2021. Retrieved from Research Computing Systems 12 May 2021.

[Reeve] Personal communications with Space Weather Prediction Center Product Subscription Service (PSS) Help, 3 June 2013

HI Observation with RTL-SDR & IF Average

Dan Kowell, AL7RS

Introduction

For some Folks getting started in RA can be a daunting task. Getting equipment, putting it all together, software, processing and getting results. My experiences have been quite a range of emotion so to say. Getting equipment together and running.... no problem, many years of HAM Radio behind me has provided some good skill. My biggest problem has been software, not growing up in the computer age is a downfall, in fact I didn't get a PC until the late 1980's and my first PC was an IBM 8088 and programs on floppy disk.

So, with that lets move on to information which I hope will help someone get started in RA and get up and running quickly. Let us start with equipment.

Equipment I am using:

- > 2.4 GHz parabolic WiFi grid dish
- > NooElec 20 Mhz – 4 Ghz LNA
- > NooElec DC Block
- > 1 – N male to SMA male Adapter (to connect LNA to Cable on Antenna)
- > RTL-SDR Dongle
- > SDR# Software with IF Average Plugin
- > 1 – USB Cable to supply power to the LNA
- > 1 – USB Cable to connect the Dongle to the PC
- > Laptop PC

Photos of the equipment I am using:



Figure 1: Antenna



Figure 2: Close up view of the N - SMA adapter, LNA, DC Block, Dongle and USB Cables, note the plastic bag which is used to protect the electronics from rain.

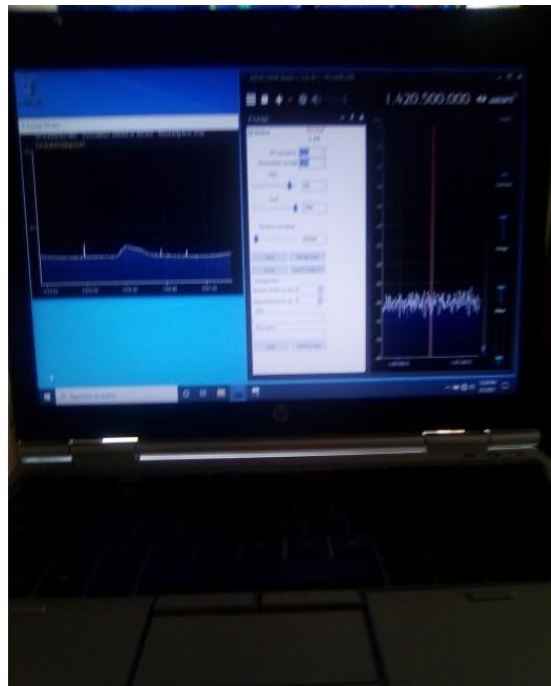


Figure 3: Laptop PC with SDR# and IF Average running (IF Average window on left side is showing HI at the time the photo was taken).

Equipment used is the same setup as in the article found on the RTLSDR website:

<https://www.rtl-sdr.com/cheap-and-easy-hydrogen-line-radio-astronomy-with-a-rtl-sdrwifiparabolic-grid-dish-1na-and-sdrsharp/>

.... with the exception of the LNA. Currently I am using the NooElec LaNA 20 MHz - 4 GHz which has a Gain of about 19 dB at 1420 MHz and a NF of about 1.2 dB. I plan on getting the NooElec SAWbird HI 1420 MHz LNA which has a Gain of about 40 dB at 1420 MHz and a NF of about 0.8 dB, (all Data from NooElec Data Sheets).

Apparently, the same equipment is found in the "Scope in a Box" available from the SARA store, although I don't know what software if any is provided in that package.

There are many Programs available for RA. Some require downloading files, compiling, make, building and host of other things before you can run them. Then, once you get them running you may or may not need to do some editing to get a plot or some other results. That is great if you are a computer specialist, but for Folks who might be like me and not so computer savvy, there are Programs that are simpler to use and do the processing then give you a plot or some other result. SDR# with the IF Average Plugin is one of these programs and will my focus here. The SDR# program with the IF Average Plugin is an easy program to use once you get it all running. The IF Average Plugin averages the FFT's from SDR# and continuously updates the Trace in the IF Average Window, almost but not quite real time.

At first, I could not get the Plugin to work in SDR#, but after obtaining a newer laptop and downloading and installing everything again into the newer laptop I was able to use the IF Average Plugin and get some clear results. So, let's dive into the Software and how I solved the issue.

Software

These instructions will deal only with Windows, I cannot help anyone with linux, mac, other OS's, compiling, building, etc . . . those are beyond my ability. (if it isn't executable, I can't run it)

I was using an old Dell D-630 laptop which was having a lot of issues and frequently programs would lock up or shut down. After installing SDR# and IF Average Plugin and finding that the Plugin would not work, I re-read the instructions and found that I was missing a component which the Plugin required. I downloaded and installed that component and still nothing. When I started SDR# I would get error messages and the program would close. Finally, I just deleted the Files for the IF Average Plugin so I could run SDR#. So, my thought at this point was: " I need a new laptop anyway " and ordered a newer laptop.

What I got:

- HP Elitebook 2560p
- x64 based PC
- Intel Core i5-2540M CPU @ 2.60 GHz
- 8 GB RAM
- MS Win 10

Next, there are some programs that the PC **must have** in order for SDR# and the IF Average Plugin to run. For SDR# **you need to Download and install the following programs first**, (if your PC doesn't already have them).

> [Microsoft .NET 5.0 or newer redistributable](#)

Note that on some computers you may also need to install the [Visual C++ Runtime](#) if it is not already installed. For the IF Average Plugin, **you need to Download and install:**

> windows desktop-runtime-5.0.2-win-x86

> microsoft-net-framework-5-0-3

> Microsoft XNA Framework 4.0 Redistributable

If any one of these programs are missing (as was in my case) the IF Average Plugin will never load or work in SDR#, (at least in my case).

Once those are installed, then Download: > [sdrsharp x86](#)

> [AVE zip \(link below \)](#)

<https://www.dropbox.com/sh/v3ul0a8x9ofagej/AADwDWqiuGUZexueFzfqEGGva?dl=0>

..... when the page opens just click the Download button at the top right hand corner of the page and the download should start, you should then have the zip file in your Downloads Folder.

(Important! **Do not run the files from within the zip file** or the following steps will fail). (Also, **do not extract into a folder within the Program Files directory**, or installation may fail as these folders are often automatically made read only by Windows).

Make a folder in C:/

(like C:/SDR#), first, extract the zipped files from [sdrsharp](#) to the new folder..... then extract the files from [AVE](#) into the same folder.

Next, open the SDR# folder and look down the list for the [Plugins XML Document File](#), Open it with notepad..... type in the magic sentence:

```
<add key="IF Average" value="SDRSharp.Average.AveragePlugin,SDRSharp.Average" />
```

click save.....

**** before performing the next step make sure you are connected to the internet as Drivers and some files get downloaded in the process.**

For Win 10

Once the previous steps have been done, (you should still have the SDR# Folder open), you can now find the [install-rtlsdr windows batch file](#) just up from the [Plugins XML File](#), right click.... run as administrator and follow the instructions..... (I had to run as administrator for Win 10).....

This will start a command prompt that will download all the drivers required to make SDRSharp work with RTL-SDR. The command prompt will automatically close after a few seconds when it is done. **If the bat file successfully ran the files rtlsdr.dll and zadig.exe will be downloaded into the SDR# directory.** If they were not downloaded then your PC or anti-virus solution may be misconfigured and may have trouble running batch files (Check that the folder is not read only, and not located in the Program Files directory).

For Win 7, x32 system (as in my old Dell D-630)

Double click on [install-rtlsdr.bat](#), This will start a command prompt that will download all the drivers required to make SDRSharp work with RTL-SDR. The command prompt will automatically close after a few seconds when it is done. **If the bat file successfully ran the files rtlsdr.dll and zadig.exe will be downloaded into the SDR# directory.** If they were not downloaded then your PC or anti-virus solution may be misconfigured and may have trouble running batch files (Check that the folder is not read only, and not located in the Program Files directory).

If [install-rtlsdr.bat](#) fails to download the dll or zadig, do a manual driver installation. **If Zadig is smaller than 5000kB (5MB), the download has failed and you should download Zadig manually.**

Once you get to this point just follow the Instructions that come with SDR# starting with "Plug in your Dongle" to finish the setup and you should be ready to set Settings and run the Programs.

Running

Before running IF Average I changed some Settings.

First, in the Configuration Panel (click the Cog in upper left corner of SDR#, I set the Sample Rate to 1.92 MSPS which on the Display Windows shows a frequency range of 1419.750 - 1421.250.

Next, I turn off the Waterfall which " I think " will be less work for the CPU.

Next, I set the IF Average Settings as follows: FFT Resolution - 1024

Intermediate Average - 1000

Gain - 350 - this setting can be used to adjust the level of the Trace in the window if the Level setting is maxed out.

Level - adjust as needed to bring the Trace into view, usually after running the Calibration. Normally I find my setting to be around 1000.

Dynamic Averaging - 902000

Calibration

You must perform the Calibration otherwise you will have a wavy and messy Trace and may not see a very weak detection.

First, I point the antenna toward the ground then open SDR#, then IF Average Control Panel and tick the "Window" box in the upper left corner to open the IF Average Window. I start SDR# and then IF Average and immediately click the "Background" button to start the calibration. (not running the calibration will give a wavy and messy trace as seen in below.



Figure 4: This is how the Trace looks on first start up before Calibration.

There will be a message in "yellow" in the upper left corner of the IF Average Window indicating that a correction scan is in progress.

Once the scan is complete (usually takes from 5 to 8 minutes) another message in "yellow" will appear saying "Corrected Background".

After Calibration you should see a nice flat Trace as in photo below: (without the HI Peak), that will come later.

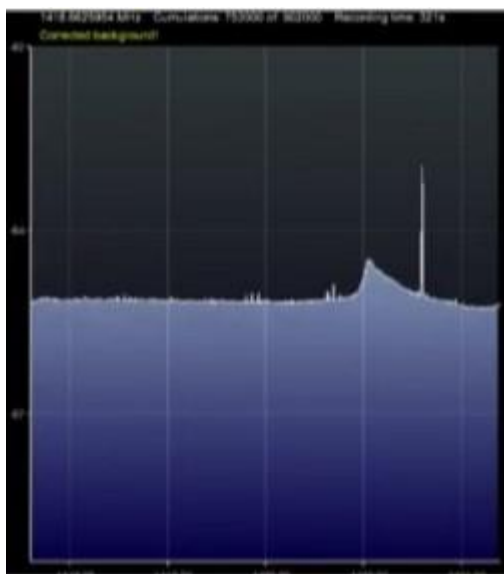


Figure 5: Corrected Background

You are now ready to begin observing.

After Calibration you can try observing HI. Your Trace will be flat, as the HI starts moving above your antenna you should see a small bump start to emerge. As the time passes the bump should grow larger and then start to dissipate and return to a fairly flat Trace as the HI moves away. Understand this process takes several hours or more.

Extra Notes

If you plan to do a 24-hour scan, make sure to change the settings in the PC that control when it goes to sleep or shuts down, not doing so means lost data collection time.

The IF Average does have a File Saving feature; however, I have not been able to find Instructions for the Plugin on how to use the program or the functions. At some point I will explore a little deeper into the File Saving Functions.

My solution is to just use the Windows Snipping Tool to capture a screen shot of the IF Average Window and save them into a folder.

Finally, there is a neat Program (Chronolapse), which is an executable program (thank God!), which saves screen shots and then later can be edited to make a movie which can show in fast motion many hours of data collection. I will not dive into this one because this is not important or necessary for RA. I will say that I have found the program to be fairly easy and straightforward to use and does have a Quick Start Guide and good Instructions.

In ending, I hope the above information will be helpful or useful to others.

Membership

New Members

Please welcome our new or returning SARA members who have joined since the last journal. If your name is missing or misspelled, please send an email to treas@radio-astronomy.org. We will make sure it appears correctly in the next Journal issue.

First name	Last name	City	State	Country	Call Sign
Simon	Gornall	San Jose	CA	USA	
Kevin	Wilson	Maryland City	MD	USA	
Steven	Ayers	Clyde	TX	USA	KE5ES
Jean	Labbe	Levis	Quebec	Canada	
Ronald	Malaya	Austin	TX	USA	
Earl	Adams	La Porte	IN	USA	
Keith	Helinsky	Middleton	MD	USA	
William	Marchant	Winchester	VA	USA	KW4WZ
Thomas	Blog	Sante Fe	NM	USA	
Raphael	Perez	Bronx	NY	USA	KI2V

Membership dues are \$20.00 US per year and all dues expire in June. Student memberships are \$5.00 US per year. Memberships must be renewed in June of each year. Or pay once and never worry about missing your dues again with the SARA Life Membership. SARA Life Memberships are now offered for a one-time payment of twenty times the basic annual membership fee (currently \$400 US).

Journal Archives & Other Promotions

The rich and diverse legacy of member contributed content is available in the SARA Journal Archives. Table of contents for journals is available online at radio-astronomy.org/store.

The entire set of The Journal of The Society of Amateur Radio Astronomers is available on USB drive. It goes from the beginning of 1981 to the end of 2017 (over 6000 pages of SARA history!) Or you can choose one of the following USB drive's or DVD:* (Prices are US dollars and include postage.)

† All SARA journals and conference proceedings are available through the previous calendar year.

Prices, US dollars, including postage

Members

Each USB drive	\$15.00	
USB drive + 1-year membership extension		\$30.00

Non-members

Each USB drive	\$25.00	
USB drive + 1-year membership	\$30.00	

Non-USA members

Each USB drive	\$20.00 (airmail)	
USB drive+ 1-year members extension	\$35.00	

*Already a member and want any or all these USB drives or DVD's? Buy any one for \$15.00 or get any three for \$35.00.

SARA Store (radio-astronomy.org/store.)

SARA offers the above USB drives, DVDs, printed Proceedings and Proceedings on USB drive and other items at the SARA Store: <http://www.radio-astronomy.org/e-store>. Proceeds from sales go to support the student grant program. Members receive an additional 10% discount on orders over \$50 US. Payments can be made by sending payment by PayPal to treas@radio-astronomy.org or by mailing a check or money order to SARA, c/o Brian O'Rourke, 337 Meadow Ridge Rd, Troy, VA 22974-3256

SARA Online Discussion Group

SARA members participate in the online forum at <http://groups.google.com/group/sara-list>. This is an invaluable resource for any amateur radio astronomer.

SARA Conferences

SARA organizes multiple conferences each year. Participants give talks, share ideas, attend seminars, and get hands-on experience. For more information, visit <http://www.radio-astronomy.org/meetings>.

Facebook

Like SARA on Facebook

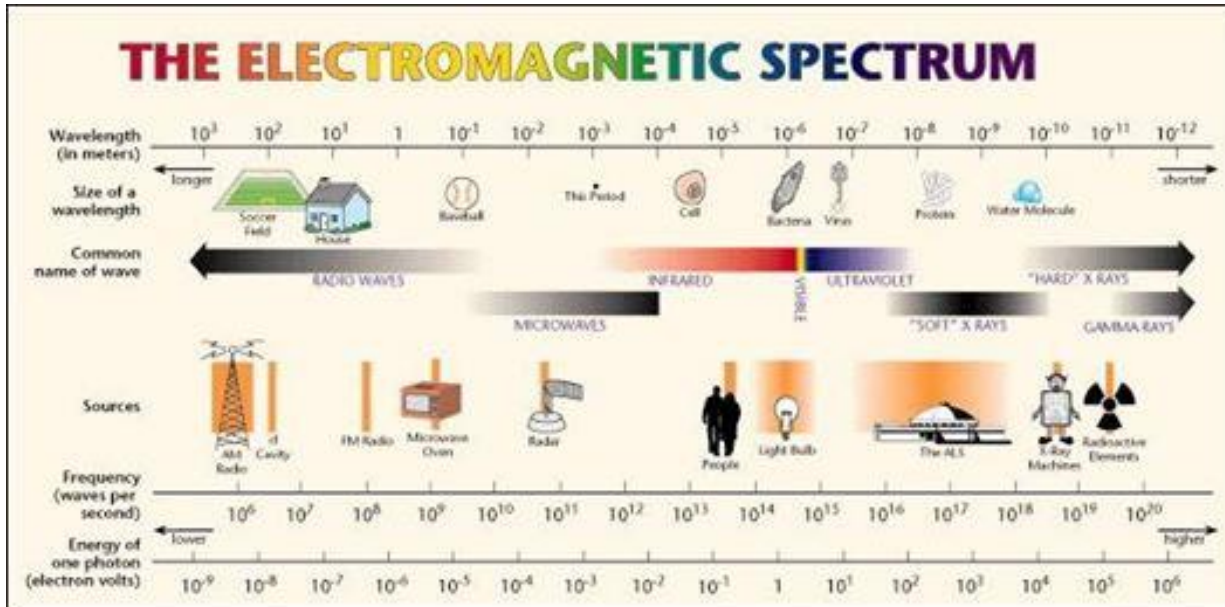
<http://www.facebook.com/pages/Society-of-Amateur-Radio-Astronomers/128085007262843>

Twitter

Follow SARA on Twitter@RadioAstronomy1

What is Radio Astronomy?

This link is for a booklet explaining the basics of radio astronomy.
<http://www.radio-astronomy.org/pdf/sara-beginner-booklet.pdf>



Administrative

Officers, directors, and additional SARA contacts

The Society of Amateur Radio Astronomers is an all-volunteer organization. The best way to reach people on this page is by email with SARA in the subject line SARA Officers.

President: Dennis Farr, WB4RJK, <http://www.radio-astronomy.org/contact/President> +1 813 833-3918

Vice President: Dr. Rich Russel, AC0UB <http://www.radio-astronomy/contact/Vicepresident>

Secretary: Bruce Randall, NT4RT, <http://www.radio-astronomy/contact/Secretary> +1 803-327-3325

Treasurer: Brian O'Rourke, K4UL, <http://www.radio-astronomy/contact/Treasurer>

Past President: Ken Redcap, tbd@radio-astronomy.org +1 319-591-1131

Founder Emeritus and Director: Jeffrey M. Lichtman, K14GIY, jeff@radioastronomysupplies.com +1 954-554-3739

Board of Directors

Name	Term expires	Email
Wayne McCain, KS0S	2021	wayne.mccain@athens.edu
Charles Osborne, K4CSO	2021	k4cso@charter.net
Ed Harfmann	2022	edharfmann@comcast.net
Steve Tzikas	2022	Tzikas@alum.rpi.edu
Keith Payea, AG6CI	2022	kbpayea@bryantlabs.net

David Westman	2022	david.westman@engineeringretirees.org
Jon Wallace	2021	wallacefj@comcast.net
Dr. Wolfgang Herrmann	2021	messbetrieb@astropeiler.de

Other SARA Contacts

All Officers	http://www.radio-astronomy.org/contact-sara	
All Directors and Officers	http://www.radio-astronomy.org/contact/All-Directors-and-Officers	
Eastern Conference Coordinator	http://www.radio-astronomy.org/contact/Annual-Meeting	
All Radio Astronomy Editors	http://www.radio-astronomy.org/contact/Newsletter-Editor	
Radio Astronomy Editors	Dr. Richard A. Russel	drrichrussel@netscape.net
Contributing Editor	Whitham D. Reeve	whitreeve@gmail.com
Educational Outreach	http://www.radio-astronomy.org/contact/Educational-Outreach	
Grant Committee	Tom Crowley	grants@radio-astronomy.org
Membership Chair	http://www.radio-astronomy.org/contact/Membership-Chair	
Technical Queries (David Westman)	http://www.radio-astronomy.org/contact/Technical-Queries	
Webmaster	Ciprian (Chip) Sufitchi, N2YO	webmaster@radio-astronomy.org

Resources

Great Projects to Get Started in Radio Astronomy

Radio Observing Program

The Astronomical League (AL) is starting a radio astronomy observing program. If you observe one category, you get a Bronze certificate. Silver pin is two categories with one being personally built. Gold pin level is at least four categories. (Silver and Gold level require AL membership which many clubs have membership. For the bronze level, you need not be a member of AL.)

Categories include

- 1) SID
- 2) Sun (aka IBT)
- 3) Jupiter (aka Radio Jove)
- 4) Meteor back-scatter
- 5) Galactic radio sources

This program is a collaboration between NRAO and AL. Steve Boerner is the Lead Coordinator and a SARA member.

For more information:

Steve Boerner

2017 Lake Clay Drive

Chesterfield, MO 63017

Email: sboerner@charter.net

Phone: 636-537-2495

<http://www.astroleague.org/programs/radio-astronomy-observing-program>

Radio Jove



The Radio Jove Project monitors the storms of Jupiter, solar activity and the galactic background. The radio telescope can be purchased as a kit or you can order it assembled. They have a terrific user group you can join. <http://radiojove.gsfc.nasa.gov/>

INSPIRE Program



The INSPIRE program uses build-it-yourself radio telescope kits to measure and record VLF emissions such as tweeks, whistlers, sferics, and chorus along with man-made emissions. This is a very portable unit that can be easily transported to remote sites for observations.

<http://theinspireproject.org/default.asp?contentID=27>

SARA/Stanford SuperSID



Stanford Solar Center and the Society of Amateur Radio Astronomers have teamed up to produce and distribute the SuperSID (Sudden Ionospheric Disturbance) monitor. The monitor utilizes a simple pre-amp to magnify the VLF radio signals which are then fed into a high definition sound card. This design allows the user to monitor and record multiple frequencies simultaneously. The unit uses a compact 1-meter loop antenna that can be used indoors or outside. This is an ideal project for the radio astronomer that has limited space. To request a unit, send an e-mail to supersid@radio-astronomy.org

Radio Astronomy Online Resources

<p>A New Radio Telescope for Mexico - ORION 2021 01 20. Dr. Stan Kurtz https://www.youtube.com/watch?v=Q9aBWr1aBVc</p>	<p>National Radio Astronomy Observatory http://www.nrao.edu</p>
<p>AJ4CO Observation of Jovian decametric emission http://www.radiojove.org/SUG/Observation%20Reports/AJ4CO/</p>	<p>NRAO Essential Radio Astronomy Course http://www.cv.nrao.edu/course/astr534/ERA.shtml</p>
<p>British Astronomical Association – Radio Astronomy Group http://www.britastro.org/baa/</p>	<p>Pulsar Sounds: Audio recordings made by professional observatories http://www.typnet.net/AJ4CO/Pulsar_Sounds/</p>
<p>CALLISTO Receiver & e-CALLISTO http://www.reeve.com/Solar/e-CALLISTO/e-callisto.htm CALLISTO data archive: www.e-callisto.org</p>	<p>Radio Astronomy calculators http://www.typnet.net/AJ4CO/Calculators/Calculators.htm</p>
<p>Deep Space Exploration Society http://DSES.science</p>	<p>Radio Astronomy Supplies http://www.radioastronomysupplies.com</p>
<p>Deep Space Object Astrophotography Part 1 -- ORION 2021 02 17. George Sradnov https://www.youtube.com/watch?v=Pm_Rs17KlyQ</p>	<p>Radio Jove Spectrograph Users Group http://www.radiojove.org/SUG/</p>
<p>European Radio Astronomy Club http://www.eraonet.org</p>	<p>Radio Sky Publishing http://radiosky.com</p>
<p>Exotic Ions and Molecules in Interstellar Space -- ORION 2020 10 21. Dr. Bob Compton https://www.youtube.com/watch?v=r6cKhp23SUo&t=5s</p>	<p>RF Associates Richard Flagg, rf@hawaii.rr.com 1721-1 Young Street, Honolulu, HI 96826 RFspace, Inc. http://www.rfspace.com</p>
<p>Forum and Discussion Group http://groups.google.com/group/sara-list</p>	<p>SARA Facebook page https://www.facebook.com/pages/Society-of-Amateur-Radio-Astronomers/128085007262843</p>
<p>GNU Radio http://www.gnu.org/licenses/gpl.html</p>	<p>SARA Twitter feed https://twitter.com/RadioAstronomy1</p>
<p>Graphs, plots, equations, miscellaneous cheat sheets http://www.typnet.net/AJ4CO/index.htm</p>	<p>SARA Web Site http://radio-astronomy.org</p>
<p>Inspire Project http://theinspireproject.org</p>	<p>SETI League http://www.setileague.org</p>

<p>Introduction to Amateur Radio Astronomy (presentation) http://www.typnet.net/AJ4CO/Publications/Intro%20to%20Amateur%20Radio%20Astronomy,%20Typinski%20(AAC,%202016)%20v2.pdf</p>	<p>Shirleys Bay Radio Astronomy Consortium marcus@propulsionpolymers.com</p>
<p>NASA Radio JOVE Project http://radiojove.gsfc.nasa.gov Archive: http://radiojove.org/archive.html</p>	<p>Simple Aurora Monitor Magnetometer http://www.reeve.com/SAMDescription.htm</p>
<p>National Radio Astronomy Observa-tory http://www.nrao.edu</p>	<p>Stanford Solar Center http://solar-center.stanford.edu/SID/</p>
<p>NRAO Essential Radio Astronomy Course http://www.cv.nrao.edu/course/astr534/ERA.shtml</p>	<p>The Arecibo Radio Telescope; It's History, Collapse, and Future - ORION 2020.12.16. Dr. Stan Kurtz, Dr. David Fields https://www.youtube.com/watch?v=rBZIPOLNX9E</p>
<p>Pulsar Sounds: Audio recordings made by professional observatories http://www.typnet.net/AJ4CO/Pulsar_Sounds/</p>	<p>The Radio JOVE Project & NASA Citizen Science – ORION 2020.6.17. Dr. Chuck Higgins https://www.youtube.com/watch?v=s6eWAXjywp8&t=5s</p>
<p>Radio Astronomy calculators http://www.typnet.net/AJ4CO/Calculators/Calculators.htm</p>	<p>UK Radio Astronomy Association http://www.ukraa.com/</p>

For Sale, Trade and Wanted

At the SARA online store: radio-astronomy.org/store.

SARA Polo Shirts

New SARA shirts have arrived.

We now have a good selection of X, XX, and XXX shirts available in all colors including white!

Shirts are \$20 at the conference and \$25 shipped.

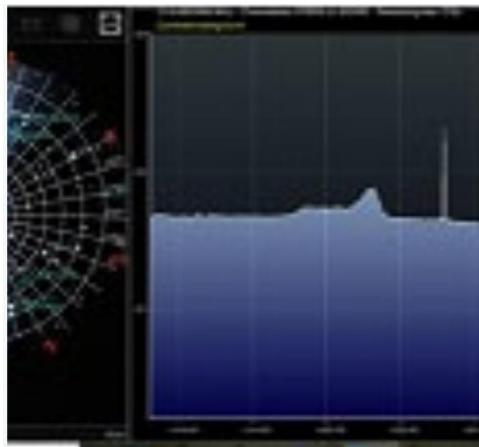
Contact the treasurer at treas@radio-astronomy.org for availability and shipping.



Scope in a Box \$295

radio-astronomy.org/store.

Kit of parts and software to build a working Radio Telescope to detect Hydrogen Line emissions. Available to USA addresses only at this time.



SuperSID Complete Kit (\$112-\$160 depending on options)

radio-astronomy.org/store.



SARA Publication, Journals and Conference Proceedings (various prices)

radio-astronomy.org/store.

SARA Journal USB Drive (\$15-\$35 depending on shipping option)

radio-astronomy.org/store.

The USB drive covers the society journal "Radio Astronomy" from the founding of the organization in 1981 thru 2020. Articles cover a wide range of topics including: cosmic radiation, pulsars, quasars, meteor detection, solar observing, Jupiter, Radio Jove, gamma ray bursts, the Itty Bitty Telescope (IBT), dark matter, black holes, the Jansky antenna, methanol masers, mapping at 408 MHz and more. This CD contains all of the above and more with over 4800 pages of articles on radio astronomy. Also included is a copy of Grote Reber's handwritten, 34 page document "Carriage and Mirror Detail" of his historic antenna now on display at the National Radio Astronomy Observatory (NRAO) in Green bank, WV. You also get an electronic copy of the 109 page "Basics of Radio Astronomy" from JPL Goldstone-Apple Valley Radio Telescope. Also included is the NRAO 40-foot radio telescope "Operators Manual", which by the way, you get to operate if you attend the Eastern SARA conference in July.

SARA Advertisements

There is no charge to place an ad in Radio Astronomy; but you must be a current SARA member. Ads must be pertinent to radio astronomy and are subject to the editor's approval and alteration for brevity. Please send your "For Sale," "Trade," or "Wanted" ads to edit@radio-astronomy.org. Please include email and/or telephone contact information. Please keep your ad text to a reasonable length. Ads run for one bimonthly issue unless you request otherwise.

Typinski Radio Astronomy, Inc., info@typinski.com

Antenna systems and feed line components for HF radio astronomy

Jeff Kruth, WA3ZKR, kmec@aol.com

RF components from HF to MMW, various types including mixers, RF switches, amplifiers, oscillators, coaxial components, waveguide components, etc. I have a very large collection of stuff and the facilities to test and provide data. Please email with your needs and I will see if I have something for you. Have fun!

Stuart and Lorraine Rumley, sales@valontechnology.com

The Valon Technology 2100 Downconverter, when combined with our 5009 frequency synthesizer module, provides a high-performance, compact receiver downconverter system. Applications include hydrogen line studies at 1420MHz and radio astronomy in the protected 30MHz segment of the 21 cm band. For more information visit <http://www.valontechnology.com/2100downconverter.html> or send an email.

Radio2Space, filippo.bradaschia@primalucelab.com

SPIDER radio telescopes and turn-key-systems designed specifically for education.

<https://www.radio2space.com>

We developed our SPIDER radio telescopes as turn-key-system just to avoid the problem you perfectly highlighted in your website: "Purchasing a radio telescope isn't like buying an optical telescope. They are harder to find, and usually require assembly and software troubleshooting. In some cases, a radio telescope must be built from components." Our SPIDER radio telescopes are not designed for amateurs that prefer to build a radio telescope but to schools, universities, museums, and other science institutes that needs for a complete and ready-to-use system, just like the optical telescopes they can normally buy!

Radio Astronomy Supplies

<http://www.radioastronomysupplies.com>

jeff@radioastronomysupplies.com

Research and Educational Radio Telescopes and all associated equipment since 1994

Membership Information

Annual SARA dues: Individual \$20, Classroom \$20, Student \$5 (US funds) anywhere in the world. Membership includes a subscription to Radio Astronomy, the bimonthly Journal of The Society of Amateur Radio Astronomers, delivered electronically (via a secure web link, emailed to you as each new issue is posted). We regret that printing and postage costs prevent SARA from providing hardcopy subscriptions to our Journal.

We would appreciate the following information included with your check or money order, made payable to SARA:

Name: _____
 Email Address : _____
(required for electronic Journal delivery)
 Ham call sign: _____ (if applicable)
 Address: _____
 City: _____
 State: _____
 Zip: _____
 Country: _____
 Phone: _____

Please include a note of your interests. Send your application for membership, along with your remittance, to our Treasurer.

For further information, see our website at:
<http://radio-astronomy.org/membership>

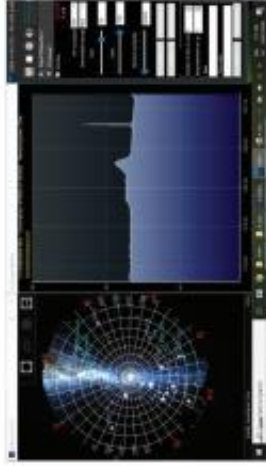


Society of Amateur Radio Astronomers, Inc.
 Founded 1981

Membership supported, nonprofit [501(c) (3)]
 Educational and Radio Astronomy Organization
**Knowledge through Common Research,
 Education and Mentoring**

How to get started?

SARA has a made a kit of software and parts to detect the Hydrogen line signal from space. This is an excellent method to get started in radio astronomy. It teaches the principles of antenna design, signal detection, and signal processing. Read more about this and other projects on our web site.



SARA members have been privileged to use this forty foot diameter drift-scan hydrogen line radio telescope every year at their annual meeting in Green Bank.

Why Radio Astronomy?

Because about sixty five percent of our current knowledge of the universe has stemmed from radio astronomy alone. The discovery of quasars, pulsars, black holes, the 3K background from the "Big Bang" and the discovery of biochemical hydrogen/carbon molecules are all the result of professional radio astronomy.

 <http://radio-astronomy.org>



The Society of Amateur Radio Astronomers

SARA was founded in 1981, with the purpose of educating those interested in pursuing amateur radio astronomy.

The society is open to all, wishing to participate with others, worldwide.

SARA members have many interests, some are as follows:

SARA Areas of Study and Research:

- ✔ Solar Radio Astronomy
- ✔ Galactic Radio Astronomy
- ✔ Meteor Detection
- ✔ Jupiter
- ✔ SETI
- ✔ Gamma Ray/High Energy Pulse
- ✔ Detection
- ✔ Antennas
- ✔ Design of Hardware / Software

The members of the society offer a friendly mentor atmosphere. All questions and inquiries are answered in a constructive manner. No question is silly!

SARA offers its members an electronic bi-monthly journal entitled Radio Astronomy. Within the journal, members report on their research and observations. In addition, members receive updates on the professional radio astronomy community and, society news.

Once a year SARA meets for a three-day conference at the Green Bank Observatory in Green Bank West Va.

There is also a spring conference held at various cities in the Western USA. Previous meetings have been at the VLA in Socorro, NM and at Stanford University.



How do I get started?

Just as a long journey begins with the first step, the project you elect must start with a clear idea of your objectives. Do you wish to study the sun? Jupiter? Make meteor counts? Do you wish to engage in imaging radio astronomy? What you decide will not only determine the type of equipment you will need, but also the local radio spectrum.

How do amateurs do radio astronomy?

Radio astronomy by amateurs is conducted using antennas of various shapes and sizes, from smaller parabolic dishes to simple wire antennas. These antennas are connected to receivers and most of these receivers are software defined radios these days. Data from the receivers are collected by computers, and the received signals will be displayed as charts, graphs or maybe even sky maps. As diverse as the observed objects, so is are the instruments and tools used. SARA members will always be supportive to find good solutions for what one wishes to observe.

Is amateur radio astronomy instrumentation expensive?

Technical information freely circulated in our monthly journal helps amateurs to obtain good low noise equipment from off the shelf assemblies, or to build their own units. The actual cash investment in radio astronomy equipment need not exceed that of any other hobby.

What are amateurs actually looking for in the received data?

The aim of the radio amateur is to find something new and unusual. Just as an amateur optical observer hopes to notice a supernova or a new comet, so does an amateur radio observer hope to notice a new radio source, or one whose radiation has changed appreciably.



The Reber Telescope at NRAO. Constructed by Grote Reber in 1937 in his back yard in Wheaton, Illinois



SARA Members discussing the IBT (itty Bitty Telescope)

